Demonstrating multilevel entanglement and optimal quantum measurements

Adetunmise Charles Dada

Submitted for the degree of *Doctor of Philosophy (PhD)*

Heriot-Watt University
Edinburgh, United Kingdom

Scottish Universities Physics Alliance (SUPA)
Institute of Photonics and Quantum Sciences (IPaQS)
School of Engineering and Physical Sciences (EPS)

February 2013

Abstract

Optimal generalised quantum measurements are important for quantum information applications in both photonic and solid state systems. However, until now, the implementations of such measurements have been optical. Entanglement is also a very important resource in quantum communication and information processing. However, high-dimensional entangled states and corresponding Bell-inequality violations are challenging to detect and demonstrate experimentally. This thesis focuses on these two aspects of signal detection.

A cavity quantum electrodynamics (QED) scheme to realise an optimised quantum measurement demonstrating the superadditivity of quantum channel capacity is proposed and analysed. The measurement is shown to be feasible using atoms in a cavity QED setup even in the presence of rather high levels of experimental errors. This is interesting because cavity QED realisations could potentially be more easily scaled to increase quantum coding gain. Experimental unambiguous discrimination between non-orthogonal states is also carried out for the first time in the solid state using the nuclear spin of a nitrogen atom associated with a defect in bulk diamond—an important step for implementations of solid-state quantum computing.

This thesis presents a method for verifying entanglement dimension using only Bell inequality test measurements. It also shows experimental results demonstrating genuine eleven-dimensional two-photon orbital angular momentum (OAM) entanglement and violations of generalised Bell inequalities up to dimension twelve. The demonstrated high-dimensional entanglement is potentially useful for closing the detection loophole in Bell-test experiments and for real-world large-alphabet quantum-cryptography applications.

Acknowledgements

I am grateful to the Scottish Universities Physics Alliance (SUPA) for a generous prize scholarship. I thank my Supervisor Dr. Erika Andersson for her kind help and support throughout the PhD project. She has been a good teacher, mentor and collaborator. I also want to express appreciation for the academic support from my Co-Supervisor Prof. Gerald Buller. He always encouraged collaboration and participation at conferences, even assisting with regards to funding the trips. He also supported the funding of many trips between Edinburgh and Glasgow during collaboration with the Glasgow Optics Group.

I warmly acknowledge other collaborators who have contributed in different ways to the results presented in this thesis. These include Dr. Mark Everitt and Dr. Vivien Kendon who were collaborators on the cavity QED project; Prof. Miles Padgett and Dr. Jonathan Leach who were collaborators on the high-dimensional entanglement experiments; Mr. Gerald Waldherr, Prof. Jörg Wrachtrup, Dr. Phillip Neumann, and Dr. Fedor Jelezko who were collaborators on the realisation of optimal measurements using NV centres in diamond.

There are also friends and colleagues with whom I have had informal chats, which have added to the success of my studies in one way or another. Of these, I would particularly like to thank Prof. Steve Barnett, Dr. Michael Hall, and all members of the Glasgow Optics Group (past and present) for fruitful discussions. I also wish to acknowledge initial discussions with Johannes Beck and Florian Rempp on NV-centre measurements. It was great fun sharing offices with Chaitanya Joshi, Frauke Izdebski, Silvia Butera and Akhil Rajan. Being a PhD student within SUPA has been a really joyful and satisfying experience, one I will not forget in a hurry.

List of Publications by the Candidate

- Dada, A. C., Leach, J., Buller, G. S., Padgett, M. J., and Andersson, E. **Experimental high-dimensional two-photon entanglement and violations of generalized Bell inequalities**. *Nature Physics* **7**, 677–680 (2011). Cover feature. The candidate carried out the preparatory simulations for the experiment, the main part of the experimental work (with guidance from Dr. Jonathan Leach), as well as data analysis including all the numerical work involved in proving high-dimensional entanglement.

- Dada, A. C., Andersson, E. **On Bell inequality violations with high-dimensional systems**. *International Journal of Quantum Information (IJQI) Special Issue* **9**, 1807-1823 (2011). The candidate contributed to the analytical derivations and performed all the numerical work.

- Dada, A. C., Andersson, E., Jones, M. L., Kendon, V. M., and Everitt, M. S. **Quantum measurements of atoms using cavity QED**. *Phys. Rev. A* **83**, 042339 (2011). The candidate derived the explicit form of the experimental implementations of the measurements.

- Waldherr, G., Dada, A. C., Neumann, P., Jelezko, F., Andersson, E., Wrachtrup, J., **Distinguishing between Nonorthogonal Quantum States of a Single Nuclear Spin**, *Phys. Rev. Lett.* **109**, 180501 (2012). The candidate derived the explicit form of the experimental implementations (such as the pulses needed), and also performed the main part of the analysis of the experimental results. He also contributed to the final execution of the experiment.

- Dalgarno, H. I. C., Dalgarno, P. A., Dada, A. C., Towers, C. E., Gibson, G. J., Parton, R. M., Davis, I. Warburton, R. J. and Greenaway, A. H. **Nanometric depth resolution from multi-focal images in microscopy**. *Journal of The Royal Society Interface* **8**, 942-951 (2011). The candidate executed some of the mathematical and statistical modelling relating to the 3D imaging system and particle tracking applications.

ACADEMIC REGISTRY
Research Thesis Submission

Name*:*	Adetunmise Charles Dada		
School/PGI:	Engineering and Physical Sciences / Institute of Photonics and Quantum Sciences		
Version: *(i.e. First, Resubmission, Final)*	Final	Degree Sought (Award **and** Subject area)	PhD (Physics)

Declaration

In accordance with the appropriate regulations I hereby submit my thesis and I declare that:

1) the thesis embodies the results of my own work and has been composed by myself
2) where appropriate, I have made acknowledgement of the work of others and have made reference to work carried out in collaboration with other persons
3) the thesis is the correct version of the thesis for submission and is the same version as any electronic versions submitted*.
4) my thesis for the award referred to, deposited in the Heriot-Watt University Library, should be made available for loan or photocopying and be available via the Institutional Repository, subject to such conditions as the Librarian may require
5) I understand that as a student of the University I am required to abide by the Regulations of the University and to conform to its discipline.

* *Please note that it is the responsibility of the candidate to ensure that the correct version of the thesis is submitted.*

Signature of Candidate*:*		Date:	

Submission

Submitted By *(name in capitals):*	
Signature of Individual Submitting:	
Date Submitted:	

For Completion in the Student Service Centre (SSC)

Received in the SSC by *(name in capitals):*			
Method of Submission *(Handed in to SSC; posted through internal/external mail):*			
*E-thesis Submitted (**mandatory for final theses)***			
Signature:		Date:	

Please note this form should bound into the submitted thesis.

Updated February 2008, November 2008, February 2009, January 2011

Contents

List of Tables

List of Figures

INTRODUCTION

Quantum signal detection

The prospect of being able to exploit quantum effects in communications and information processing schemes continues to capture the interest of scientists. An indispensable aspect of all such schemes is the detection stage. This is because, in quantum information processing and quantum communication protocols, information is encoded in and carried by a quantum system [1], and it is only by doing a detection can the final state of the system or the result of the performed task be determined. Indeed, the concept of the state of a quantum system remains mysterious and controversial even after one century of quantum mechanics (please see [2]). Also, the quantum state itself is not a quantum mechanical observable [3] and is not directly accessible [4]. Be that as it may, quantum measurements provide a means to peer into the quantum world.

Since von Neumann put quantum theory on a firm mathematical basis in 1932 [5], the topic of detecting quantum signals has grown into a rich interdisciplinary area of research and many quantum communication and information processing schemes have been developed. In recent years, quantum information processing and communication has progressed greatly due to better precision of measurement and control, as well as longer coherence times of photonic and solid state quantum systems. Spontaneous parametric downconversion (SPDC) [6, 7] sources have been the workhorse for generating entangled photons [8], which are useful for communication tasks such as quantum key distribution [9] and quantum teleportation [10]. Also, as evidenced by the recent Nobel Prize in Physics [11], cavity QED techniques [12] are of wide international interest and impact because they allow for precise control and measurement of single quantum systems such as photons, atoms or a combination of these. Nitrogen-vacancy centres in diamond offer long lived coherence at room temperature [13, 14, 15]. This thesis considers specific aspects of signal detection pertaining to these systems. In particular, it explores the experimental implementations of quantum measurements in the context of (a) Bell inequality violation for high-dimensional entanglement demonstration, and (b) quantum state discrimination using non-photonic systems.

The motivation for the latter is that, generally speaking, some optimal quantum mea-

surements are difficult to generalise using linear optics. This is due to the large overhead costs of effective large-scale photon-photon interactions [16, 17]. Therefore, it is useful to study how to realise such measurements in other physical systems. In particular, non-orthogonal state discrimination has received considerable attention mostly theoretically, but also experimentally in the last 5-10 years and has led to important developments in operational quantum information processing [18, 19]. This thesis presents the first solid-state demonstration of optimal discrimination of non-orthogonal quantum states. Although this concept has already been demonstrated in photonic systems, developing the techniques for solid-state implementations of such schemes is an important step towards large-scale quantum information processing in the solid state. This is because solid-state systems face completely different challenges (such as dephasing, state detection errors and pulse calibration errors) from those of single photons (such as photon losses and non-deterministic gates). The studies reported here deal with facing the complexity that comes with working with the experimental complications of solid-state systems.

High-dimensional bipartite entanglement also enables very promising applications including teleportation of qudit states [10, 20], generalised dense coding (i.e., with pairs of entangled d-level systems) [21], and certain quantum key distribution protocols [9]. More generally, schemes like quantum secret sharing [22], and measurement based quantum computation [23], apply multi-particle entanglement. However, such applications are only practical when it is possible to experimentally detect high-dimensional entangled states. This makes the ability to verify high-dimensional entanglement between physical qudits of crucial importance. Various techniques exist for witnessing entanglement, and in particular, high-dimensional entanglement (see [24] and references within). However, for practical applications, it is usually desirable that the resource state is not only entangled, but that the entanglement is of the type that can violate a Bell inequality. The use of Bell inequality violation for entanglement verification is favoured here since it is closer to a direct application: in entanglement-based large alphabet quantum key distribution, the presence of an eavesdropper is determined using a Bell inequality test.

Demonstrations of high-dimensional two-photon entanglement using time bins [25, 26] and OAM bring entanglement-based applications such as quantum key distribution (QKD) systems (sharing larger number of bits per photon) closer to their real-world applications. In addition to enabling larger information capacity [27, 28], such systems have been shown to have a security advantage over QKD based on two-dimensional systems which share one bit per photon pair [29].

This thesis is organised as follows. Chapter 1 introduces and defines some of the key tools and concepts applied throughout the rest of thesis. The chapters are written in a rather self-contained fashion as they discuss original results obtained from the PhD project as well as the motivation, background information and results for each of the respective

short projects reported.

Chapter 2 and 3 respectively present original results on a feasible scheme for demonstration of superadditivity of quantum channel capacity using cavity QED, and experimental realisation of optimal schemes for unambiguous discrimination between nonorthogonal nuclear-spin states of a nitrogen atom associated with a nitrogen-vacancy (NV) centre in diamond.

Chapter 4 discusses fair sampling in tests of the Clauser-Horne-Shimony-Holt Bell inequality and its generalisation in systems having an arbitrary number of dimensions. Theoretical results leading to an experimentally feasible scheme for determining entanglement dimension from Bell test measurements are also presented. Chapter 5 then describes experimental results demonstrating genuine eleven-dimensional entanglement in OAM for photons generated by SPDC using Bell-inequality tests.

Chapter 6 finally gives a summary and overview over the results of the thesis as well as future outlook.

CHAPTER 1

Underpinning concepts

1.1 Quantum measurements

A signal is ultimately encoded onto the state of a physical system, such as a photon or atom. Therefore, signal detection is fundamentally a *quantum measurement*—a process by which one extracts information about the state of the quantum system.[1]

1.1.1 Quantum states

Quantum mechanics dictates that any isolated or *closed* physical system is assigned a *Hilbert space* $\mathcal{H}$, which is a complex vector space equipped with inner product. This is known as the *state space* of the system. The state of a physical system is represented mathematically as complex vector known as the *state vector*. The simplest quantum mechanical system is the *qubit*, a discrete variable system that has a two-dimensional state space. Discrete variable systems having Hilbert space dimensions greater than two are sometimes referred to as *qudits*.

Qubits can be physically encoded in the polarisation state of a photon as well as electronic or nuclear spin states of atoms. Suppose $|0\rangle$ and $|1\rangle$ form the orthonormal basis for the state space. An arbitrary state vector in the state space can be written as

$$|\psi\rangle = \alpha\,|0\rangle + \beta\,|1\rangle\,, \tag{1.1}$$

where α and β are complex numbers. The condition that $|\psi\rangle$ be a unit vector is known as the normalisation condition for state vectors. One may write Equation 1.1 as

$$|\psi\rangle = e^{i\gamma}(\cos\frac{\theta}{2}\,|0\rangle + e^{i\phi}\sin\frac{\theta}{2}\,|0\rangle), \tag{1.2}$$

where θ, ϕ, γ are real numbers. Ignoring the global phase factor $e^{i\gamma}$, we can effectively write

$$|\psi\rangle = \cos\frac{\theta}{2}\,|0\rangle + e^{i\phi}\sin\frac{\theta}{2}\,|0\rangle\,, \tag{1.3}$$

[1] The descriptions of quantum states and quantum measurements provided in this chapter can be found in Refs. [30] and [31].

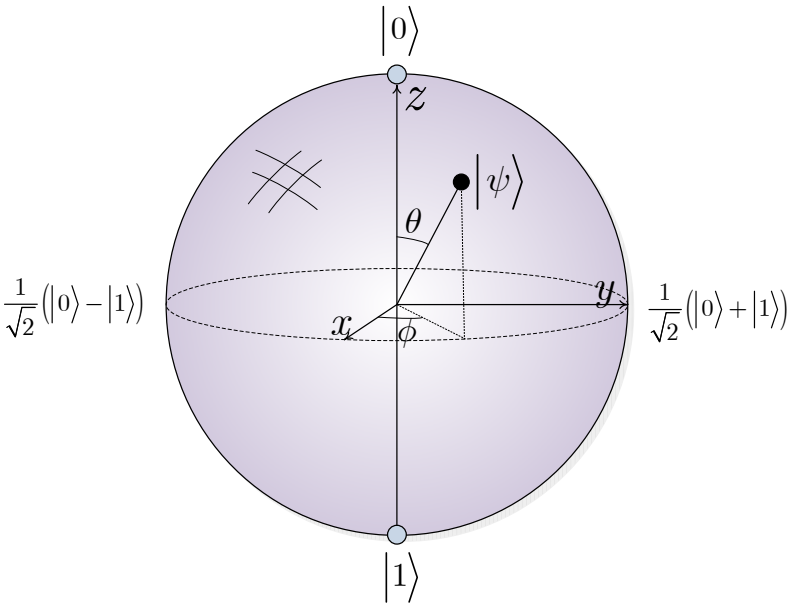

Figure 1.1: Bloch sphere representation of a qubit.

The numbers θ and ϕ define a point on the unit three-dimensional sphere illustrated in Figure 1.1. This is often called the *Bloch sphere* and it gives a useful geometric representation of the qubit. Qudits can be physically encoded in the OAM states of photons. These have high-dimensional state spaces and do not have a simple Bloch sphere representation.

The *density operator* or *density matrix* provides a convenient means for describing quantum systems whose state is not completely known (i.e., which are not in pure states), that is, the so called *mixed states*. Suppose, a quantum system is in one of a number of states $|\psi_i\rangle$, where i is an index, with respective probabilities p_i. $\{p_i, |\psi_i\rangle\}$ is called an *ensemble* of pure states. The density operator for the system is then defined by the equation

$$\hat{\rho} = \sum_i p_i |\psi_i\rangle \langle\psi_i| . \tag{1.4}$$

The state space of a *composite system* is the tensor product of the state spaces of the subsystems. In other words, if two systems are assigned Hilbert spaces $\mathcal{H}_1$ and $\mathcal{H}_2$, then the composite system is described by $\mathcal{H} = \mathcal{H}_1 \otimes \mathcal{H}_2$, where $\otimes$ denotes tensor product. Moreover, if we have systems numbered 1 to n, and the system number i is prepared in the state $|\psi_i\rangle$ or $\hat{\rho}_i$, then the joint state of the total system is

$$|\psi\rangle = |\psi_1\rangle \otimes |\psi_2\rangle \otimes \ldots \otimes |\psi_n\rangle = |\psi_1 \psi_2 \ldots \psi_n\rangle, \text{ or} \tag{1.5}$$

$$\hat{\rho} = \hat{\rho}_1 \otimes \ldots \otimes \hat{\rho}_n. \tag{1.6}$$

States which can be written in the form of Equations (1.5) and (1.6) are said to be *separable*. Such states of the Hilbert space of a composite system are a measure-zero subset, whose complement is a dense open subset composed of states which are said to be *entan-*

gled (see Section 1.2).

1.1.2 Evolution and measurement

The evolution of a closed quantum system is described by a unitary transformation. That is, the state $|\psi\rangle$ or $\hat{\rho}$ of the system at the time t_1 is related to the state $|\psi'\rangle$ or $\hat{\rho}'$ of the system at the time t_2 by a unitary[1] operator $\mathbf{U}$ which depends on the times t_1 and t_2. The evolved state is expressed as

$$|\psi'\rangle = \mathbf{U}|\psi\rangle, \tag{1.7}$$

$$\hat{\rho}' = \mathbf{U}\hat{\rho}\mathbf{U}^{\dagger}. \tag{1.8}$$

A few useful single qubit unitary transformations are [32]

$$\hat{\sigma}_x = \begin{bmatrix} 0 & 1 \\ 1 & 0 \end{bmatrix}, \quad \hat{\sigma}_y = \begin{bmatrix} 0 & -i \\ i & 0 \end{bmatrix}, \quad \hat{\sigma}_z = \begin{bmatrix} 1 & 0 \\ 0 & -1 \end{bmatrix}, \tag{1.9}$$

$$\hat{R}_y(\theta) = \begin{bmatrix} \cos\theta/2 & \sin\theta/2 \\ -\sin\theta/2 & \cos\theta/2 \end{bmatrix}, \quad \hat{R}_z(\alpha) = \begin{bmatrix} e^{i\alpha/2} & 0 \\ 0 & e^{-i\alpha/2} \end{bmatrix},$$

$$\Phi(\delta) = \begin{bmatrix} e^{i\delta} & 0 \\ 0 & e^{i\delta} \end{bmatrix}, \tag{1.10}$$

where $\hat{\sigma}_x$, $\hat{\sigma}_y$ and $\hat{\sigma}_z$ are the *Pauli spin matrices*; $\hat{R}_y(\alpha)$ and $\hat{R}_z(\alpha)$ are rotations of the qubit by θ and α about the y and z axes on the Bloch sphere respectively; and $\Phi(\delta)$ is a phase shift of δ.

Further, the continuous time evolution of the state of a closed quantum system is described by the *Schrödinger equation*,

$$i\hbar\frac{d|\psi\rangle}{dt} = H|\psi\rangle. \tag{1.11}$$

Here, $\hbar$ is the *Planck constant*. H is a *Hermitian* (i.e. self-adjoint) operator known as the *Hamiltonian* of the closed system. Thus, in principle, if we know the Hamiltonian of a closed system, then (together with the knowledge of $\hbar$) we understand its dynamics completely. For most physical systems however, the Hamiltonian is not exactly solvable and formal solutions as well as approximations have to be sought.

To extract information about the state of a physical system, such as a photon, an external system has to interact with it. This interaction makes the measured system no longer closed and thus not necessarily subject to unitary evolution. Quantum measurements in general are described by a collection of measurement operators $\{M_i\}$. These are opera-

[1] unitarity of $\mathbf{U}$ implies that $\mathbf{U}^{\dagger}\mathbf{U} = \mathbb{I}$

tors acting on the state space of the system being measured and the index i refers to the measurement outcomes that may occur in the experiment. If the state of the system is $|\psi\rangle$ just before the measurement, then the probability that result i occurs is given by

$$p(i) = \langle\psi| M_i^\dagger M_i |\psi\rangle\,, \tag{1.12}$$

and the state after measurement is

$$\frac{M_i|\psi\rangle}{\sqrt{\langle\psi| M_i^\dagger M_i |\psi\rangle}}. \tag{1.13}$$

The measurement operators satisfy the *completeness relation*

$$\sum_i M_i^\dagger M_i = \mathbb{I}, \tag{1.14}$$

which expresses the fact that the outcome probabilities sum up to unity, i.e.

$$\sum_i \langle\psi| M_i^\dagger M_i |\psi\rangle = \sum_i p(i) = 1, \tag{1.15}$$

$\forall\, |\psi\rangle$. In terms of the density operator,

$$p(i) = \mathrm{Tr}(M_i^\dagger M_i \hat{\rho}), \tag{1.16}$$

where Tr denotes the trace. A very important consequence of Equation (1.13) is that a measurement performed on a quantum state will disturb it, unless the state is known to be an eigenstate of the measurement operator. This limits the amount of information extractable from the system through measurement.

1.1.3 Distinguishing quantum states

In a communication system, the task of the detector is often to determine which one of a set of states a system was prepared in. This is essentially a discrimination between signal states. The knowledge of the signal encoding as well as the desired probability for each outcome is applied to implement specific optimisations in detection.

In the classical world, different states of an object are usually distinguishable, at least in principle. For example we can always identify which side a cast die has landed on. However, quantum mechanically, this not generally the case. To illustrate, consider the metaphor of a game involving two parties *Alice* and *Bob*, representing the *encoder* and the *detector* respectively. Suppose Alice chooses a state $|\psi_i\rangle$ $(1 \leq i \leq n)$ from some fixed set of states known to both parties. She gives $|\psi_i\rangle$ to Bob, whose task is to identify the index i of the state he has been given.

Suppose the $|\psi_i\rangle$ states are orthonormal. Then Bob can do a quantum measurement to distinguish these states by defining a measurement operator

$$M_i \equiv |\psi_i\rangle\langle\psi_i|, \tag{1.17}$$

one for each possible index i, and an additional measurement operator defined as the positive operator $\mathbb{I} - \sum_{i\neq 0} |\psi_i\rangle\langle\psi_i|$. These operators satisfy the completeness relation, and if the state $|\psi_i\rangle$ is prepared, then $p(i) = \langle\psi_i|M_i|\psi_i\rangle = 1$, so the result i occurs with a certainty, and Bob does not have to guess. Thus it is possible to reliably distinguish between the orthonormal states $|\psi_i\rangle$. However, if the states are not orthonormal, *there is no quantum measurement capable of distinguishing the states with certainty*. The idea is that Bob will do a measurement described by measurement operators M_j, with outcome j. Depending on the outcome of the measurement Bob tries to guess what the index i was. To see why Bob cannot distinguish between the two non-orthogonal states $|\psi_1\rangle$ and $|\psi_2\rangle$, consider that $|\psi_1\rangle$ can be decomposed into a (non-zero) component parallel to $|\psi_2\rangle$, and another orthogonal to it. Suppose j is a measurement outcome which indicates to Bob that the state was $|\psi_1\rangle$. However, because of the component of $|\psi_2\rangle$ parallel to $|\psi_1\rangle$, there is a non-zero probability of getting the outcome j when $|\psi_2\rangle$ is prepared, so Bob will sometimes make an error in identifying the prepared state.

1.1.4 Projective measurements

Loosely speaking, a projective measurement is one which simply 'asks' the system which one of n orthonormal states it is in, and then leaves it in the state corresponding to the outcome. In more concrete terms, a projective measurement is described by an *observable* $\mathbf{M}$, a Hermitian (i.e., self adjoint) operator on the state of the system being observed, which can be written as

$$\mathbf{M} = \sum_m m P_m, \tag{1.18}$$

where P_m is the projector onto the eigenspace of $\mathbf{M}$ with eigenvalue m. The possible outcomes of the measurement correspond to the eigenvalues m, of the observable. Upon measuring the state $|\psi\rangle$, the probability of getting result m is given by

$$p(m) = \langle\psi|P_m|\psi\rangle \tag{1.19}$$

The state of the system immediately after measurement, given that outcome m occurred is

$$\frac{P_m|\psi\rangle}{\sqrt{p(m)}} \tag{1.20}$$

Thus one readily identifies the projector as

$$P_m = |\psi_m\rangle\langle\psi_m|, \tag{1.21}$$

where the states $|\psi_i\rangle$ are orthonormal. The states $|\psi_i\rangle$ are said to form the *measurement basis*.

The projective measurements can be seen as a case of the measurement described in Section 1.1.2 above where the measurement operators, in addition to satisfying the completeness relation $\sum_i M_i^\dagger M_i = \mathbb{I}$, also satisfy the conditions that $\{M_i\}$ are orthogonal projectors, that is they are Hermitian.

A simple example demonstrating this idea is the measurement of a qubit encoded in the *polarisation state of a photon*. With the photon initially in state

$$|\psi\rangle = \alpha|H\rangle + \beta|V\rangle, \tag{1.22}$$

and using measurement operators $\{M_H, M_V\}$ with $M_H = |H\rangle\langle H|$ and $M_V = |V\rangle\langle V|$, one realises that the measurement outcome probabilities are $p(H) = |\alpha|^2$ and $p(V) = |\beta|^2$. The measurement operators here could, for example, be implemented using polarising beam splitters with photon detectors at each of the reflection and transmission output ports for the detection of horizontal and vertical polarisations respectively. In this picture, the quantum system being measured and the measuring device altogether are a part of a larger, isolated, quantum mechanical system.

1.1.5 POVM measurements

POVM stands for positive operator-valued measure, otherwise known as probability-operator measure (POM). POVM measurements are also known as *generalised measurements*. Suppose a measurement described by measurement operators M_i is performed on a quantum system in the state $|\psi\rangle$. Then the probability of outcome i is given by $p(i) = \langle\psi|M_i^\dagger M_i|\psi\rangle$. Suppose we define

$$\Pi_i \equiv M_i^\dagger M_i. \tag{1.23}$$

It is clear then that Π_i is a positive operator such that $\sum_i \Pi_i = I$ and $p(i) = \langle\psi|\Pi_i|\psi\rangle$. Thus the set of operators Π_i are sufficient to determine the probabilities of the different measurement outcomes. The operators Π_i are known as the POVM elements associated with the measurement. The complete set $\{\Pi_i\}$ is known as POVM. Note that the POVM elements are not necessarily projectors, and so POVM measurements are more general than projective measurements. This will be described further in subsequent chapters.

1.2 Quantum entanglement

The mathematical definition of entanglement versus separability is straightforward for pure states: a pure state $|\psi\rangle$ is *separable* if and only if it can be written as

$$|\psi\rangle = |\psi_1\rangle \otimes |\psi_2\rangle, \tag{1.24}$$

otherwise it is *entangled*. An example of a separable pure state is $|\psi\rangle = |00\rangle$, while examples of entangled pure states are the *Bell states*

$$\left|\phi^{\pm}\right\rangle = \frac{1}{\sqrt{2}}(|00\rangle \pm |11\rangle) \quad \text{or} \quad \left|\psi^{\pm}\right\rangle = \frac{1}{\sqrt{2}}(|01\rangle \pm |10\rangle). \tag{1.25}$$

Of interest for the example in the next section is the *singlet state*

$$\left|\psi^{-}\right\rangle = \frac{1}{\sqrt{2}}(|01\rangle - |10\rangle). \tag{1.26}$$

A mixed state is *separable* if and only if it can be written as [33]

$$\hat{\rho} = \sum_j p_j |\psi_1^j\rangle\langle\psi_1^j| \otimes |\psi_2^j\rangle\langle\psi_2^j|, \tag{1.27}$$

otherwise it is *entangled*. The coefficients p_j here are probabilities and the states need not be orthogonal i.e. $\langle\psi_n^j|\psi_n^k\rangle \neq \delta_{jk}$ in general, where $n = 1, 2$. Such a state can be prepared through local operations and classical communication. An example of a separable mixed state containing only classical correlations is

$$\hat{\rho} = \frac{1}{2}(|00\rangle\langle 00| + |11\rangle\langle 11|), \tag{1.28}$$

while an example of an entangled mixed state is a Werner state [33]

$$\hat{\rho} = (1-p)\frac{1}{4}\mathbb{I} + p(|\phi^+\rangle\langle\phi^+|, \tag{1.29}$$

where the probability p is such that $\frac{1}{3} < p < 1$.

1.2.1 EPR paradox and Bell inequality

In their argument [34], Einstein, Podolsky and Rosen (EPR) introduced a requirement which they claimed was a sufficient condition for a physical property to satisfy *realism*, namely, that it be possible to predict the value that property will have irrespective of whether a measurement is performed or not. Bell's original inequality [35] was key to the

experimental investigation of the validity of the EPR argument. Clauser, Horne, Shimony and Holt [36] further put Bell's inequality into a more experimentally verifiable form.

Using the EPR reasoning, the CHSH-Bell inequality can be arrived at by constructing a scenario where a source prepares two particles and sends one to *Alice* and the other to *Bob*. Assume that Alice measures her particle on reception and has two detector settings A and a, and that she chooses randomly which one to use for each arriving particle only upon receiving it. Also, let the same conditions be true for Bob with his detector settings represented as B and b. For simplicity, assume that the outcomes can be either $+1$ or -1 for any of the measurements. Also, if we assume that Bob's measurement cannot affect the result of Alice's measurement and vice versa, then $A,a,B,b \in \{-1,+1\}$ implies that

$$\begin{aligned}
&(A-a, A+a) \in \{(0,\pm 2),(\pm 2,0)\},\\
&(A-a)\,B-(A+a)\,b \in \{-2,2\},\\
&-2 \leq \langle AB - Ab - aB - ab\rangle \leq 2,\\
&S = \mid \langle AB\rangle - \langle Ab\rangle - \langle aB\rangle - \langle ab\rangle \mid \leq 2\,.
\end{aligned} \tag{1.30}$$

S is known as the *CHSH-Bell parameter*.

However, repeating the same thought experiment with quantum mechanical calculations suggests a possibility of violating this inequality. This involves adopting a quantum mechanical description of the particle states. For example, let the two particles be prepared in the singlet state (Equation (1.26)) with $|0\rangle$ and $|1\rangle$ representing up and down spins respectively, and let Alice and Bob perform measurements along the spin directions

$$\begin{aligned}
\hat{A} &= \cos\theta_A \hat{\sigma}_x + \sin\theta_A \hat{\sigma}_y,\\
\hat{a} &= \cos\theta_a \hat{\sigma}_x + \sin\theta_a \hat{\sigma}_y,\\
\hat{B} &= \cos\theta_B \hat{\sigma}_x + \sin\theta_B \hat{\sigma}_y,\\
\hat{b} &= \cos\theta_b \hat{\sigma}_x + \sin\theta_b \hat{\sigma}_y.
\end{aligned} \tag{1.31}$$

The joint measurement outcomes are

$$\begin{aligned}
\left\langle \psi^- \middle| \hat{A}\otimes\hat{B} \middle| \psi^- \right\rangle &= -\cos(\theta_A - \theta_B) = -\cos\theta_{AB},\\
\left\langle \psi^- \middle| \hat{A}\otimes\hat{b} \middle| \psi^- \right\rangle &= -\cos(\theta_A - \theta_b) = -\cos\theta_{Ab},\\
\left\langle \psi^- \middle| \hat{a}\otimes\hat{B} \middle| \psi^- \right\rangle &= -\cos(\theta_a - \theta_B) = -\cos\theta_{aB},\\
\left\langle \psi^- \middle| \hat{a}\otimes\hat{b} \middle| \psi^- \right\rangle &= -\cos(\theta_a - \theta_b) = -\cos\theta_{ab}.
\end{aligned} \tag{1.32}$$

The Bell parameter is thus found to be

$$\begin{aligned} S_{QM} &= |\langle AB\rangle - \langle Ab\rangle - \langle aB\rangle - \langle ab\rangle| \\ &= |-\cos\theta_{AB} + \cos\theta_{Ab} + \cos\theta_{aB} + \cos\theta_{ab}|. \end{aligned} \tag{1.33}$$

Clearly, the Bell inequality does not necassarily hold under quantum mechanical assumptions. In fact, if we choose

$$\begin{aligned} \hat{A} &= \sigma_x, \\ \hat{B} &= (\sigma_y - \sigma_x)/\sqrt{2}, \\ \hat{a} &= \sigma_y, \\ \hat{b} &= (\sigma_y + \sigma_x)/\sqrt{2}, \end{aligned} \tag{1.34}$$

then

$$S_{QM} = 2\sqrt{2} > 2. \tag{1.35}$$

This result which is obtainable with entangled systems cannot be simulated by any classical theory based on local hidden variables.

Although quantum mechanical correlations can lead to a violation of Bell inequalities, there is an upper limit to the amount of violation quantum mechanically possible for a given Bell inequality. This is known as *Tsirelson Bound*, named after Tsirelson (or Cirel'son) who derived the bound for the CHSH Bell inequality i.e. $S_{QM} \leq 2\sqrt{2}$ [37]. This limit is in general lower than the algebraic limit. For example, the Tsirelson bound for the CHSH inequality is less than the largest algebraically possible value of S (Equation 1.30), i.e., 4.

1.2.2 High-dimensional entanglement

The CHSH-Bell inequality admits two outcomes per measurement and is thus well suited to two dimensional systems or qubits, i.e. systems with only two basis states; with their classical analogues being bits. Other versions of Bell inequalities exist for higher dimensional systems (e.g. see Ref. [38]) with bounds different from 2 and $2\sqrt{2}$ for the CHSH version. This will be explored further in Chapters 4 and 5. Indeed, dichotomic measurements can also be used for systems of higher dimensions, even continuous-variable systems.

Let us note briefly here that any bipartite pure state can be written in the form

$$|\psi\rangle = \sum_{j=1}^{d} \lambda_j |a_j\rangle \otimes |b_j\rangle. \tag{1.36}$$

This is known as Schmidt decomposition (see [3]), and d is the Schmidt number of the pure state. Such a state is here referred to as having d-dimensional entanglement.

1.3 Superadditivity of quantum channel capacity

The transmission characteristics of a communications channel is determined by its noise characteristics as well as the quantities of the available transmission resources. As well brought out in [39], a feature of classical communication theory is that the amount of transmissible information is *at most* doubled when one doubles the transmission resource (such as code length, signal power, bandwidth) for fixed noise characteristics of the channel. However, this is not generally the case in quantum communication theory, i.e. by optimising the detection or quantum measurement strategy, it might be possible to increase the amount of transmissible information by more than twice. This is called the *superadditivity* of the capacity of the quantum channel.

In communication, individual signals (e.g. $\{0,1\}$) in a transmitted message are referred to as *letters*. Sometimes, it is desirable to encode the individual signals respectively into block sequences of letters. Each block is referred to as a *codeword*. By *channel*, we mean the set of physical codeword states $\{x_j\}$ as well as the possible outputs $\{y_j\}$, and the channel matrix with each matrix element given by the conditional probability $P(y_j|x_i)$ of obtaining an output y_j given that the input was x_i. Each element of the channel matrix is called a *channel transition probability*. The mutual information defined between the input variable $X = \{x_i; P(x_i)\}$ and $Y = \{y_j; P(y_j)\}$ can be expressed in terms of the Shannon entropies $H(X)$, $H(Y)$ and the joint entropy $H(X,Y)$ as [40]

$$I(X:Y) = H(X) + H(Y) - H(X,Y). \tag{1.37}$$

Using the expressions

$$\begin{aligned}
H(X) &= -\sum_i P(x_i)\log_2 P(x_i) = -\sum_i\sum_j P(x_i,y_j)\log_2 P(x_i), && (1.38)\\
H(Y) &= -\sum_j P(y_j)\log_2 P(y_j) = -\sum_i\sum_j P(x_i,y_j)\log_2 P(y_j), && (1.39)\\
H(X,Y) &= -\sum_i\sum_j P(x_i,y_j)\log_2 P(x_i,y_j) \quad \text{and} && (1.40)\\
P(x_i,y_j) &= P(x_i)P(y_j|x_i) \quad (\text{Bayes}'\text{rule}), && (1.41)
\end{aligned}$$

we obtain

$$I(X:Y) = \sum_i P(x_i)\sum_j P\left(y_j|x_i\right)\log_2\left[\frac{P\left(y_j|x_i\right)}{\sum_k P(x_k)\,P\left(y_j|x_k\right)}\right]. \tag{1.42}$$

1.3.1 Classical channel capacity

In classical communication theory where one considers coding for a given fixed channel model $\{P(y_j|x_i)\}$, the capacity (for a memoryless channel) is defined as the maximum mutual information with respect to the prior distribution of the encoded letters $P(x_i)$,

$$C = \max_{\{P(x_i)\}} I(X:Y). \tag{1.43}$$

1.3.2 Quantum channel capacity

However, in quantum communications only the input variable X and the corresponding set of quantum states at the receiver denoted as $\{\hat{\rho}_x(i)\}$ are given. It is possible to seek for the output variable Y by an optimum *POVM measurement*. Let the POVM elements be $\{\hat{M}_{y(j)}\}$, and let $\hat{\Pi}_{y(j)} = \hat{M}^{\dagger}_{y(j)}\hat{M}_{y(j)}$. The channel matrix is

$$P(y_j|x_i) \equiv \mathrm{Tr}(\hat{\Pi}_{y(j)}\hat{\rho}_{x(i)}) \tag{1.44}$$

The maximum extractable information or *accessible information* is defined as

$$I_{Acc} = \max_{\{\hat{\Pi}_j\}} I(X:Y) \tag{1.45}$$

This quantity when further optimised with respect to the prior probabilities will give

$$C_1 = \max_{\{P(x_i)\}} \max_{\{\hat{\Pi}_{y(j)}\}} I(X:Y). \tag{1.46}$$

This is the limit of the capacity when the initial channel $\{P(y_j|x_i)\}$ is used with classical channel coding and a quantum signal detection. However, this is not the maximum capacity that quantum mechanics allows *per use of the channel*.

One could convey the code words in quantum states which are product states of the letter states $\hat{\psi}_{\mathbf{x}} = \hat{\rho}_{x_1} \otimes \cdots \otimes \hat{\rho}_{x_n}$, and use the best measurement allowed by quantum mechanics described by the POVM $\{\hat{\Pi}_{\mathbf{y}}\}$ on the extended space where $\{\mathbf{y}\}$ are the decoded codewords. The channel matrix for this extended channel is given by

$$P(\mathbf{y}|\mathbf{x}) \equiv \mathrm{Tr}(\hat{\Pi}_{\mathbf{y}}\hat{\psi}_{\mathbf{x}}). \tag{1.47}$$

Replacing the codeword states $\{x_i\}$ and outputs $\{y_j\}$ with the extended codeword states $\{\mathbf{x_i}\}$ and outputs $\{\mathbf{y_j}\}$ in Equation (1.42), we may then define the mutual information for

this extended channel as

$$I(X^n : Y^n) = \sum_i P(\mathbf{x_i}) \sum_j P\left(\mathbf{y_j}|\mathbf{x_i}\right) \log_2 \left[\frac{P\left(\mathbf{y_j}|\mathbf{x_i}\right)}{\sum_k P(\mathbf{x_k}) P\left(\mathbf{y_j}|\mathbf{x_k}\right)} \right]. \tag{1.48}$$

The channel capacity of the order n is defined as

$$C_n = \max_{\{P(x_i)\}} \max_{\left\{\hat{\Pi}_j\right\}} I(X^n : Y^n). \tag{1.49}$$

For a quantum channel, it may hold that

$$C_n > nC_1, \tag{1.50}$$

in which case the quantum channel is said to exhibit *superadditivity* in classical information capacity.

Very few schemes of coding and detection exhibiting superadditivity are known (see [40] and references therein). Chapter 2 will consider a simple example of superadditivity.

CHAPTER 2

Quantum measurements of atoms using cavity QED

2.1 Introduction

This chapter describes how to realise two non-standard quantum measurements using cavity quantum electrodynamics (QED). The first measurement unambiguously distinguishes between two non-orthogonal quantum states in an optimal way. The second example is a measurement that demonstrates superadditive quantum coding gain. The main contribution in this chapter is the derivation of the explicit form of these measurements in a cavity-QED setup, demonstration of the optimality of the proposed scheme in terms of cavity usage, and an estimation of the effect of experimental errors. The experimental tools used are single-atom unitary operations effected by Ramsey pulses and two-atom Tavis-Cummings interactions. This chapter shows how the superadditive quantum coding gain is affected by errors in the field-ionisation detection of atoms, and that even with rather high levels of experimental imperfections, a reasonable amount of superadditivity can still be seen. Apart from the realisation reported in this thesis, these types of measurement have only been realised optically. It is of great interest to have realisations using other physical systems for fundamental reasons, as well as in order to circumvent the limitations of photonic realisations. For example, quantum coding gain in general increases with code word length, and a realisation using atoms could potentially be scaled more easily than the existing realisation using photons [39] due to the possibility of strong atom-atom interactions.

Generalised quantum measurements or probability operator measures (POMs), also called positive operator valued measures (POVMs), are important mathematical tools for quantum communication and quantum information processing [41]. They are naturally able to describe imperfections and errors in real experimental measurements. In addition, there are also situations where it is advantageous to deliberately engineer a measurement that is not a projective measurement. This is frequently the case when distinguishing between quantum states [41, 42]. The simplest such example is when distinguishing between two non-orthogonal states without error [43, 44, 45]. In addition, knowledge of optimal measurement strategies may be useful in placing tight bounds on other quantum

operations such as quantum cloning [42, 46].

This chapter describes how to realise two examples of non-standard quantum measurements using the tools of cavity QED. The methods proposed could, however, be applied also more generally for realising other generalised quantum measurements using the same system. The first measurement is optimal unambiguous discrimination of non-orthogonal quantum states, also known as the Ivanovic-Dieks-Peres (IDP) measurement. This task is important for quantum information and communication systems as well as for quantum key distribution (QKD) [47]. In fact, the IDP measurement is optimal for the B92 QKD protocol [48], although this was not realised initially. Prior to this work, all the realisations of the IDP measurement have been optical [49, 50, 51]. However, generalised quantum measurements could also be realised on atoms using existing experimental techniques [52, 53, 54], on single nuclear spins in the solid state (as Chapter 3 will discuss), or using nuclear magnetic resonance [55].

The second example is the measurement required to demonstrate that quantum channel capacities can be superadditive (see Sec. 1.3). In this case, at least two uses of a quantum channel, and a collective measurement (i.e. using entangled measurement basis states) of the resulting code block, is required. The quantum coding gain in general grows with the length of the code blocks [40]. Superadditivity has so far only been demonstrated using linear optics [56]. Quantum source coding for message compression is another type of quantum coding scheme that has been optically demonstrated [57], using similar techniques as for the optical demonstration of quantum superadditivity. In both cases, the two uses of the quantum channel were encoded using the path and polarisation degrees of freedom of a single photon and the states are manipulated using basic linear optical elements (polarising beam splitters and wave plates). While this demonstrated the principle of the measurement, extension of the coding to longer code blocks would be impractical due to problems of scalability. Scalability would require effective photon-photon interactions, which are challenging to realise due to the large resource overhead [16, 17].

A cavity-QED demonstration of superadditivity might use two atomic qubits and encode each usage of the quantum channel in the state of one atom. This could in principle be scaled to longer codewords using resources which do not scale exponentially, whereas the existing optical realisation uses polarization and path to encode the two uses of the channel, making it difficult to scale [39]. Also, other coding schemes, including quantum source coding, or any other realisation of collective quantum measurements, could be realised in a cavity QED setting employing similar methods. It is also useful to estimate how experimental imperfections would affect the measurement. Cavity QED techniques have indeed been applied extensively in exploring the quantum dynamics of atoms and photons in cavities and has been used, for example, in preparing entangled states of atoms [58], performing phase gate operations [59], doing quantum non-demolition measurements of

cavity fields [60], and in experimental studies of the process of decoherence in quantum measurements [61]. In addition, there are a number of QED-type systems in which a cavity QED based scheme can be easily implemented. These include circuit and photonic crystal based systems [62, 63].

This chapter is organised as follows. Section 2.2 describes the IDP measurement of an atom in a cavity QED realisation. In Section 2.3, the superadditive measurement and a cavity QED scheme to realise it are presented. Section 2.4 discusses how experimental imperfections, such as state misidentification, might affect the proposed scheme. Finally, Section 2.5 gives a summary of the chapter's conclusions and a few other remarks.

2.2 Distinguishing between two non-orthogonal states

Generalised quantum measurements are extensions of projective or von Neumann measurements. Just as for projective quantum measurements, probabilities $p(j)$ for measurement outcomes are calculated using the trace rule

$$p(j) = \mathrm{Tr}(\hat{\rho}\hat{\Pi}_j), \tag{2.1}$$

where $\hat{\rho}$ is the measured state and $\hat{\Pi}_j$ is the POVM element corresponding to outcome j. The fact that probabilities are positive means that all eigenvalues of the $\hat{\Pi}_j$ are positive, which is written $\hat{\Pi}_j > 0$, and consequently also that the $\hat{\Pi}_j$ are Hermitian. Also, since the probabilities for all possible outcomes should sum to 1, it follows that

$$\sum_j \hat{\Pi}_j = \hat{\mathbf{I}}, \tag{2.2}$$

where $\hat{\mathbf{I}}$ is the identity operator. Generalised quantum measurements are different from projective measurements in that the measurement operators do not have to be projectors. This means that there can be more or less measurement outcomes than the number of dimensions of the measured quantum system.

The Ivanovic-Dieks-Peres (IDP) measurement [43, 44, 45] is a generalised measurement that distinguishes between two non-orthogonal states without error, in other words, unambiguously. For the measurement to be error-free, however, one must accept that it will sometimes be inconclusive. The IDP measurement is optimal in the sense that it minimises the probability of an inconclusive measurement outcome. Suppose that one wishes

to distinguish without error between two non-orthogonal quantum states

$$|\psi_1\rangle = \cos\theta|1\rangle - \sin\theta|2\rangle \quad (2.3)$$

$$|\psi_2\rangle = \cos\theta|1\rangle + \sin\theta|2\rangle, \quad 0 < \theta < \pi/4, \quad (2.4)$$

of a single quantum system e.g. an atom for which $|1\rangle \equiv |g\rangle$, $|2\rangle \equiv |e\rangle$, and $|3\rangle \equiv |i\rangle$, where $|g\rangle, |e\rangle, |i\rangle$ are ground, excited and higher excited states respectively. First, the optimal measurement will depend on the probabilities for preparing these states, i.e. the prior probabilities. Note also that making a projective measurement in the basis $\{|\psi_1\rangle, |\psi_1^\perp\rangle\}$, with $|\psi_1^\perp\rangle = \sin\theta|1\rangle + \cos\theta|2\rangle$ and obtaining the outcome $|\psi_1^\perp\rangle$ necessarily indicates that the prepared state was $|\psi_2\rangle$. If one obtains $|\psi_1\rangle$, then one cannot be sure which state was prepared, and the outcome is inconclusive. Similarly, if one chooses to measure in the basis $\{|\psi_2\rangle, |\psi_2^\perp\rangle\}$, then an outcome $|\psi_2^\perp\rangle$ indicates that the state was certainly $|\psi_1\rangle$ and the outcome $|\psi_2\rangle$ yields an inconclusive result. If one is restricted to standard von Neumann measurements, choosing to measure in one or the other basis is the best that can be done in terms of minimising the probability of an inconclusive outcome for the unambiguous discrimination.

This procedure above is however not always optimal. If the respective probabilities of preparing $|\psi_1\rangle$ and $|\psi_2\rangle$, i.e., the prior probabilities, are similar, then the generalised measurement that gives the lowest possible probability for the inconclusive result has the measurement operators

$$\hat{\Pi}_1 = k|\psi_2^\perp\rangle\langle\psi_2^\perp|, \;\; \hat{\Pi}_2 = k|\psi_1^\perp\rangle\langle\psi_1^\perp|, \;\; \hat{\Pi}_? = \hat{\mathbf{I}} - \hat{\Pi}_1 - \hat{\Pi}_2, \quad (2.5)$$

where k is a positive number which is as large as the positivity of $\hat{\Pi}_?$ will allow, that is, $k = 1/(1 + \langle\psi_1|\psi_2\rangle)$. The minimum probability for the inconclusive result is then given by $p(?)=|\langle\psi_1|\psi_2\rangle|$. Let us denote the prior probabilities as p_1 and $p_2 = 1 - p_1$.

The measurement described in Eq. (2.5) can be physically realised as a measurement in a higher dimensional Hilbert space in an orthonormal basis. This follows from Naimark's theorem which states that any generalised measurement can be realised in this way [41]. The IDP measurement can then be realised in terms of such a projective measurement in an extended Hilbert space by

(a) Extending the initial 2D Hilbert space into a 3D space by adding an extra state $|3\rangle$ which is orthogonal to both initial states $|\psi_1\rangle$ and $|\psi_2\rangle$, resulting in an orthonormal basis $\{|1\rangle, |2\rangle, |3\rangle\}$.

(b) Measuring in a basis $\{|\Pi_1\rangle, |\Pi_2\rangle, |\Pi_3\rangle\}$ where $|\Pi_1\rangle \perp |\psi_2\rangle$ and $|\Pi_2\rangle \perp |\psi_1\rangle$. This measurement can be implemented in two steps:

(i) Performing a unitary operation $\hat{U}$ given by

$$\hat{U} = |1\rangle\langle\Pi_1| + |2\rangle\langle\Pi_2| + |3\rangle\langle\Pi_?|. \tag{2.6}$$

(ii) Doing a standard projective measurement in the $\{|1\rangle, |2\rangle, |3\rangle\}$ basis. A detection in the states $|1\rangle$ or $|2\rangle$ would unambiguously indicate that the unknown state was $|\psi_1\rangle$ or $|\psi_2\rangle$ respectively, while a detection result $|3\rangle$ would make the measurement inconclusive.

The detection probabilities will therefore be

$$\begin{aligned} p(1|1) &= |\langle\Pi_1|\psi_1\rangle|^2, \\ p(2|2) &= |\langle\Pi_2|\psi_2\rangle|^2, \\ p(1|2) &= p(2|1) = |\langle\Pi_1|\psi_2\rangle|^2 = |\langle\Pi_2|\psi_1\rangle|^2 = 0, \\ p(?|1) &= p(?|2) = |\langle\psi_1|\psi_2\rangle|. \end{aligned} \tag{2.7}$$

Here $p(k|j)$ denotes the probability of obtaining a result k given a state j.

Using the basis state vectors $|1\rangle \equiv [1,0,0]^T$, $|2\rangle \equiv [0,1,0]^T$ and $|3\rangle \equiv [0,0,1]^T$, one works out the unitary operation in (2.6) for the optimum measurement to be

$$\hat{U} = \frac{1}{\sqrt{2}} \begin{bmatrix} \tan\theta & -1 & -\sqrt{1-\tan^2\theta} \\ \tan\theta & 1 & -\sqrt{1-\tan^2\theta} \\ \sqrt{2(1-\tan^2\theta)} & 0 & \sqrt{2}\tan\theta \end{bmatrix} \tag{2.8}$$

For experimental realisation, an $n \times n$ discrete unitary operator $\hat{U}$ may be decomposed into a product of unitary operators, $T_{j,k}$, coupling only two levels, j and k, at a time [64]. This involves finding matrices $T_{j,k}$ such that

$$T^\dagger_{n-1,n} \cdots T^\dagger_{2,n} \cdots T^\dagger_{2,4} T^\dagger_{2,3} \cdots T^\dagger_{1,n} \cdots T^\dagger_{1,3} T^\dagger_{1,2} \hat{U} = I$$

From which one then deduces that

$$\hat{U} = T_{1,2} T_{1,3} \cdots T_{1,n} \cdots T_{2,3} T_{2,4} \cdots T_{2,n} \cdots T_{n-1,n}.$$

$T^\dagger_{j,k}$ are $n \times n$ unitary matrices which successively transform $\hat{U}$ into a diagonal matrix by reducing the off-diagonal elements to zero, one at a time.

Furthermore, especially when there are many outcomes, this decomposition for a generalised quantum measurement may be optimised to use the minimum number of such pairwise operations [65]. In this case, there is only one extra atomic state, and the reali-

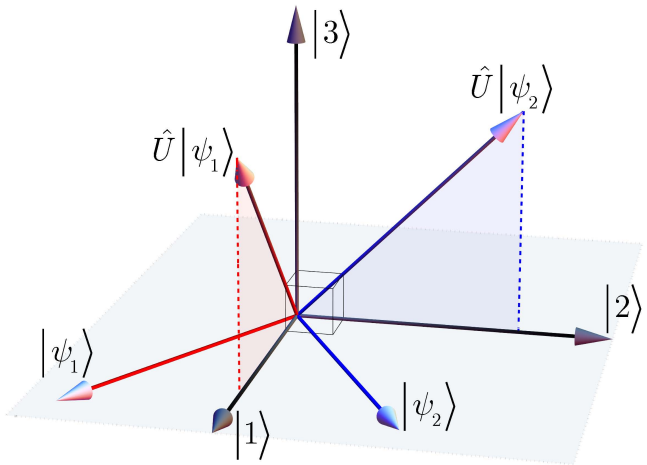

Figure 2.1: Geometrical representation of the IDP measurement. The initial two-dimensional Hilbert space, where $|\psi_1\rangle$ and $|\psi_2\rangle$ live, is spanned by $\{|1\rangle, |2\rangle\}$. This is extended to three dimensions by adding an extra state $|3\rangle$ which is orthogonal to each of the two initial basis states. The measurement consists of a unitary operation $\hat{U}$, followed by a standard projective measurement in the $\{|1\rangle, |2\rangle, |3\rangle\}$ basis. The transformed states $\hat{U}|\psi_1\rangle$ and $\hat{U}|\psi_2\rangle$ are orthogonal to $|2\rangle$ and $|1\rangle$ respectively.

sation is straightforward,

$$\hat{U} = \hat{T}_{1,2}\hat{T}_{1,3}, \tag{2.9}$$

where

$$\hat{T}_{1,2} = \begin{pmatrix} \frac{1}{\sqrt{2}} & -\frac{1}{\sqrt{2}} & 0 \\ \frac{1}{\sqrt{2}} & \frac{1}{\sqrt{2}} & 0 \\ 0 & 0 & 1 \end{pmatrix}, \text{ and} \tag{2.10}$$

$$\hat{T}_{1,3} = \begin{pmatrix} \tan\theta & 0 & -\sqrt{1-\tan^2\theta} \\ 0 & 1 & 0 \\ \sqrt{1-\tan^2\theta} & 0 & \tan\theta \end{pmatrix}. \tag{2.11}$$

In summary, one performs $\hat{T}_{1,3}$, followed by $\hat{T}_{1,2}$ on the input state $|\psi\rangle \in \{|\psi_1\rangle, |\psi_2\rangle\}$ to obtain $|\psi\rangle'$, followed by a projective measurement of $|\psi\rangle'$ in the basis $\{|1\rangle, |2\rangle, |3\rangle\}$. This will yield an error probability of zero and a minimum probability of an inconclusive result $p(?) = \cos 2\theta$. It is useful to note that when realising this measurement, one may choose to use an ancillary qubit instead, i.e. an extra atom, rather than an extra atomic level in one atom. In this case one reassigns the states as $|1\rangle \to |11\rangle$, $|2\rangle \to |12\rangle$, $|3\rangle \to |21\rangle$ and instead of Eqn. 2.6, perform a unitary operation given by

$$\hat{U} = |11\rangle\langle\Pi_1| + |12\rangle\langle\Pi_2| + |21\rangle\langle\Pi_?| + |22\rangle\langle 22| \tag{2.12}$$

before a detection in the computational basis.

2.2.1 Cavity QED implementation

The interaction between an atom and a classical field, resonant or quasi-resonant with the atomic transition between two states $|g\rangle$ and $|e\rangle$, can be used to realise the IDP measurement outlined above. The required unitary operations result from the action of the atom-field Hamiltonian, which is [66]

$$\tilde{H} = \frac{\hbar\Delta_r}{2}\sigma_z - i\hbar\frac{\Omega_r}{2}\left[e^{-i\varphi}\sigma_+ + e^{i\varphi}\sigma_-\right]. \tag{2.13}$$

Here $\sigma_z = |g\rangle\langle g| - |e\rangle\langle e|$ is the Pauli-Z operator, and $\sigma_\pm$, the atomic raising and lowering operators, are defined as $\sigma_+ = |g\rangle\langle e|$ and $\sigma_- = |e\rangle\langle g|$. Ω_r and Δ_r are respectively the classical Rabi frequency and the atom-field detuning, and φ is the phase of the classical field with respect to the atomic transition dipole.

It can be shown from Eq. (2.13) that an interaction lasting for a time $t = \theta/\Omega_r$ with a resonant field having a phase φ effects the transformations

$$\begin{aligned} |g\rangle &\longrightarrow \quad \cos(\theta/2)|g\rangle + \sin(\theta/2)e^{i\varphi}|e\rangle, \\ |e\rangle &\longrightarrow -\sin(\theta/2)e^{-i\varphi}|g\rangle + \cos(\theta/2)|e\rangle. \end{aligned} \tag{2.14}$$

This transformation corresponds to the operation of $R_{g,e}(\theta,\varphi) \equiv \exp(-i\tilde{H}t/\hbar)$, which is a unitary operator coupling only two levels at a time, that is, the states denoted by $|e\rangle$ and $|g\rangle$. If we use the notation $|g\rangle \equiv [1,0]^T$ and $|e\rangle \equiv [0,1]^T$, then $R_{g,e}(\theta,\varphi)$ is given as

$$R_{g,e}(\theta,\varphi) = \begin{pmatrix} \cos\frac{\theta}{2} & -e^{-i\varphi}\sin\frac{\theta}{2} \\ e^{i\varphi}\sin\frac{\theta}{2} & \cos\frac{\theta}{2} \end{pmatrix}. \tag{2.15}$$

Returning to the definition of the basis $\{|1\rangle, |2\rangle, |3\rangle\}$ above, one may perform the unitary operator $\hat{U}$ for the IDP measurement by setting

$$\hat{T}_{1,2} = R_{1,2}(\pi/2, 0) \tag{2.16}$$

$$\hat{T}_{1,3} = R_{1,3}(\vartheta, 0), \tag{2.17}$$

where $\vartheta = \cos^{-1}(\frac{1}{\sqrt{3}})$, and the $R_{g,e}$ is realised using a Ramsey pulse resonant with the transition $|g\rangle \leftrightarrow |e\rangle$.

The physical states representing $|1\rangle$, $|2\rangle$, and $|3\rangle$ could be chosen based on convenience of experimental realisation. In doing this, one may wish to bear in mind, for example, that a direct coupling between $|2\rangle$ and $|3\rangle$ will not be necessary, and that at the detection stage, outcome $|3\rangle$ represents an inconclusive result. A possible choice of states could be a ^{85}Rb ladder of Rydberg states; $|e\rangle \equiv 63P$, $|g\rangle \equiv 61D$ and $|i\rangle \equiv 62P$, which are coupled using standard micromaser transitions [67]. The ladder of circular Rydberg states

with principal quantum numbers $n = 49, 50, 51$ could also be used [61]. A final projective measurement which determines the energy level of the atom would be required. This is commonly done by means of state selective field-ionisation detection [68, 69, 70, 71], which involves passing the Rydberg atoms through an increasing electric field and measuring the energy at which the atom is ionised.

2.3 Measurement demonstrating superadditivity of quantum channel capacity

As mentioned in Section 1.3.2, quantum channels may display superadditivity in classical information capacity [40, 72, 73]. This means that

$$C_n > nC_1, \tag{2.18}$$

where C_1 is the classical information capacity of a single use of the channel, and C_n is the classical information capacity of a combination of n uses of the channel. For classical channels, it holds that

$$C_n = nC_1, \tag{2.19}$$

meaning that superadditivity is a purely quantum effect as it is displayed only by quantum channels. This makes it interesting to experimentally demonstrate the superadditivity of quantum channel capacity. In order to do this, it is necessary to carry out quantum coding followed by an appropriate collective quantum measurement. One possible scheme is outlined below.

2.3.1 Trine letter states

Consider a channel coding for sending classical information through a quantum channel with a given ensemble of quantum states representing the letter states. A clear and simple example of an ensemble which can be used to demonstrate superadditivity in classical capacity of a quantum channel is the qubit trine states. Consider the set of ternary symmetric states of a qubit, that is $\{|\psi_0\rangle, |\psi_1\rangle, |\psi_2\rangle\}$ known as the *qubit trine states*, with

$$\begin{aligned} |\psi_0\rangle &= |0\rangle, \\ |\psi_1\rangle &= -\frac{1}{2}|0\rangle - \frac{\sqrt{3}}{2}|1\rangle, \\ |\psi_2\rangle &= -\frac{1}{2}|0\rangle + \frac{\sqrt{3}}{2}|1\rangle, \end{aligned} \tag{2.20}$$

to transmit information, where $\{|0\rangle, |1\rangle\}$ is the orthonormal basis set. Using one quantum state drawn from this ensemble one can transmit at most $C_1 = 0.6454$ bits. This is achieved by sending any two of the states $|\psi_j\rangle$ with probability 1/2 each and distinguishing between these with the optimal measurement, which, for this specific case, coincides with the minimum-error or Helstrom measurment [39, 56, 74]. The Helstrom measurement is discussed in more detail in Chapter 3.

Using two qubits, there are nine possible states. It has been shown [72] that if only three of these are used, namely

$$\begin{aligned} |\psi_{xx}\rangle &= |\psi_x\rangle \otimes |\psi_x\rangle \\ &= \frac{1}{2}(1+\cos\varphi_x)|00\rangle + \frac{1}{2}\sin\varphi_x\,(|01\rangle + |10\rangle) \\ &\quad + \frac{1}{2}(1-\cos\varphi_x)|11\rangle, \end{aligned} \tag{2.21}$$

with $\varphi_x = 2\pi x/3$, where $x = 0,\ 1,\ 2$, then $I_2 = 1.3690$ bits of information can be retrieved if the code word states are used with equal probabilities. This is larger than $2C_1 (= 1.2908)$. The superadditive quantum coding gain (SQCG), per use of the channel, is

$$(I_2 - 2C_1)/2 = (1.3690 - 1.2908)/2 = 0.0391. \tag{2.22}$$

The measurement used to decode the codewords is the *square-root measurement* with the measurement basis states $\left|\Pi_{yy}\right\rangle$ defined as

$$\left|\Pi_{yy}\right\rangle \equiv \left(\sum_x |\psi_{xx}\rangle\langle\psi_{xx}|\right)^{-1/2} |\psi_{yy}\rangle. \tag{2.23}$$

In explicit form the codeword states are

$$\begin{aligned} |\psi_{00}\rangle &= |00\rangle, \\ |\psi_{11}\rangle &= [|00\rangle + \sqrt{3}\,(|01\rangle + |10\rangle) + 3|00\rangle]/4, \\ |\psi_{22}\rangle &= [|00\rangle - \sqrt{3}\,(|01\rangle + |10\rangle) + 3|00\rangle]/4, \end{aligned} \tag{2.24}$$

and the optimal measurement basis is given by

$$\begin{aligned} |\Pi_{00}\rangle &= \cos(\gamma/2)\,|00\rangle - \sin(\gamma/2)\,|11\rangle, \\ |\Pi_{11}\rangle &= [\sin(\gamma/2)\,|00\rangle + \cos(\gamma/2)\,|11\rangle]/\sqrt{2} + (|01\rangle + |10\rangle)/2, \\ |\Pi_{22}\rangle &= [\sin(\gamma/2)\,|00\rangle + \cos(\gamma/2)\,|11\rangle]/\sqrt{2} - (|01\rangle + |10\rangle)/2, \\ |A\rangle &= [|01\rangle - |10\rangle]]/\sqrt{2}, \end{aligned} \tag{2.25}$$

where

$$\begin{aligned} \cos(\gamma/2) &= (\sqrt{2}+1)/\sqrt{6}, \text{ and} \\ \sin(\gamma/2) &= (\sqrt{2}-1)/\sqrt{6}. \end{aligned} \tag{2.26}$$

The outcome corresponding to the state $|A\rangle$ will never occur, since all codeword states are orthogonal to $|A\rangle$. This state merely completes the 4-dimensional basis.

The states (2.25) define an entangled measurement basis, and the implementation of the measurement will require similar resources as a Bell measurement, including entangling interactions. The Bell states are the maximally entangled states

$$\begin{aligned} |\Phi^{\pm}\rangle &= (|00\rangle \pm |11\rangle)/\sqrt{2} \\ |\Psi^{\pm}\rangle &= (|01\rangle \pm |10\rangle)/\sqrt{2}, \end{aligned} \tag{2.27}$$

and a Bell measurement is a projection in this basis. This can be achieved by first performing a unitary transformation $\hat{U}_B$

$$\hat{U}_B = |00\rangle\langle\Psi^+| + |01\rangle\langle\Phi^+| + |10\rangle\langle\Psi^-| + |11\rangle\langle\Phi^-| \tag{2.28}$$

on the input Bell state, followed by a projective measurement in the $\{|00\rangle, |01\rangle, |10\rangle, |11\rangle\}$ basis, which is referred to here as the computational basis. Any other transformation which takes each of the Bell states respectively to any permutation of the computational basis states, up to global phases, would also do.

The superadditive measurement can be realised in a similar fashion by making a unitary transformation $\hat{U}_{\text{sa}}$ on the input states, and following this by a projective measurement in the computational basis. From Eq. (2.25), $\hat{U}_{\text{sa}}$ is given as

$$\hat{U}_{\text{sa}} = |00\rangle\langle\Pi_{00}| + |01\rangle\langle\Pi_{11}| + |10\rangle\langle A| + |11\rangle\langle\Pi_{22}|. \tag{2.29}$$

In matrix notation, it takes the form

$$\hat{U}_{\text{sa}} = \frac{1}{2}\begin{bmatrix} 2\cos(\gamma/2) & 0 & 0 & -2\sin(\gamma/2) \\ \sqrt{2}\sin(\gamma/2) & 1 & 1 & \sqrt{2}\cos(\gamma/2) \\ 0 & \sqrt{2} & -\sqrt{2} & 0 \\ \sqrt{2}\sin(\gamma/2) & -1 & -1 & \sqrt{2}\cos(\gamma/2) \end{bmatrix}. \tag{2.30}$$

Superadditivity can in general only be achieved when an appropriate *collective* POM is chosen, namely, detection in an entangled measurement basis [39]. An SQCG of 0.011 ± 0.003 has been experimentally demonstrated by the previously mentioned optical implementation which uses polarisation and path to encode two qubits [40].

2.3.2 Cavity QED realisation

The unitary operation $\hat{U}_{\text{sa}}$ needed to realise this measurement can be decomposed in terms of single atom operation and entangling interactions. The single atom rotations correspond to Ramsey pulses $\hat{R}_1(\theta,\varphi)$ and $\hat{R}_2(\theta,\varphi)$. In the four-dimensional Hilbert space spanned by the joint basis states of the two 2-level atoms, the unitary transformation $\hat{R}_1(\theta,\varphi)$ effected by a Ramsey pulse on atom 1 is

$$\hat{R}_1(\theta,\varphi) = \hat{R}(\theta,\varphi)\otimes\hat{I}, \tag{2.31}$$

while a Ramsey pulse on atom 2 is

$$\hat{R}_2(\theta,\varphi) = \hat{I}\otimes\hat{R}(\theta,\varphi), \tag{2.32}$$

where $\otimes$ denotes the tensor product operation.

The entangling operations, on the other hand, can be realised using the interactions between atoms and a cavity field governed by the two-atom Tavis-Cummings Hamiltonian in the limit of large detuning [75, 76]. This produces an effective Hamiltonian in which the field is removed as a degree of freedom, eliminating atom-field entanglement, but allowing interactions between the two atoms through virtual excitation of the field. This ensures that no quantum information is exchanged between the atoms and the cavity, so that the cavity merely mediates interactions between the atoms. Each atom is effectively a two-state system, detuned from the cavity resonance by Δ. Let g denote the atom-cavity dipole coupling constant. In the limit of large Δ, the effective Hamiltonian is

$$\widetilde{H}_{\text{eff}} = -\frac{\hbar g^2}{\Delta}\left(\sigma_{eg,eg}+\sigma_{ge,ge}+\sigma_{eg,ge}+\sigma_{ge,eg}\right). \tag{2.33}$$

This corresponds to a unitary transformation

$$\hat{T}_{\text{TC}}(t) = \begin{bmatrix} 1 & 0 & 0 & 0 \\ 0 & e^{-it\phi}\cos(t\phi) & -ie^{-it\phi}\sin(t\phi) & 0 \\ 0 & -ie^{-it\phi}\sin(t\phi) & e^{-it\phi}\cos(t\phi) & 0 \\ 0 & 0 & 0 & 1 \end{bmatrix}, \tag{2.34}$$

where $\phi = g^2/\Delta(s^{-1})$ is the effective coupling constant and $|00\rangle \equiv |gg\rangle \equiv [1,0,0,0]^T$, $|01\rangle \equiv |ge\rangle \equiv [0,1,0,0]^T$, $|10\rangle \equiv |eg\rangle \equiv [0,0,1,0]^T$ and $|11\rangle \equiv |ee\rangle \equiv [0,0,0,1]^T$ denote the computational basis states.

To elucidate the process of deriving the superadditive measurement using these building blocks, it is instructive to first consider the Bell measurement briefly. The Bell measurement can be performed with a combination of the operations in Eqs. (2.31), (2.32)

and (2.34). This will yield a transformation which rotates each of the Bell states, into some permutation of the computational basis states up to global phases.

This can be done in only four steps. The principle of the process is to take the entangled states to states that are as close as possible to the separable basis states with each step. The Tavis-Cummings operations are the available two-qubit operations for disentangling the Bell states. However, it turns out that the detuned Tavis-Cummings operation on its own cannot disentangle $|\Psi^{\pm}\rangle$. It is necessary to precede it with a Ramsey rotation which produces a relative phase shift of $\pi/2$ between $|01\rangle$ and $|10\rangle$. In previous work [66, 75], the phase shifting effect has been achieved using an extra atomic level $|i\rangle$. This is done by performing a Ramsey operation resonant with the $|e\rangle \leftrightarrow |i\rangle$ transition, before, and then after the Tavis-Cummings operation. Another proposal suggests introducing a slight delay between the passage of the two atoms through the cavity [77].

The approach used here is different. As a first step, it involves applying a Ramsey pulse to the atom 2, i.e., $\hat{U}_1 = \hat{R}_2\left(\pi, \frac{3\pi}{4}\right)$. This gives the following transformation of the Bell states:

$$\begin{aligned} \hat{U}_1|\Phi^{\pm}\rangle &= (|01\rangle \pm i|10\rangle)/\sqrt{2} \\ \hat{U}_1|\Psi^{\pm}\rangle &= (|00\rangle \pm i|11\rangle)/\sqrt{2}. \end{aligned} \tag{2.35}$$

The second step is the operation $\hat{U}_2 = \hat{T}_{\mathrm{TC}}(\frac{3\pi}{4\phi})$ to have

$$\begin{aligned} \hat{U}_2\hat{U}_1|\Psi^{+}\rangle &= (|00\rangle - i|11\rangle)/\sqrt{2} \\ \hat{U}_2\hat{U}_1|\Phi^{+}\rangle &= |01\rangle \\ \hat{U}_2\hat{U}_1|\Phi^{-}\rangle &= |10\rangle \\ \hat{U}_2\hat{U}_1|\Psi^{-}\rangle &= (|00\rangle + i|11\rangle)\sqrt{2}. \end{aligned} \tag{2.36}$$

The combination of a preceding Ramsey operation on atom 2 and the detuned Tavis-Cummings operation effectively carries out a transformation which disentangles the $|\Psi^{+}\rangle$ and $|\Phi^{-}\rangle$ states.

The third step is a Ramsey operation $\hat{U}_3 = \hat{R}_2(\pi, 0)$. The effect of this operation is simply to interchange $|00\rangle$ with $|01\rangle$, and $|11\rangle$ with $|10\rangle$ simultaneously. We have

$$\begin{aligned} \hat{U}_3\hat{U}_2\hat{U}_1|\Psi^{+}\rangle &= (|01\rangle - i|10\rangle)/\sqrt{2} \\ \hat{U}_3\hat{U}_2\hat{U}_1|\Phi^{+}\rangle &= |00\rangle \\ \hat{U}_3\hat{U}_2\hat{U}_1|\Phi^{-}\rangle &= |11\rangle \\ \hat{U}_3\hat{U}_2\hat{U}_1|\Psi^{-}\rangle &= (|01\rangle + i|10\rangle)\sqrt{2}. \end{aligned} \tag{2.37}$$

The resulting entangled states can now be disentangled with a Tavis-Cummings operation

in a final step before detection. Using $\hat{U}_4 = \hat{T}_d(\frac{3\pi}{4\phi})$ will then give:

$$\begin{aligned}
\hat{U}_4\hat{U}_3\hat{U}_2\hat{U}_1|\Psi^+\rangle &= |01\rangle \\
\hat{U}_4\hat{U}_3\hat{U}_2\hat{U}_1|\Phi^+\rangle &= |00\rangle \\
\hat{U}_4\hat{U}_3\hat{U}_2\hat{U}_1|\Phi^-\rangle &= |11\rangle \\
\hat{U}_4\hat{U}_3\hat{U}_2\hat{U}_1|\Psi^-\rangle &= |10\rangle. \qquad (2.38)
\end{aligned}$$

Detection results $|00\rangle$, $|01\rangle$, $|10\rangle$ and $|11\rangle$ would now indicate that the inputs were the Bell states $|\Psi^+\rangle$, $|\Phi^+\rangle$, $|\Psi^-\rangle$ and $|\Phi^-\rangle$ respectively. This realisation is similar in its construction to the realisation on atoms considered in [78].

A similar method is applicable for the superadditive measurement. It is worth noting that since the outcome corresponding to $|A\rangle$ should never occur, it would be sufficient to make a unitary transformation $\hat{U}'_{\rm sa}$ which takes two of the three states $|\Pi_{00}\rangle$, $|\Pi_{11}\rangle$ and $|\Pi_{22}\rangle$ uniquely into two of the four computational basis states in the four-dimensional Hilbert space, say $|\Pi_{22}\rangle \rightarrow |01\rangle$ and $|\Pi_{11}\rangle \rightarrow |11\rangle$; and the remaining measurement basis state, say $|\Pi_{00}\rangle$, and $|A\rangle$ each into superpositions of the two other computational basis states, say $|00\rangle$ and $|10\rangle$. This is used here as it may reduce the number of steps in the experimental realisation.

Obtaining a realisation of $\hat{U}_{\rm sa}$ involves finding a sequence of operations which transforms $\hat{U}^\dagger_{\rm sa}$ into a matrix of the form $P_\pi D$, where P_π is a permutation matrix and D is a diagonal matrix. This could be a sequence of unitary operations coupling two basis states at a time [64]. As with most physical setups, not all pairwise coupling operations are available in the cavity-QED setup under consideration. This is because of the restriction to operations $\hat{T}_{\rm TC}(t)$, which couple the pair of basis states $|01\rangle$ and $|10\rangle$, and single qubit operations $\hat{R}_1(\theta,\varphi)$ and $\hat{R}_2(\theta,\varphi)$, which each couple two pairs of basis states at the same time. The strategy for obtaining a realisation in terms of these is as follows. Since the operation $\hat{T}_{\rm TC}$ couples basis states $|01\rangle$ and $|10\rangle$, it is natural to first use a Tavis-Cummings interaction to disentangle these components of the measurement states in Eq. (2.25). In order to do this, it turns out that one needs to precede the Tavis-Cummings interaction by two Ramsey pulses as with the Bell measurement explained above. This first pulse sequence then takes the states $|A\rangle(=|\Psi^-\rangle)$ and $|\Psi^+\rangle$ into the disentangled states $|A'\rangle = |01\rangle$ and $|10\rangle$. Next, in order to use a Tavis-Cummings interaction to disentangle the $|00\rangle$ and $|11\rangle$ components, one needs to first swap the states $|0\rangle$ and $|1\rangle$ for any one of the atoms using Ramsey pulses. It turns out that at the end of this process, which thus comprises two Tavis-Cummings interactions and a number of Ramsey pulses, $|A\rangle$ and the measurement basis state $|\Pi_{00}\rangle$ are both mapped to superpositions of $|00\rangle$ and $|10\rangle$, and Ramsey pulses would be needed in order to map these superpositions to $|00\rangle$ and $|10\rangle$. As remarked above, these last Ramsey rotations are not necessarily required.

This leads to a realisation in seven steps. The first step is a Ramsey rotation on the atom 2, $\hat{U}_1' = \hat{R}_2(\pi,\pi)$. The second step is another Ramsey rotation on atom 2, $\hat{U}_2' = \hat{R}_2(\pi,3\pi/4)$. The third step involves passing the two atoms simultaneously through the first detuned cavity with the effective interaction time $t_1 = 3\pi/(4\phi)$ giving a detuned Tavis-Cummings interaction described by $\hat{U}_3' = \hat{T}_{\mathrm{TC}}(t_1)$. Step four is another Ramsey pulse applied to atom 2 defined as $\hat{U}_4' = \hat{R}_2(\pi,\pi/2)$. The fifth step is a second detuned Tavis-Cummings type interaction, $\hat{U}_5' = \hat{T}_d(t_2)$ with duration $t_2 = \frac{\gamma}{2\phi}$. The sixth and seventh steps effectively rotate $|A'\rangle$ into a superposition. This is achieved using $\hat{U}_6' = \hat{R}_2(\pi,(\gamma-\pi/2)/4)$ as the sixth step and $\hat{U}_7' = \hat{R}_2(\pi/2,0)$ as the seventh step.

These steps lead to the effective unitary operation

$$\hat{U}_{\mathrm{sa}}' = \frac{e^{-i\gamma/4}}{2}\begin{bmatrix} -e^{-i\gamma/2}C & -e^{i\gamma/2} & e^{i\gamma/2} & e^{-i\gamma/2}S \\ -e^{-i\gamma/2}C & e^{i\gamma/2} & -e^{i\gamma/2} & e^{-i\gamma/2}S \\ -S & 1 & 1 & -C \\ S & 1 & 1 & C \end{bmatrix}, \tag{2.39}$$

where $S = \sqrt{2}\sin(\gamma/2)$ and $C = \sqrt{2}\cos(\gamma/2)$. To clarify the assignment of measurement results, consider the alternative form

$$\begin{aligned} \hat{U}_{\mathrm{sa}}' \equiv \; & \tfrac{1}{\sqrt{2}}(|00\rangle + |10\rangle)\langle\Pi_{00}| + \tfrac{1}{\sqrt{2}}(|00\rangle - |10\rangle)\langle A| \\ & + |01\rangle\langle\Pi_{22}| + |11\rangle\langle\Pi_{11}|. \end{aligned} \tag{2.40}$$

This makes it clear that $\hat{U}_{\mathrm{sa}}'$ ideally yields the same value as $\hat{U}_{\mathrm{sa}}$ for the mutual information, but is slightly different from $\hat{U}_{\mathrm{sa}}$, since final detection in either $|00\rangle$ or $|10\rangle$ correspond to $|\Pi_{00}\rangle$. Recall that all three signal states are orthogonal to $|A\rangle$. When $\hat{U}_{\mathrm{sa}}$ is used, the final measurement outcome corresponding to $|A\rangle$ should never occur. When experimental imperfections are included, the mutual information and consequently SQCG may be different for $\hat{U}_{\mathrm{sa}}$ and $\hat{U}_{\mathrm{sa}}'$. This will be made clear shortly.

After performing the seven steps, a subsequent detection in the computational basis will complete the measurement. The mutual information is given by (see Equations 1.38–1.42)

$$\begin{aligned} I_2 &= I(X:Y) \\ &= \sum_j P(x_j)\sum_k P(y_k|x_j)\log_2\left[\frac{P(y_k|x_j)}{\sum_m P(x_m)P(y_k|x_m)}\right], \end{aligned} \tag{2.41}$$

where X and Y denote the sender and receiver respectively, and x_j and y_k denote the signal states that were transmitted and received respectively, $k, j, m = 1, 2, 3, \ldots$.

The channel matrix resulting from applying the derived pulse sequence and a subse-

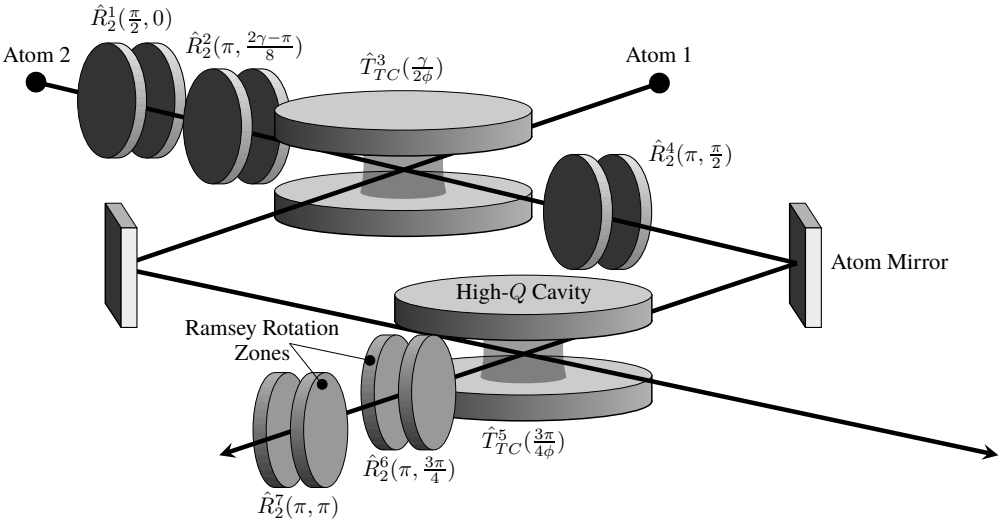

Figure 2.2: Schematic diagram of proposed cavity QED implementation of the POM for superadditive decoding. This figure shows the scheme for the unitary operation performed before the final projective measurement by field-ionisation detectors. Atom mirrors have been implemented using electric, magnetic and light-induced forces (see [79], [80] and references therein). If required, it could be realised in this scheme also by using an additional Tavis-Cummings operation to swap the state from one atom to that of a fresh one traveling perpendicularly. The superscripts on the operators indicate the order of their application to the two atom state. These operations are defined in Equations (2.31), (2.32), and (2.34).

quent projective measurement to the input state $\hat{\rho}_x = |\psi_x\rangle\langle\psi_x|$ are

$$P(y|x) = \mathrm{Tr}(\hat{\Pi}'_y \hat{\rho}_x), \tag{2.42}$$

where $\hat{\Pi}'_y = |\Pi'_{yy}\rangle\langle\Pi'_{yy}|$. Substituting the resulting channel matrix elements into Eq. (1.42), and using prior probabilities

$$p\left(x_j\right) = \frac{1}{3}, \quad (j = 1,2,3) \tag{2.43}$$

gives SQCG of $I_2/2 - C_1 = 0.0391$. A schematic diagram outlining the derived implementation is shown in Fig. 2.2.

2.3.3 Optimality

The question of determining the optimality of a given realisation of a POM using certain building blocks in a physical setting is non-trivial. For the superadditive measurement, the optimality of the proposed realisation can be checked simply in terms of the total number of steps, excluding the more experimentally challenging steps as much as possible. The Tavis-Cummings interaction is clearly more difficult to realise than the single-atom Ramsey operations because it involves a synchronous passage of two atoms through a high-Q

cavity.

Below is a short proof by contradiction that at least two detuned Tavis-Cummings interactions is required to realise the superadditive decoding. The canonical Cartan decomposition of a two-qubit unitary operator $\mathrm{U} \in \mathrm{SU}(4)$ [81] shows that if a single detuned Tavis-Cummings interaction could be used to implement $\hat{U}_{\mathrm{sa}}$ (or $\hat{U}'_{\mathrm{sa}}$), then there would exist w'_1, w_2, v'_1, v_2, W'_1, W_2, V'_1, and $V_2 \in \mathrm{SU}(2)$ such that

$$\hat{U}_{\mathrm{sa}} = (w'_1 \otimes w_2) T_d(\phi) (v'_1 \otimes v_2) \tag{2.44}$$

and

$$T_d(\phi) = (W'_1 \otimes W_2) \hat{U}_{\mathrm{sa}} (V'_1 \otimes V_2). \tag{2.45}$$

Equation (2.45) is a system of 16 equations. It is easily verified that this system of equations has no solution. This concludes the proof and gives evidence of the optimality of our proposed scheme with respect to the number of Tavis-Cummings interactions needed. Jaynes-Cummings interactions through sequential passage of the atoms through the cavity can also be used for entangling interactions between atoms. This has proved suitable for preparing specific entangled two-atom states [58, 75, 77]. However, a main disadvantage of using the Jaynes-Cummings interactions is the possibility of leakage of atomic excitation into cavity field modes having more than one excitation, since the field has an infinite number of levels besides $\{|0\rangle, |1\rangle\}$.

2.4 Experimental imperfections

Both the IDP measurement and the measurement to demonstrate quantum superadditivity will be affected by experimental imperfections. In particular, when errors are present, error-free or unambiguous state discrimination in general becomes impossible, and one should aim for a maximum confidence measurement strategy instead [82, 83, 84]. As for the measurement that demonstrates superadditivity, it is natural to ask how robust the superadditive quantum coding gain is with respect to imperfections. This is considered next.

Experimental imperfections that could adversely affect the overall quality of the realisations of the superadditive measurement, and the SQCG, include initial state preparation fidelity, Ramsey operation fidelity, Tavis-Cummings operation fidelity and detection errors. The initial state preparation fidelity would depend largely on the fidelity of the Ramsey operations since they are used to carry out these preparations. In turn, the fidelity of the Ramsey operations depend on the accuracy to which the parameters θ and φ can be set.

Let us consider how the delay between the atoms affect the results and ultimately the

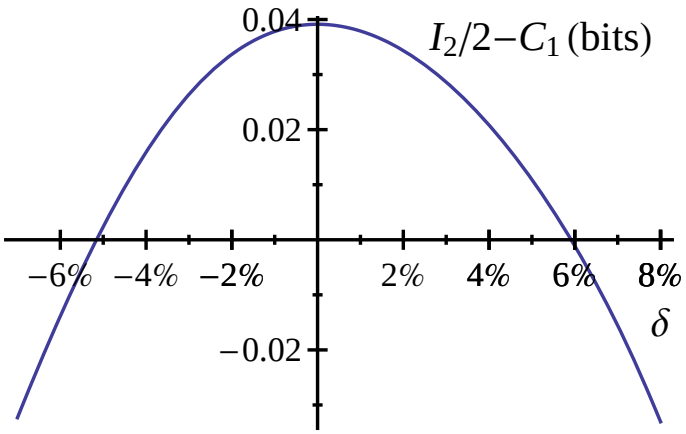

Figure 2.3: Plot of the superadditive coding gain as a function of δ, where δ is the delay $t_d(s)$ as a percentage of the time t_2 (s) spent by both atoms in the second cavity. The same delay is applied in both cavities.

SQCG. Zheng and Guo [75] have estimated the effect of such a delay on the preparation of an EPR pair of the form

$$|\Psi_{EPR}\rangle = \frac{1}{\sqrt{2}}\left(|e,g\rangle + i|g,e\rangle\right), \tag{2.46}$$

which can be prepared by a single Tavis-Cummings operation. This was done by considering a delay of $t_d = 0.01t$ between the atoms, where t is the time each atom spends in the cavity. In this situation, a fidelity of 0.99 was estimated.

Applying this same idea, the time spent in the cavity by the two atoms is then no longer t but $t - t_d$. Such a delay yields an imperfect Tavis-Cummings operation which affects the coding gain. Fig. 2.3 shows the superadditive coding gain as a function of δ, where δ is the delay as a percentage of the longest cavity interaction time in the sequence, that is, t_2 (s) spent in cavity 2. A delay up to 5% of the longest cavity interaction time in the sequence, which occurs in the second cavity interaction, still gives an SQCG of 0.011 bits.

In the photonic realisation [56], the detection efficiency η, which is the photon count probability, does not degrade the result on its own. This is because the SQCG is calculated using a normalised channel matrix. However, when combined with dark counts which arise from background radiation as well as from carriers generated in a detector even when no photons are incident, the SQCG is degraded since this effectively results in a finite probability of misidentification of states.

In a cavity QED realisation, the detection efficiency could be even more problematic if it depends on the atomic states, for example. Even if the detection efficiency were independent of the atomic state, state misidentification is a usual problem in detection. Consider a detection to determine whether a two level atom is in a state $|0\rangle$ or $|1\rangle$. In the

perfect case, the detection would be an ideal von Neumann measurement which can be described by the two projectors

$$\hat{P}_0 = |0\rangle\langle 0|, \;\; \hat{P}_1 = |1\rangle\langle 1|. \tag{2.47}$$

A non-ideal detector, however, might record the wrong state with some probability. This is the case in atomic state detection schemes where projective measurements are carried out using field-ionisation detectors, in which the ionisation energy of the atoms serves as an indicator of the state. This means that for a two-level atom in the state $|0\rangle$, the measurement will give the result 1 with probability p and the result 0 with probability $1-p$. In a realistic experimental scenario, the probability of misidentification might not be symmetric. For instance, it might be more likely to misidentify the atomic state $|1\rangle$ as $|0\rangle$ than conversely. Let us denote the probability of misidentifying the $|0\rangle$ and $|1\rangle$ states as $p(0|1) \equiv p$ and $p(1|0) \equiv q$ respectively. Introducing these errors, the effective measurement is a POM with elements defined as the operators

$$\begin{aligned} \hat{\pi}_0 &= (1-p)\hat{P}_0 + q\hat{P}_1 \\ \hat{\pi}_1 &= (1-q)\hat{P}_1 + p\hat{P}_0. \end{aligned} \tag{2.48}$$

This is incorporated into the calculations of the SQCG by first calculating the resulting single channel capacity C_1 and then the mutual information for length-two coding I_2. The resulting C_1 is calculated using Eq. (2.41), where the channel matrix corresponding to the single channel case is used. From this, the SQCG is obtained and plotted in Fig. 2.4 as a function of the probabilities of misidentification p and q when $\hat{U}_{\rm sa}$ is realised exactly. The affected channel matrix is given as

$$P(y|x) = \mathrm{Tr}(\hat{U}_{\rm sa}\hat{\rho}_x\hat{U}_{\rm sa}^{\dagger}\hat{M}_y). \tag{2.49}$$

Here, x and y label the matrix elements. $\hat{M}_1 = \hat{\pi}_0 \otimes \hat{\pi}_0$, $\hat{M}_2 = \hat{\pi}_0 \otimes \hat{\pi}_1$, $\hat{M}_3 = \hat{\pi}_1 \otimes \hat{\pi}_0$, and $\hat{M}_4 = \hat{\pi}_1 \otimes \hat{\pi}_1$ are the elements of the POM describing the imperfect projective measurement in the computational basis. The resulting SQCG plot shows that, even with rather high probabilities of misidentification, a reasonable amount of superadditive quantum coding gain can still be accessed. Fig. 2.4 also indicates a symmetric trade-off effect between probabilities p and q.

Let us now use the proposed realisation which effects the unitary transformation $\hat{U}'_{\rm sa}$. In this case, the channel matrix elements then become

$$P(y|x) = \mathrm{Tr}(\hat{U}'_{\rm sa}\hat{\rho}_x\hat{U}'^{\dagger}_{\rm sa}\hat{M}_y). \tag{2.50}$$

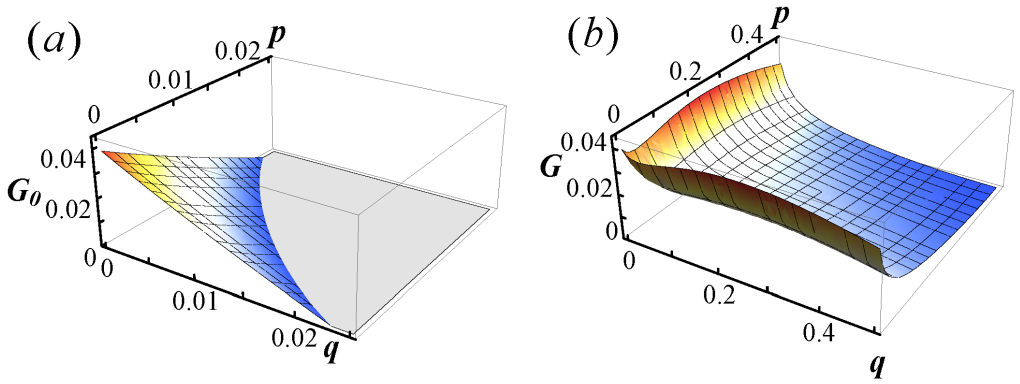

Figure 2.4: Effects of detection errors when $\hat{U}_{\rm sa}$ is used to realise the superadditive measurement. (a) Plot of the difference G_0 (bits) between the length-two coding mutual information and the ideal single channel capacity, $G_0 = I_2/2(p,q) - C_1(p=0,q=0)$. (b) Plot of the actual superadditive coding gain G_0 (bits), $G = I_2/2(p,q) - C_1(p,q)$. G_0 and G are plotted as functions of the probabilities, p and q, of misidentifying states $|0\rangle$ and $|1\rangle$ of a two-level atom respectively.

The corresponding values of mutual information for the double channel and the SQCG are plotted in Fig. 2.5 as functions of the probabilities of misidentification p and q. As shown in Fig. 2.5(b), reasonable amounts of SQCG can be seen even with rather high levels of detection errors. Since, in the proposed scheme $\hat{U}'_{\rm sa}$, the SQCG favors combinations of higher values of p with lower values q, the physical states representing $|0\rangle$ and $|1\rangle$ may need to be chosen to ensure that $p > q$ if there is considerable difference between p and q. Values for the probabilities of state misidentification p (and/or q) of as low as 0.013, for selective detection of some adjacent Rydberg states, have been reported [85]. For a given pair of adjacent Rydberg states, it is also noted that these error probabilities can be considerably lowered at the expense of the overall detection efficiency, since the misidentification probabilities are the crucial factors in this scheme.

Finally, it is important to consider feasibility in terms of lifetimes of the atomic states and cavity decay. The earlier mentioned circular Rydberg states, with principal quantum numbers $n = 50, 51$ have radiative lifetimes of $T_r \simeq 30$ ms, and coupling constant $g = 2\pi \times 24$ kHz. Using an estimated detuning of $10g$, the atom-atom interaction time will be on the order of $10\pi/g \simeq 0.2$ ms [61]. The time for the entire sequence of operations is on the order of 2 ms, which is a lot less than T_r. It is also worth noting that whilst in the detuned cavities, the Purcell effect [86] is suppressed and hence the spontaneous emission rate is further reduced, leading to longer lifetimes. Cavity decay times of up to 130 ms have been achieved [87], allowing for interactions to take place long before the dissipative processes due to the cavity begin to set in. Moreover, since only virtual excitations of the cavity are to be used in the proposed scheme described here, the effect of cavity decay is reduced much further. With all these taken into consideration, the proposed scheme is realisable within the lifetime of available Rydberg states using current or shortly available

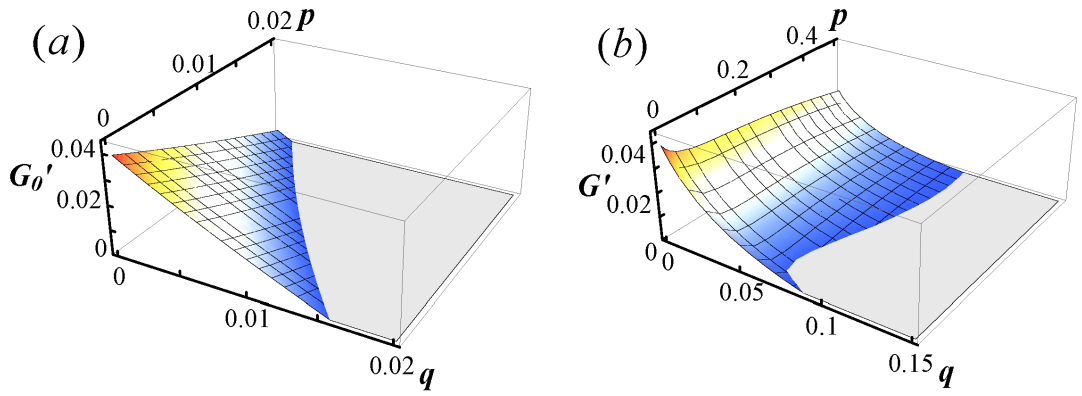

Figure 2.5: Effects of detection errors when $\hat{U}'_{\rm sa}$ is used to implement the superadditive measurement. (a) Plot of the difference G'_0(bits) between the length-two coding mutual information and the ideal single channel capacity, $G'_0 = I'_2/2(p,q) - C_1(p=0,q=0)$. (b) Plot of the actual superadditive coding gain G' (bits) for our proposed scheme, where $G' = I'_2/2(p,q) - C_1(p,q)$. G'_0 and G' are plotted as functions of the probabilities, p and q, of misidentifying states $|0\rangle$ and $|1\rangle$ of a two-level atom respectively.

technologies.

2.5 Conclusion

In conclusion, explicit cavity-QED schemes for experimental realisation of two generalised quantum measurement strategies have been proposed and explained in this chapter. These were unambiguous discrimination of two non-orthogonal quantum states, the so-called IDP measurement, and the measurement to demonstrate superadditive quantum coding using a ternary quantum alphabet. Realisations of the minimum-error measurements to distinguish between the trine states in Eq. (2.20) [41] and between mirror-symmetric states [88] would require analysis similar to the IDP measurement outlined here. Also, similar methods can be used to implement any generalised quantum measurement using cavity QED.

The results above show that these realisations are feasible using current or shortly available cavity QED technologies. A simple proof confirmed the optimality of the realisation of the measurement that demonstrates quantum superadditivity in terms of cavity usage. The superadditive quantum coding gain is affected by imperfect detection of the basis states, and even with rather high levels of such experimental imperfections, a reasonable amount of superadditivity can be seen. These results do not address the fact that in the presence of experimental imperfections, the measurement that one should attempt to implement in order to demonstrate maximum coding gain might change. It is thus conceivable that even with experimental errors, it may be possible to see a somewhat larger quantum coding gain than indicated in the results above. In other words, these estimates

are lower bounds on the superadditive quantum coding gain, given the assumed level of errors in the implementation. An example where the optimal quantum measurement changes in the presence of experimental imperfections is when comparing two coherent states [89].

The fact that atoms can interact strongly via cavity fields makes it possible to experimentally investigate the implementation of superadditive coding with longer code words using cavity QED-type systems. It is also interesting to further study realisations of other generalised quantum measurements which are difficult to realise using linear optics. The next chapter considers the implementations of optimal quantum measurements using nuclear spins associated with a nitrogen-vacancy centre in diamond.

CHAPTER 3

Optimal quantum measurements of a single ^{14}N nuclear spin

3.1 Introduction

An important non-trivial quantum information processing task, which until now has only been realised optically, is optimal unambiguous discrimination between two non-orthogonal quantum states, otherwise known as the Ivanovic-Dieks-Peres (IDP) measurement [43, 44, 45]. This chapter presents and compares experimental realisations of optimal quantum measurements for distinguishing between two non-orthogonal quantum states encoded in a single ^{14}N nuclear spin at a nitrogen-vacancy defect in diamond. This is the first time these measurements on a quantum system are realised in the solid state. The main contributions focused on in this chapter are the derivation of the explicit form of the experimental implementations (such as the pulses needed etc.), and the analysis of the experimental results and errors. Nitrogen-vacancy (NV) centers in diamond are very attractive for quantum information processing (QIP), since their associated spins have been shown to have long-lived quantum coherence at room temperature [13, 14]. The measurement schemes implemented include optimal unambiguous state discrimination (known as IDP) measurement, unambiguous state discrimination using a standard projective measurement, and minimum-error measurement (known as Helstrom measurement). The realisation of the last two measurements allows a benchmarking of the IDP measurement against standard projective measurements and to demonstrate the advantage of the generalised measurement over the best standard projective measurement for unambiguous discrimination in this system. Measurement efficiencies are found to be above 80% for all schemes and reach a value of 90% for the IDP measurement.

As discussed in Chapter 2, it is sometimes advantageous to perform a quantum measurement that, by design, is not a standard projective measurement. This is the case when distinguishing between non-orthogonal quantum states, for instance. This is not possible to achieve perfectly with certainty. Nevertheless, one can for example minimise the error [41], or measure in such a way that when a result is obtained it is guaranteed to be correct. This can be achieved at the expense of sometimes obtaining an inconclusive result, and such a measurement is referred to as unambiguous [90].

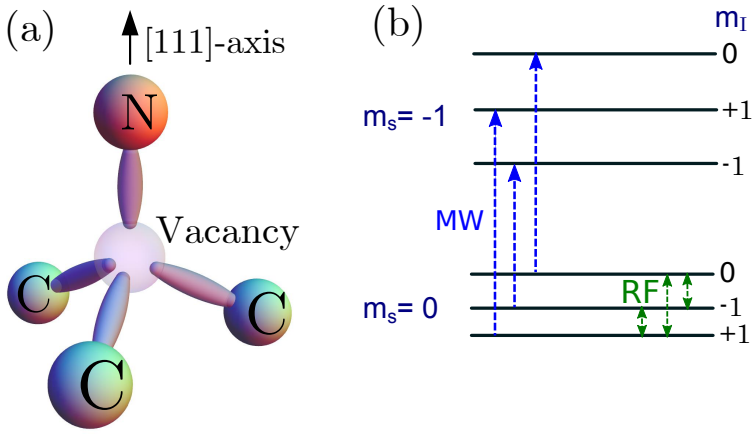

Figure 3.1: (a) Atomic structure of the nitrogen-vacancy defect in diamond. It consists of a substitutional nitrogen atom and a neighbouring vacancy in the diamond carbon lattice. (b) Energy-level scheme of the electron spin $m_S = 0, -1$ states showing the hyperfine structure in a magnetic field. MW pulses selectively map the nuclear spin state onto the electronic spin state which are then read out optically.

For a given task, the optimal quantum measurement will not necessarily be a standard projective measurement, but rather a generalised measurement. For example, while the minimum-error measurement when distinguishing between two equiprobable nonorthogonal states is a projective measurement known as the Helstrom measurement, the optimal unambiguous state discrimination (USD) measurement is a generalised measurement known as the Ivanovic-Dieks-Peres (IDP) measurement [43, 44, 45].

This type of measurement is relevant for important quantum information tasks in quantum cryptography [48, 91] and in entanglement swapping protocols [92]. Moreover, it can be useful for quantum communication, when the two signal states are nonorthogonal after passing through a channel. Yet, while it has been implemented optically [50, 93], an implementation in solid state has been lacking until now. In order to perform advanced QIP tasks, the ability to perform such optimal (i.e. possibly generalised) quantum measurements is a basic requirement.

3.2 Experimental realisation

The experiments reported in this chapter are carried out on the ^{14}N nuclear spin (spin $I = 1$) of a negatively charged nitrogen-vacancy (NV^-) defect in diamond and utilise a quantum non-demolition (QND) single-shot readout method [94] to measure the spin states. The structure of the NV^- defect is shown in Figure 3.1 (a). It consists of a substitutional nitrogen atom and a neighbouring vacancy site inside the diamond lattice. It has an electron spin triplet ground state, that can be prepared and read out by laser illumination. The hyperfine structure of the ^{14}N nuclear spin is shown in Figure 3.1 (b).

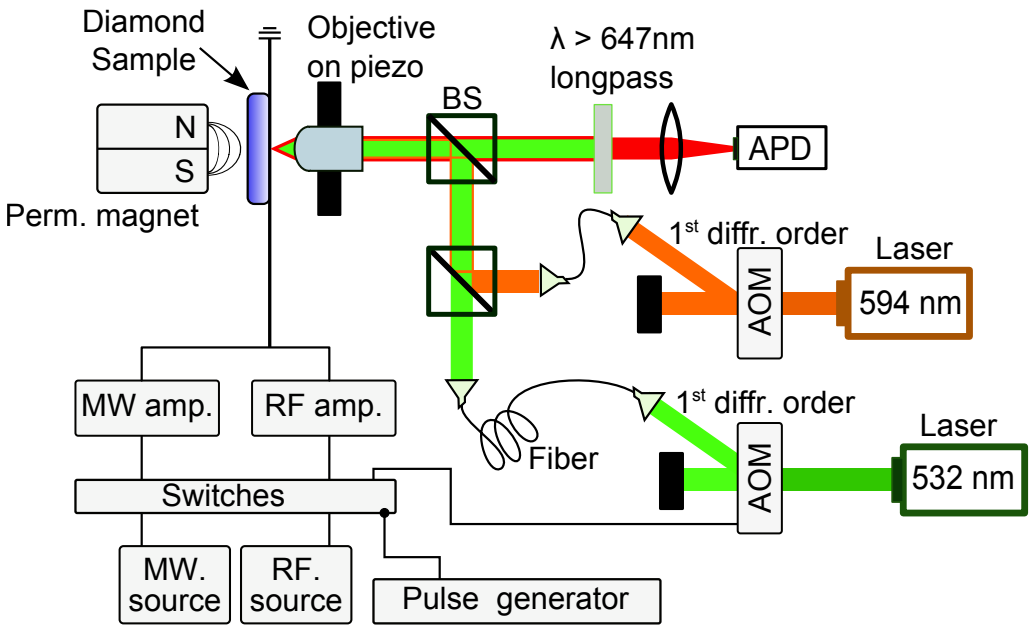

Figure 3.2: Experimental setup for quantum measurements on ^{14}N nuclear spin associated with an NV$^-$ centre on diamond. The charge state post-selection is carried out using the 594 nm orange laser. RF pulses rotate the nuclear spin, which are then coupled to the electronic spin states using MW pulses. These are in turn read out by means of fluorescence measurements using the green laser. The readout process destroys the electronic spin states but the nuclear spin states are kept robust by means of a strong magnetic field.

Microwave (MW) pulses can be used to repetitively map the nuclear spin state onto the electron spin, which can then be optically measured, allowing quantum non-demolition (QND) single-shot readout of the nuclear spin state. These additional features make it a promising system for QIP [14, 94, 95, 96, 97, 98]. A schematic diagram of the experimental setup is shown in Fig. 3.2. A confocal microscope objective which was mounted on a piezoelectric nanometer scale scanner was used to optically address individual NV centers.

To summarise, the quantum non-demolition measurement of the nuclear spin state is as follows. The MW pulses selectively map the nuclear spin state onto the electronic spin states (see Fig. 3.1). The specific MW pulse chosen is determined by the nuclear spin state to be projected onto to ensure that the NV is taken to the $m_S = -1$ state only when the nuclear spin is in the probed state, and otherwise it remains in $m_S = 0$. The (532 nm) green light takes the NV$^-$ to an excited state while a high magnetic field ($B \simeq 0.64T$) maintains the nuclear spin polarisation. From this excited state, there are two different decay paths depending on the electronic spin state. For $m_S = 0$, there will be predominantly radiative decay into the $m_S = 0$ ground state, while for $m_S = -1$, an inter-system crossing to a metastable state is more likely to occur from where it decays non-radiatively to the $m_S = 0$ ground state. The fluorescence is therefore lower for $m_S = -1$ than for $m_S = 0$. This enables optical state detection and also leaves the NV$^-$ in the $m_S = 0$ ground state, with

the nuclear spin state intact. A similar procedure using the orange laser is used to measure the charge state of the NV enabling charge state post-selection[1].

For both measurements, consider the case where the system has been prepared, with equal prior probabilities $p_a = p_b = 1/2$, in one of the two non-orthogonal states

$$|a\rangle = \cos\theta|0\rangle - \sin\theta|-1\rangle, \;\; |b\rangle = \cos\theta|0\rangle + \sin\theta|-1\rangle, \tag{3.1}$$

where $0 \leq \theta < \pi/4$, and θ is half the angle between $|a\rangle$ and $|b\rangle$, and $\{|0\rangle, |1\rangle\}$ form an orthonormal basis. Since the states $|a\rangle$ and $|b\rangle$ are not orthogonal, they cannot be distinguished from each other with certainty.

The ^{14}N nuclear spin is prepared in these states as follows (see Fig. 3.3(a)). First, it is initialised to the $|m_{\mathrm{I}} = 0\rangle$ state by a QND measurement [94]. This preparation is successful whenever the measurement result is $m_I = 0$. In addition, a charge state postselection is performed on the NV using a charge state measurement as done in [99]. The charge state is successfully prepared when the outcome of this measurement yields NV^-, and only these instances are used.

The next step is to prepare the two non-orthogonal states (3.1) by applying a 2θ-pulse resonant with the $|m_{\mathrm{I}} = 0\rangle \leftrightarrow |m_{\mathrm{I}} = -1\rangle$ transition, with phases 0 and π, producing states $|a\rangle$ and $|b\rangle$ respectively, see Fig. 3.1. One may then try to distinguish between these two states using different measurement schemes. Each scheme basically corresponds to a particular measurement basis.

To implement the measurement in a given basis, the experiment employs radio frequency (RF) pulses resonant with the ^{14}N spin transitions $|m_{\mathrm{I}} = 0\rangle \leftrightarrow |m_{\mathrm{I}} = -1\rangle$ and $|m_{\mathrm{I}} = 0\rangle \leftrightarrow |m_{\mathrm{I}} = +1\rangle$, which are applied such that the required basis is rotated onto the $\{|m_{\mathrm{I}} = 0\rangle, |m_{\mathrm{I}} = +1\rangle, |m_{\mathrm{I}} = -1\rangle\}$-basis. The final projective measurements are performed by consecutive single-shot readout measurements on the spin states, where the first positive result is counted as the outcome (please see Figure 3.3 (b) for an example of readout of one of three orthogonal spin states). Due to the possibilities of spin flips and/or errors in each readout measurement in the sequence, there is a probability to obtain multiple or no positive result at all leading to imperfect detection efficiencies. Details for these errors in the specific cases are given below.

3.2.1 Unambiguous state discrimination (USD)

USD requires $p(a|b) = p(b|a) = 0$, where $p(a|b)$ is the probability to obtain result "a" given that the state was $|b\rangle$, and vice versa for $p(b|a)$. A simple way to achieve this is to perform projective measurement in the two-dimensional space spanned by $|0\rangle$ and $|-1\rangle$, either in the basis $\{|a\rangle, |a^{\perp}\rangle\}$ or the basis $\{|b\rangle, |b^{\perp}\rangle\}$, where $|a^{\perp}\rangle = \sin\theta|0\rangle + \cos\theta|-1\rangle$

[1] See Ref. [99] for more details about the charge state postselection.

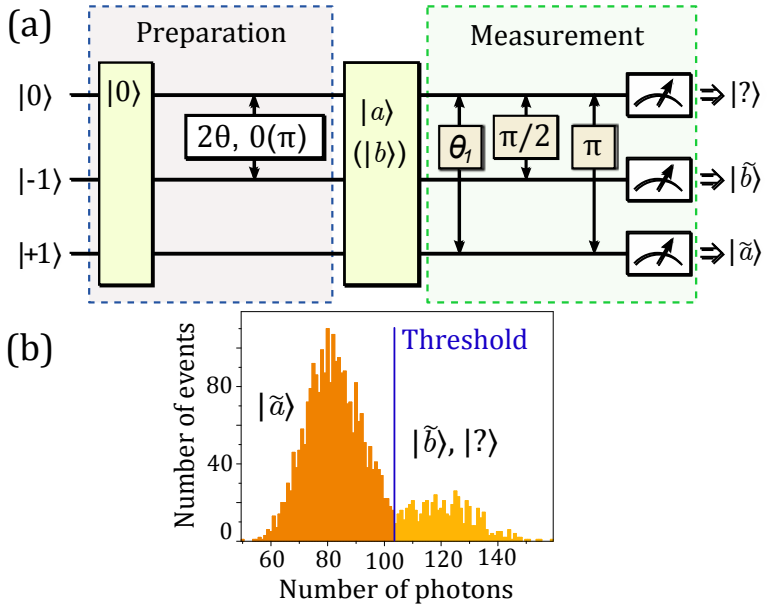

Figure 3.3: (a) Illustration of the applied radio frequency pulses to prepare the non-orthogonal states and perform the IDP measurement. For the Helstrom measurement, the θ_1 pulse is omitted. (b) Histogram of results for single-shot readout of $|\tilde{a}\rangle$ for several preparations of a single NV center in the state $|a\rangle$ with $\theta = \pi/4$. In each event (preparation and detection), a level of photocounts below the threshold is taken to correspond to a detection in the state $|\tilde{a}\rangle$ and the system having been prepared in the state $|a\rangle$.

is orthogonal to $|a\rangle$, and $|b^{\perp}\rangle = \sin\theta|0\rangle - \cos\theta|-1\rangle$ is orthogonal to $|b\rangle$. The result "$a^{\perp}$" then guarantees that the state must have been $|b\rangle$, and vice versa for "$b^{\perp}$", while the results "a" and "b" are inconclusive. In the following, this method is referred to as standard unambiguous state discrimination (SUSD). The probability of such an inconclusive outcome is $p_? = p_i + p_j|\langle i|j\rangle|^2$, $i,j = a,b$. If the prior probabilities p_a and p_b are equal, then $p_? = (1+|\langle a|b\rangle|^2)/2 \geq 1/2$ for either measurement. If the prior probabilities are not equal, it will be best to always choose the one with the higher probability. The main drawback of this protocol is the high probability of an inconclusive result.

3.2.1.1 Standard USD

In order to realise the SUSD measurement in the basis $\{|a\rangle, |a^{\perp}\rangle\}$ and in the basis $\{|b\rangle, |b^{\perp}\rangle\}$, unitary operations $\hat{U}_a$ and $\hat{U}_b$ are respectively performed, followed by a detection in the $\{|0\rangle, |1\rangle\}$ basis. The unitary operations $\hat{U}_a = |0\rangle\langle a| + |1\rangle\langle a^{\perp}|$ and $\hat{U}_b = |0\rangle\langle b| + |1\rangle\langle b^{\perp}|$ are carried out by RF 2θ and -2θ-pulses, respectively, on the $|m_{\mathrm{I}} = 0\rangle \leftrightarrow |m_{\mathrm{I}} = -1\rangle$ transition. Additionally, the scheme applies a π-pulse on the $|m_{\mathrm{I}} = 0\rangle \leftrightarrow |m_{\mathrm{I}} = +1\rangle$ transition, and the final projective measurement is performed in the basis $\{|m_{\mathrm{I}} = +1\rangle, |m_{\mathrm{I}} = -1\rangle\}$. This is for a technical reason explained in Sec. 3.3. This SUSD was implemented as outlined above. In the results of the experimental realisation, the overall probability to obtain a result (or detection efficiency) was ~84.6 %. This includes ~1%

of multiple positive results. The state $|m_{\mathrm{I}} = -1\rangle$ then corresponds to $|a^{\perp}\rangle$ and $|b^{\perp}\rangle$, depending on the chosen basis, and the state $|m_{\mathrm{I}} = +1\rangle$ corresponds to the inconclusive result $|a\rangle$ and $|b\rangle$ respectively.

3.2.1.2 IDP measurement

The optimal USD (i.e., the IDP measurement) however has three outcomes, corresponding to "a", "b", and "inconclusive". It is optimal in the sense that the probability of an inconclusive result is the lowest possible for unambiguous determination of the prepared state, that is for results "a" and "b". The measurement can be understood as a projective measurement in an extended three-dimensional space as illustrated in Fig. 3.4(a). This requires an auxiliary basis state which is provided by the third ^{14}N nuclear spin state, since there are three spin basis states (I=1). In three dimensions, as Fig. 3.4 (a) shows, there exist orthonormal states $|\tilde{a}\rangle, |\tilde{b}\rangle$ and $|?\rangle$, such that $|\tilde{a}\rangle$ is perpendicular to $|b\rangle$, and $|\tilde{b}\rangle$ is perpendicular to $|a\rangle$. A possible choice of such states is given by

$$\begin{aligned} |\tilde{a}\rangle &= \frac{1}{\sqrt{2}}\left(\tan\theta|0\rangle - |-1\rangle - \sqrt{1-\tan^2\theta}|+1\rangle\right), \\ |\tilde{b}\rangle &= \frac{1}{\sqrt{2}}\left(\tan\theta|0\rangle + |-1\rangle - \sqrt{1-\tan^2\theta}|+1\rangle\right), \\ |?\rangle &= \sqrt{1-\tan^2\theta}|0\rangle + \tan\theta|+1\rangle. \end{aligned} \tag{3.2}$$

Using a projective measurement in the basis $\{|\tilde{a}\rangle, |\tilde{b}\rangle, |?\rangle\}$, the unambiguity condition $p(a|b) = p(b|a) = 0$ holds as required, and the probability $p_?$ for an inconclusive outcome is given by the overlap $|\langle a|b\rangle|$–the minimum possible value for unambiguous state discrimination. The Hilbert space can be extended either using an ancillary level, as done here, or using an ancillary qubit as suggested in the proposal of Chapter 2, or as done in the optical realisation where the system and ancilla qubits are polarisation and path respectively [50]. A general method for working out how to realise generalised quantum measurements is given in Ref. [52]. The measurement in the basis $\{|\tilde{a}\rangle|\tilde{b}\rangle, |?\rangle\}$ can be implemented for example by first performing a unitary operation

$$\hat{U} = |0\rangle\langle\tilde{a}| + |-1\rangle\langle\tilde{b}| + |+1\rangle\langle?|, \tag{3.3}$$

followed by a projective measurement in the $\{|0\rangle, |-1\rangle, |+1\rangle\}$ basis. Detection in $|0\rangle$ or $|-1\rangle$ now unambiguously indicates that the unknown state was $|a\rangle$ or $|b\rangle$ respectively, while the result $|+1\rangle$ is inconclusive. The conditional probabilities for different results

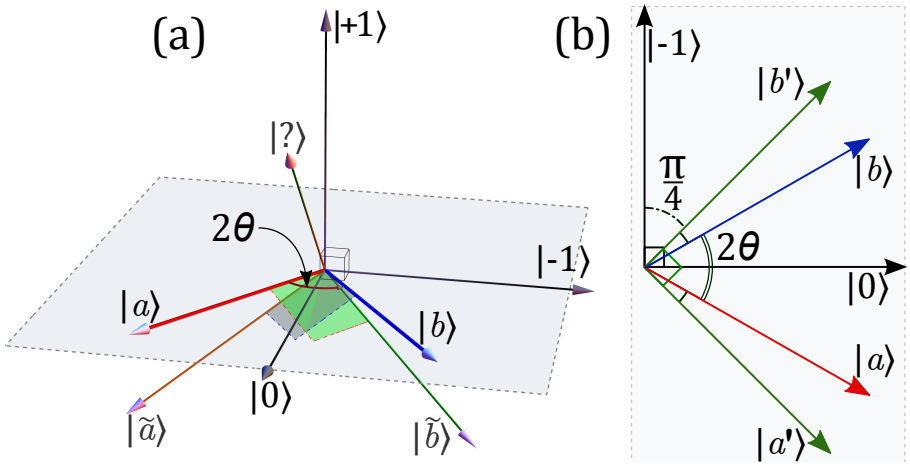

Figure 3.4: Geometrical representation of (a) the IDP measurement. The initial two-dimensional Hilbert space, where $|a\rangle$ and $|b\rangle$ live, is spanned by $\{|0\rangle, |-1\rangle\}$. The measurement is a projective measurement in the basis $\{|\tilde{a}\rangle|\tilde{b}\rangle, |?\rangle\}$, where $|\tilde{a}\rangle$ is orthogonal to $|b\rangle$ and $|\tilde{b}\rangle$ is orthogonal to $|a\rangle$. It can be realised by first making the unitary operation $\hat{U}$ in Eq. (3.5), followed by a projective measurement in the $\{|0\rangle, |-1\rangle, |+1\rangle\}$ basis. (b) The Helstrom measurement basis $\{|a'\rangle, |b'\rangle\}$.

are [43, 44]

$$\begin{aligned} p(a|a) &= |\langle\tilde{a}|a\rangle|^2 = 1 - |\langle a|b\rangle| = p(b|b) = |\langle\tilde{b}|b\rangle|^2 \\ p(a|b) &= p(b|a) = |\langle\tilde{a}|b\rangle|^2 = |\langle\tilde{b}|a\rangle|^2 = 0 \\ p(?|a) &= p(?|b) = |\langle a|b\rangle|. \end{aligned} \tag{3.4}$$

Here $p(j|k)$ denotes the conditional probability of obtaining a result $|j\rangle$ given a state $|k\rangle$, with $j,k = a,b$. The average probability of correctly identifying a prepared state is then $p_{\text{corr}} = p(a|a)p_a + p(b|b)p_b$, where p_j are the prior probabilities, i.e., for preparing states $|j\rangle$. Also, the average error probability is $p_{\text{err}} = p(b|a)p_a + p(a|b)p_b$, while the average probability of an inconclusive outcome is $p_? = p(?|a)p_a + p(?|b)p_b$.

Defining the basis vectors as $|0\rangle \equiv [1,0,0]^T$, $|-1\rangle \equiv [0,1,0]^T$ and $|+1\rangle \equiv [0,0,1]^T$, where the superscript T denotes transpose, $\hat{U}$ can be written as [43, 44, 45]

$$\hat{U} = \frac{1}{\sqrt{2}} \begin{bmatrix} \tan\theta & -1 & -\sqrt{1-\tan^2\theta} \\ \tan\theta & 1 & -\sqrt{1-\tan^2\theta} \\ \sqrt{2(1-\tan^2\theta)} & 0 & \sqrt{2}\tan\theta \end{bmatrix}. \tag{3.5}$$

$\hat{U}$ may then be decomposed into a product of unitary operators coupling two levels at a time [52, 64]. For experimental convenience, the scheme employs a decomposition of

the form $\hat{U} = \hat{T}_{0,-1}\hat{T}_{0,+1}$ [93], where

$$\hat{T}_{0,-1} = \frac{1}{\sqrt{2}} \begin{pmatrix} 1 & -1 & 0 \\ 1 & 1 & 0 \\ 0 & 0 & \sqrt{2} \end{pmatrix}, \tag{3.6}$$

$$\hat{T}_{0,+1} = \begin{bmatrix} \tan\theta & 0 & -\sqrt{1-\tan^2\theta} \\ 0 & 1 & 0 \\ \sqrt{1-\tan^2\theta} & 0 & \tan\theta \end{bmatrix}. \tag{3.7}$$

This corresponds to a pulse sequence consisting of a $\theta_1 = 2\arcsin(\sqrt{1-\tan^2\theta})$ RF pulse resonant with the $|m_\mathrm{I}=0\rangle \leftrightarrow |m_\mathrm{I}=+1\rangle$ transition, followed by a $\theta_2 = \pi/2$ pulse resonant with the $|m_\mathrm{I}=0\rangle \leftrightarrow |m_\mathrm{I}=-1\rangle$ transition. As before, a RF π-pulse is applied on the $|m_\mathrm{I}=0\rangle \leftrightarrow |m_\mathrm{I}=+1\rangle$ transition, such that if the RF pulses have no effect due to improper electron initialisation, the measurement result will be inconclusive since the spin will stay in $|m_\mathrm{I}=0\rangle$, which gives an inconclusive result (see Fig. 3.1). The detection is completed with a projective measurement in the basis $\{|m_\mathrm{I}=0\rangle,|m_\mathrm{I}=-1\rangle,|m_\mathrm{I}=+1\rangle\}$. A positive result on $|m_\mathrm{I}=-1\rangle$ ($|m_\mathrm{I}=+1\rangle$) corresponds to state $|a\rangle$ ($|b\rangle$), and a positive result on $|m_\mathrm{I}=0\rangle$ corresponds to an inconclusive result. The IDP measurement was implemented as outlined above. In the results of the experimental realisation, the average detection efficiency of the final readout is $\sim$90.2%. This includes $\sim$10.2% of multiple positive results.

3.2.2 Minimum-error (Helstrom) measurement

The Helstrom measurement minimises the error in the result in the case where inconclusive outcomes are not allowed. It gives a higher probability to obtain a correct result than an unambiguous measurement, but at a cost—an obtained result is not guaranteed to be correct. For the two equiprobable states $|a\rangle$ and $|b\rangle$ under consideration, the Helstrom measurement is simply a projective measurement in a two-dimensional orthonormal basis $\{|a'\rangle,|b'\rangle\}$ which is symmetric around $|a\rangle$ and $|b\rangle$ (see Fig. 3.4 (b)), such that $|a\rangle$ has a larger overlap with $|a'\rangle$ and $|b\rangle$ a larger overlap with $|b'\rangle$. In our case,

$$|a'\rangle = \frac{1}{\sqrt{2}}(|0\rangle - |-1\rangle) \tag{3.8}$$

$$|b'\rangle = \frac{1}{\sqrt{2}}(|0\rangle + |-1\rangle). \tag{3.9}$$

A detection in state $|a'\rangle$ corresponds to $|a\rangle$, and a detection in state $|b'\rangle$ to $|b\rangle$. For two states $|a\rangle$ and $|b\rangle$ with prior probabilities p_a and p_b, the Helstrom measurement has an

error probability given by [41]

$$p_{\text{err}}^{\text{opt}} = \frac{1}{2}(1 - \sqrt{1 - 4p_a p_b |\langle a|b\rangle|^2}). \tag{3.10}$$

This optimum result is obtained when the states $|a'\rangle$ and $|b'\rangle$ are modified based on the prior probabilities. The probability to obtain a correct result is given by $p_{\text{corr}} = 1 - p_{\text{err}}^{\text{opt}}$, which is the highest possible probability to identify the state correctly. For two equiprobable states $|a\rangle$ and $|b\rangle$ the Helstrom measurement is implemented by performing only the rotation (3.6), i.e, the RF $\pi/2$-pulse on the $|m_{\text{I}} = 0\rangle \leftrightarrow |m_{\text{I}} = -1\rangle$ transition. Again, an RF π-pulse on the $|m_{\text{I}} = 0\rangle \leftrightarrow |m_{\text{I}} = +1\rangle$ transition is applied to take care of possible electronic spin initialisation errors. Finally, the scheme uses a projective measurement in the basis $\{|m_{\text{I}} = +1\rangle, |m_{\text{I}} = -1\rangle\}$, corresponding to the outcomes "a" and "b", with an efficiency of $\sim$83.1%, including $\sim$1.1% of multiple positive results in the experimental realisation.

A summary of the three measurement schemes in shown in Table 3.1. The results of the three measurements are shown in Fig. 3.5, where it shows the average probability of correctly identifying a prepared state $p_{\text{corr}} = p(a|a)p_a + p(b|b)p_b$, the average probability for an inconclusive result $p_? = p(?|a)p_a + p(?|b)p_b$, and the average probability for conclusive but incorrect identification $p_{\text{err}} = p(b|a)p_a + p(a|b)p_b$ (i.e. making an error). The conditional probabilities are found to be similar, that is $p(a|a) \approx p(b|b)$, $p(b|a) \approx p(a|b)$, and $p(b|a) \approx p(a|b)$ in our experiments.

First, it is useful to compare the generalised quantum measurement (IDP) with the simpler SUSD measurement, to see how the increased experimental complexity affects its performance. In Fig. 3.5 (a) and (b), it is evident that the probability of a conclusive result and the probability for an inconclusive result is always better for the IDP measurement than for the SUSD measurement, as expected. However, Fig. 3.5 (c) shows that this is also partly due to a higher error probability for the IDP measurement for large $\langle a|b\rangle$. The reason for these errors is discussed below, and is expected to reduce with improvement in the experimental control of the NV.

While the Helstrom measurement minimises errors when no inconclusive results are allowed, USD measurements are supposed to give unambiguous (error-free) results by allowing an inconclusive outcome. However, the results of the experimentally realised unambiguous measurements are not guaranteed to be correct either, due to inevitable experimental imperfections. It is therefore important to check how the errors resulting from imperfections in the realisation of the unambiguous measurement compare with the error probability of the ideal optimal minimum-error measurement, as well as with the error probability in an experimental realisation of the minimum-error measurement.

As expected, Fig. 3.5 (a) shows that the probability of obtaining a correct result is

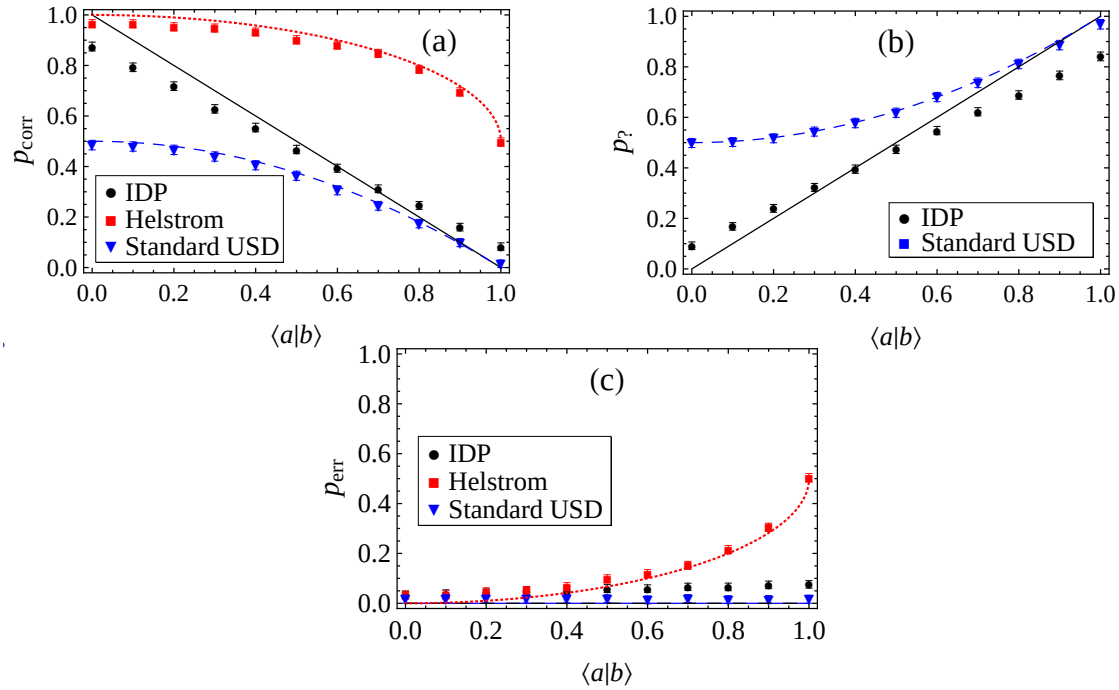

Figure 3.5: Experimental results of unambiguous and minimum-error discrimination of non-orthogonal states. The two non-orthogonal states $|a\rangle$ and $|b\rangle$ are prepared with equal prior probabilities, $p_a = p_b = 1/2$. The probabilities for correct identification $p_{\rm corr} = p(a|a)p_a + p(b|b)p_b$, inconclusive outcomes $p_? = p(?|a)p_a + p(?|b)p_b$ and incorrect outcomes $p_{\rm err} = p(b|a)p_a + p(a|b)p_b$ are shown in figures(a), (b) and (c) respectively. Probabilities are plotted as functions of overlap $\langle a|b\rangle = \cos 2\theta$. The experimental error bars account only for uncertainty due to measurement shot noise.

highest for the Helstrom measurement. The probability of making an error is shown in Fig. 3.5 (c). This shows that for small overlap $|\langle a|b\rangle|$, this probability is only a few percent for the three measurement protocols. Also, the error in the implementation of the IDP measurement is never greater than that of the Helstrom measurement. Only for small overlap does the error in the implementation of the IDP measurement slightly exceed the ideal minimum-error bound.

3.3 Error discussion

The main source of errors, which lead to discrepancies between ideal theoretical predictions and the experimental results, is decoherence due to the limited lifetime of the nuclear spin during the QND readout. One effect this has is a reduction of the available time for fluorescence measurements which in turn reduces the photon count for single-shot readout, thereby increasing measurement uncertainty due to photon shot noise. For example, even though the spin is in the state $|m_{\rm I} = +1\rangle$, the count rate corresponding to state $|m_{\rm I} = 0\rangle$ or $|m_{\rm I} = -1\rangle$ is detected. Also, there is a finite probability for the nuclear

Measurement	d	unambiguous	error %	efficiency %
SUSD	2	yes	~ 3.5	84.6
IDP	3	yes	$4-7.5$	90.2
Helstrom	2	no	> 3.5	83.1

Table 3.1: A summary of the IDP, Helstrom and SUSD experimental measurement results. d is the dimension of the Hilbert space used for the measurement. While the IDP and SUSD measurements have zero error probability in the ideal case, the Helstrom measurement has an inherent error probability which adds to errors due to experimental imperfections. The indicated error is the overall observed in the experimental realisation of each scheme. The ideal efficiency for each of the measurements is 100%.

spin state to flip during the measurement and this is especially important when consecutive projections are being done on all three spin states. Due to these errors, it is possible to obtain more than one positive result for the measurement, or none at all. Since the probability for the spin flip increases with time, the first positive result is counted as the outcome since subsequent positive results are more likely to be due to errors.

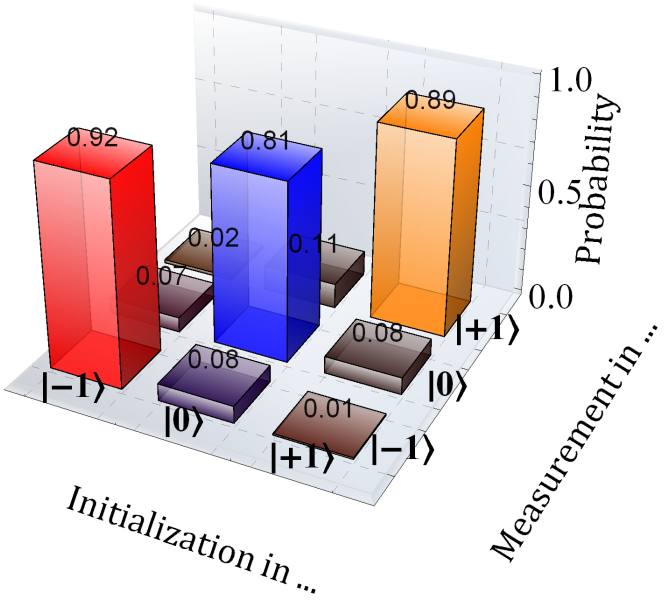

Figure 3.6: Measured spin flip probabilities due to limited single-shot readout fidelity. The plot shows the transition matrix calculated from analysing $\approx 16,800$ state preparations. This is obtained by initialising the NV center in state $|m_I = -1\rangle$, $|m_I = 0\rangle$ or $|m_I = +1\rangle$ and thereafter performing a readout of the state in the $\{|m_I = -1\rangle, |m_I = 0\rangle, |m_I = +1\rangle\}$ basis.

The probability to get a false positive result is increased if a neighbouring spin state (with $\Delta m_I = \pm 1$) is highly populated. To highlight this, Fig. 3.6 shows an example of measurement results demonstrating typical values of single-shot readout error probability. This is why the error probability of the IDP measurement is higher for large $\langle a|b\rangle$ compared to the standard unambiguous measurement in Fig. 3.5 (c), since for the IDP measurement the inconclusive result corresponds to $|m_I = 0\rangle$ and the conclusive result

$|m_{\mathrm{I}} = -1\rangle$ or $|m_{\mathrm{I}} = +1\rangle$, whereas for the standard unambiguous measurement the inconclusive result corresponds to $|m_{\mathrm{I}} = +1\rangle$ and the conclusive result $|m_{\mathrm{I}} = -1\rangle$.

Another point to consider is the imperfect electronic initialisation, either due to errors in the charge state postselection (see Ref. [99]), or because the electron spin is not properly polarised. In both cases, this affects the nuclear spin transition frequencies by hyperfine interaction, and the RF pulses, which are designed for the electron being in the $m_{\mathrm{S}} = 0$ NV^- ground state, will have no effect on the nuclear spin. In this case, the nuclear spin will stay in the initialised state, which is $m_{\mathrm{I}} = 0$. By applying a final π pulse on the $|m_{\mathrm{I}} = 0\rangle \leftrightarrow |m_{\mathrm{I}} = +1\rangle$ transition, this scheme ensures that the state $|m_{\mathrm{I}} = 0\rangle$ is either not used (for the standard unambiguous and Helstrom measurements), or counted as inconclusive (for the IDP measurement).

3.4 Conclusion

In conclusion, this chapter has discussed an experimental realisation and comparison of three different measurement schemes to distinguish between non-orthogonal quantum states—an important task in quantum information processing. These measurements include optimal unambiguous state discrimination and the minimum-error or Helstrom measurement. Previously, optimal unambiguous state discrimination had only been realised using photons [50, 93]. The ability to perform generalised measurements on NV^- centres is of interest for implementations of solid-state quantum computing. The realised IDP measurement for NV^- centres outperforms standard projective measurements, and gives further evidence that NV^- centres in diamond are a favourable candidate for solid state quantum information processing at room temperature.

CHAPTER 4

Fair sampling, Bell inequalities and entanglement dimension

4.1 Introduction

Quantum correlations resulting in violations of Bell inequalities have generated a lot of interest in quantum information science and fundamental physics. This chapter addresses some open questions that become relevant in Bell-type tests involving systems with local dimension greater than 2. For CHSH-Bell tests within 2-dimensional subspaces of such high-dimensional systems, it has been suggested that experimental violation of Tsirelson's bound (see Sec. 1.2.1) indicates that more than 2-dimensional entanglement was present. This chapter explains that the overstepping of Tsirelson's bound is due to violation of fair sampling (a condition that the sample of detected pairs is representative of the pairs emitted), and can in general be reproduced by a separable state, if fair sampling is violated. The main contribution in this chapter is to demonstrate that for a class of Bell-type inequalities generalised to d-dimensional systems, a certain level of violation would guarantee d-dimensional entanglement of the tested state, when fair sampling is satisfied. It is also shown that this can be used as an experimentally feasible test of d-dimensional entanglement for up to quite high values of d. This is done through analytical derivation of bounds on the violations as well as the numerical calculations of the bounds for some specific cases.

Bell inequalities [35, 36] must be obeyed by any local hidden-variable theory, but are violated by quantum mechanics. Many experiments have shown violation of Bell inequalities, see e.g. Refs. [100, 101, 102, 103]. To date, all photon-based Bell test experiments suffer from the fair sampling or *detection loophole*. This refers to the possibility of obtaining a violation of a Bell inequality with a local hidden-variable theory due to loss [36, 104, 105, 106, 107]. In order to close the detection loophole without making any assumptions regarding the fairness of the sampling, detection efficiencies must be above certain threshold values, [108, 109, 110, 111, 112, 113, 114, 115] and this has been achieved in tests using ions [103]. The bound on loss may vary according to the setting considered. In particular, it has recently been shown that bounds on loss may be less stringent for tests using high-dimensional systems [116]. Imperfections in

experimental coincidence detection schemes may also result in false violations of Bell inequalities [117, 118].

A standard form of the fair sampling condition requires that loss be independent of measurement settings [36, 100, 119, 120]. It has however been shown that this is not necessary; the loss may depend on the measurement settings. To test local hidden-variable theories, it is necessary and sufficient that the detection efficiency factorises as a function of the measurement settings and the tested state [121]. This is a more relaxed condition than the form of fair sampling assuming that loss is independent of the measurement settings. It is important to note that, in order to judge whether fair sampling is satisfied or not, the detection efficiencies that should be considered refer not only to the efficiency of the final detection, that is, the efficiencies of the actual detectors used. The detection efficiency must take all of the measurement process into account, including for example the losses associated with the selection of measurement bases. Fair sampling may be violated even if the final detection process is very efficient.

Bell inequalities involve probabilities for certain combinations of outcomes to occur, when measurements are made on different parts of a quantum system. Experiments, however, usually measure these probabilities in terms of count rates normalised by total count rates. The total rate is usually given by the sum of the count rates for all the outcomes obtained with a particular combination of measurement settings. The total count rate may not correspond in a simple way to the total probability for the source to emit a state. Normalising using underestimated "total count rates" may lead to anomalous "Bell violations" even for separable states, and violation of Tsirelson's bound [37] for entangled states.

Postselection schemes that do not satisfy fair sampling may thus be used to increase Bell violation both for separable and entangled states, see e.g. Refs. [121, 122, 123, 124, 125, 126, 127]. In addition to this, certain kinds of postselection, while preserving the separable state bound, lead to a violation of Tsirelson's bound with two-qubit entangled states [121, 124]. This chapter considers situations that are especially relevant for tests of Bell inequalities with high-dimensional systems, such as when using the orbital angular momentum of light. Recently, a number of experiments have reported violations of Bell inequalities using subspaces of high-dimensional quantum systems, [128, 129, 130] and it has been suggested that Tsirelson's bound may be violated using a similar setup as a demonstration of high-dimensional entanglement [131]. It is therefore important to be aware of the exact forms the violation of fair sampling could take for such experiments. This chapter demonstrates that the fair sampling assumption may be violated in more subtle ways using current setups if care is not taken. In particular, for high-dimensional systems, the fair sampling assumption can be violated even if the final detection efficiency is 100% in the tested subspaces.

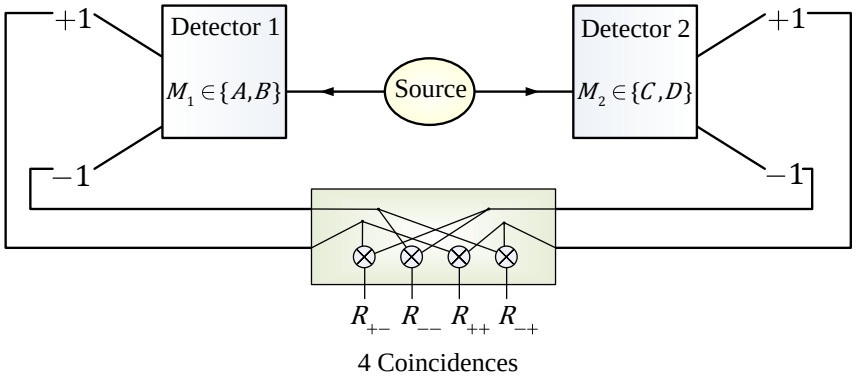

Figure 4.1: Schematic view of a CHSH-Bell test. Each of the two detectors has two possible settings. The outputs from the detectors give four different pairwise coincidence rates for each combination of detector settings. The four different combinations of detector settings give in total 4×4=16 coincidence rates, that are used for calculating the CHSH-Bell parameter S.

The rest of the chapter begins by reviewing the Clauser-Horne-Shimony-Holt (CHSH) Bell inequality and the use of postselection and fair sampling. Through examples which are especially relevant for experiments using the orbital angular momentum of light, it then illustrates how fair sampling may be violated in non-standard ways. In such cases, it is possible to incorrectly infer "violations" of the CHSH inequality even for a separable state independent of the efficiency of the final detection. Also, an entangled state may produce anomalously high Bell inequality violations. An example where the different measurement settings do satisfy the fair sampling condition is then considered. In this case, the maximal violation for a quantum state is $2\sqrt{2}$ in agreement with Tsirelson's bound. The final part of this chapter considers what may be deduced from the level of violation about the dimensionality of entanglement present in the tested state, in the case of a family of generalised Bell-type inequalities.

4.2 The CHSH-Bell inequality

The most common form of Bell inequality [35] is due to Clauser, Horne, Shimony and Holt [36]. Suppose that one can choose to measure either observable A or B on one quantum system, and either observable C or D on a second system, see Figure 4.1. The measurement outcomes for these observables are denoted by a, b, c, d, respectively, and can take values ± 1. If, for an individual experimental run, definite values can actually be assigned to these measurement outcomes, independent of whether the corresponding measurements are made or not (realism), and independent of what measurement is made on the other quantum system (locality), then these individual measurement outcomes must satisfy

$$ac + ad + bc - bd = a(c+d) + b(c-d) = \pm 2. \tag{4.1}$$

Let us denote the average of ac when the measurements are repeated many times for identically prepared states by

$$E(a,c) = p(a=c) - p(a=-c), \tag{4.2}$$

and similar for the other measurement combinations. If Eq. (4.1) is averaged over many experimental runs, then this results in the familiar CHSH-Bell inequality,

$$S = |E(a,c) + E(a,d) + E(b,c) - E(b,d)| \leq 2, \tag{4.3}$$

where S is the Bell parameter. Violation of this inequality means either that a value cannot be assigned to an individual measurement outcome independently of that measurement being made, or independently of a measurement on a distant quantum system being made, or both. Experimental violation of this inequality therefore cannot be explained using a local realist theory. For a singlet state $|\Psi^-\rangle = 1/\sqrt{2}(|+-\rangle - |-+\rangle)$ of two spin-1/2 quantum systems, one obtains $E(a,c) = -\mathbf{a}\cdot\mathbf{c}$ if spin is measured along the direction $\mathbf{a}$ on the first system and along $\mathbf{c}$ on the second system. $S = 2\sqrt{2}$ may be obtained e.g. by choosing measurement directions $\mathbf{a} = \mathbf{z}, \mathbf{b} = \mathbf{x}, \mathbf{c} = -(\mathbf{z}+\mathbf{x})/\sqrt{2}$ and $\mathbf{d} = (\mathbf{z}-\mathbf{x})/\sqrt{2}$. For a quantum state, $2\sqrt{2}$ is the maximal possible violation of the CHSH inequality, referred to as Tsirelson's bound [37]. Indeed, for any entangled quantum state, there is a maximal amount of violation which is possible. In general, this corresponds to the maximum eigenvalue of the corresponding Bell operator as described below.

4.3 Postselection and fair sampling

In an experiment, one cannot directly measure the probabilities $p(a=c)$, $p(a=-c)$, $p(a=d)$, and so on. Instead, what is measured, in optical experiments for example, are count rates, such as coincidence count rates $R(a=c)$, $R(a=-c)$, $R(a=d)$ etc. for different combinations of measurement settings. Typically, one then calculates

$$\widetilde{E}(a,c) = \frac{R(a=c) - R(a=-c)}{R(a=c) + R(a=-c)}, \tag{4.4}$$

and similar for other combinations of measurement settings. Taking into account only the detected outcomes constitutes postselection. The CHSH-Bell inequality with postselection is

$$S = \widetilde{E}(a,c) + \widetilde{E}(a,d) + \widetilde{E}(b,c) - \widetilde{E}(b,d) \leq 2. \tag{4.5}$$

Similar expressions can be formed for measurements with more than two outcomes and Bell inequalities for high-dimensional systems. In using Eq. (4.5) instead of Eq. (4.3),

one assumes that the detected events are representative also of the undetected events. In particular, one assumes that $R_{tot}(a,c) = R(a=c) + R(a=-c)$, and similar for other combinations, are total count rates for which the detection efficiencies satisfy the fair sampling condition. Detection efficiencies are essentially the count rates, for particular measurement settings and the state measured, divided by the total emission rate of the source. For example, $R_{tot}(a,c) = \mathcal{E}(A,C,\hat{\rho})R_{source}$, where R_{source} is the total emission rate for the source and $\mathcal{E}(A,C,\hat{\rho})$ is the measurement efficiency for settings A,C and measured state (or hidden variable) $\hat{\rho}$. Note that the analogously defined efficiencies for different outcomes for one measurement setting and a given state need not be equal for us to be able to define an "overall" efficiency for that measurement setting and state.

As mentioned earlier (Section 4.1), a more relaxed version of the fair sampling condition states that in order to rule out local hidden-variable theories, it is necessary and sufficient that the single-party efficiencies factorise as a function of the measurement settings and the state or hidden variable. That is, detection efficiencies must factorise as $\mathcal{E}(k,\rho) = \mathcal{E}(k)\mathcal{E}(\hat{\rho})$ for all settings k for measurements on a subsystem, and for all states $\hat{\rho}$ [121]. Moreover, if this condition holds, then any value of a Bell parameter that can be obtained with a separable state using postselection can also be obtained without postselection, with some other separable state. Also for entangled states, a violation that can be obtained with postselection can also be obtained without postelection. This means that if the fair sampling assumption is satisfied, then Tsirelson's bound cannot be violated.

Both versions of the fair sampling condition (i.e. the one that requires that detection efficiencies be independent of measurement settings and the one that only requires that the efficiencies factorise into functions of measurement setting and the state) may fail explicitly especially when a Bell inequality is tested on high-dimensional systems, if the different measurement settings do not equally sample the same parts of the Hilbert space. Essentially, this leads to "too low" total count rates for different measurement settings, and consequently too high values of $\widetilde{E}$. This will become clearer when one considers the fair sampling condition in terms of measurement operators.

4.3.1 Fair sampling for quantum measurements

The necessary and sufficient fair sampling assumption can also be stated in the context of quantum measurements [121]. If the measurement operators are known, e.g. one knows what quantum measurements one aims for in an experiment, one may easily check if the fair sampling condition is satisfied. Consider a test of a Bell inequality. Each measurement on one of the subsystems is described by positive measurement operators $\hat{\Pi}_{k,m}$ where k labels the measurement setting and the index m runs over the possible outcomes.

The sum of the measurement operators for a setting k is given by the positive operator

$$\hat{Q}_k = \sum_m \hat{\Pi}_{k,m} \leq \mathbf{1}, \tag{4.6}$$

which can be less than the identity operator in the space of the concerned subsystem, in order to model loss. (If a measurement operator $\hat{\Pi}_{k,0}$ corresponding to "no detection" is added, then $\hat{Q}_k + \hat{\Pi}_{k,0} = \mathbf{1}$, the identity operator on the concerned subsystem.) The single-party detection efficiency for measurement setting k, when the state $\hat{\rho}$ is measured, is given by $\mathcal{E}(k,\rho) = \mathrm{Tr}(\hat{Q}_k\hat{\rho})$, and is equal to the total probability to obtain an outcome for measurement setting k and state $\hat{\rho}$. In terms of measurement operators, the fair sampling condition $\mathcal{E}(k,\rho) = \mathcal{E}(k)\mathcal{E}(\rho)$ is equivalent to

$$\hat{Q}_k = \mathcal{E}(k)\hat{Q}, \tag{4.7}$$

where $0 < \mathcal{E}(k) \leq 1$ and the positive operator $\hat{Q} \leq \mathbf{1}$ is independent of k. This means that the different measurements for the k settings must sample different parts of the Hilbert space in an equal way, and can only differ in their overall efficiency $\mathcal{E}(k)$.

This also directly shows how *entanglement concentration* [132, 133] works in this context (see Sec. 5.5). An operator $\hat{Q}$ in (4.7) that is not proportional to the identity operator (on the relevant Hilbert space) means that parts of the incident state are "unequally" filtered out. This filtering can be done either as part of the measurements for the different settings, as implicit in the above treatment, or by first performing a measurement with measurement operators $\hat{Q}$ and $\mathbf{1} - \hat{Q}$, where $\mathbf{1} - \hat{Q}$ corresponds to the loss in the filtering. If the outcome corresponding to $\hat{Q}$ is obtained, the entanglement concentration has succeeded, the state is transformed to $\hat{Q}^{1/2}\hat{\rho}\hat{Q}^{1/2}/\mathrm{Tr}(\hat{Q}\hat{\rho})$, and one can proceed with a further measurement. Any such filtering is consistent with fair sampling, and cannot lead to apparent violation of a Bell inequality by a separable state, or violation of Tsirelson's bound for an entangled state. Within these bounds, specific choices of $\hat{Q}$ for particular input states may lead to enhancement of the violation.

4.4 Violation of fair sampling for high-dimensional quantum systems

If the different measurement settings on one subsystem do not equally sample the same parts of the Hilbert space, that is, $\hat{Q}_k \neq \mathcal{E}(k)\hat{Q}$, then the fair sampling assumption is violated. This can lead to anomalously high Bell violations both for separable and entangled states $\hat{\rho}$. That is, fair sampling can be explicitly violated with local measurements due to bias in the postselection. This is especially relevant for Bell experiments with

high-dimensional systems, for example, using the orbital angular momentum of light (OAM) [128, 129, 130]. A high-dimensional Bell-test experiment using photon OAM states is introduced and described in Chapter 5. However, let us briefly note here that the eigenstates of the angular momentum operator $\hat{L}_z$ in the paraxial limit are Laguerre-Gaussian modes of light with an azimuthal angular phase dependence of $\exp(-i\ell\phi)$, where ℓ is an integer. Such beams carry an orbital angular momentum of $\ell\hbar$ per photon [134]. In contrast to polarisation, which gives a two-dimensional state space, using the OAM of light in principle allows us to access an infinite-dimensional space. In practice, the number of OAM eigenstates considered is limited due to experimental constraints, but as explained in Chapter 5, violation of Bell inequalities in 12×12 dimensions has been observed using the OAM of entangled twin beams.

In experiments using the orbital angular momentum of light, detection is often done using either etched phase plates, or computer-controlled spatial light modulators (SLMs) acting as reconfigurable holograms. In the rest of this chapter, both are referred to as 'SLMs'. An SLM can be used to change a chosen superposition of OAM eigenmodes to the mode with $\ell = 0$. This beam can then be focused onto a pinhole detector and detected. The eigenmode with $\ell = 0$ is the only eigenmode with a non-zero intensity on the beam axis. Any eigenmode with $\ell \neq 0$ necessarily has zero intensity on the beam axis, because of the phase singularity there, and will not give any signal. For example, one can configure the SLM to add an OAM of $2\hbar$ per photon. An incident $\ell = -2$ beam will then be changed into an $\ell = 0$ beam and detected, while a beam with any other ℓ will result in no signal.

In the ideal case, detection using an SLM is essentially described by measurement operators $|\phi\rangle\langle\phi|, \mathbf{1} - |\phi\rangle\langle\phi|$, where $|\phi\rangle$ may be an angular momentum eigenstate $|\ell\rangle$ or a superposition of such eigenstates. The measurement operator $|\phi\rangle\langle\phi|$ corresponds to a detector firing, whereas the outcome $\mathbf{1} - |\phi\rangle\langle\phi|$ corresponds to no detector firing. This assumes that the efficiency of the final detection, including any optics used for the beam focusing, is 100%, and that there are no dark counts. In a more realistic case (but still with no dark counts) the measurement can be described using measurement operators $p|\phi\rangle\langle\phi|, \mathbf{1} - p|\phi\rangle\langle\phi|$, where $0 \leq p < 1$. The examples given here correspond to $p = 1$, since they are meant to illustrate that irrespective of detector efficiency, fair sampling may be violated. It is straightforward to extend these examples to cases where $p \neq 1$, with identical conclusions.

When testing CHSH-type Bell inequalities using the orbital angular momentum of light, two-outcome measurements may be realised using two different settings of an SLM in one light beam, and registering the count rate in each case. The settings can be described using the projectors $|\phi\rangle\langle\phi|$ and $|\phi^{\perp}\rangle\langle\phi^{\perp}|$. The rest of the Hilbert space is effectively not sampled. One also assumes that the count rates would remain the same if

projections onto both states were simultaneously made. Multidimensional measurements may be realised with more settings of the SLM. If care is not taken, this technique may give measurements on the subsystems that explicitly violate the fair sampling condition (4.7).

An experiment to demonstrate violation of Bell inequalities in up to 12×12 dimensions is described in Chapter 5. There, the alteration of a single parameter of the state of a reconfigurable SLM was sufficient to change between the d basis states required for one measurement setting, thus sampling a high-dimensional space. In this case, the d states of the SLMs were chosen so that the resulting measurements did obey the fair sampling condition. In general, however, keeping the configuration of an SLM the same while, for example, physically rotating it relative to the beam axis, does not guarantee that different measurement settings so obtained sample the same state space and obey the fair sampling condition. Quite obviously, one could e.g. choose any pair of the basis states used in that experiment for one d-outcome measurement setting (with $d > 2$), and the result would be a two-outcome projection onto some orthogonal states $|\theta\rangle$ and $|\theta^{\perp}\rangle$. Picking another pair would give a projection onto two other states $|\phi\rangle$ and $|\phi^{\perp}\rangle$. Clearly, unless the pairs are the same, it holds that $|\theta\rangle\langle\theta| + |\theta^{\perp}\rangle\langle\theta^{\perp}| \neq |\phi\rangle\langle\phi| + |\phi^{\perp}\rangle\langle\phi^{\perp}|$, meaning that these two measurement settings explicitly violate the fair sampling condition irrespective of the detection efficiencies within the sampled subspaces. The example below demonstrates this in further detail. Other similar examples are easy to construct, and violation of the fair sampling condition is the reason for the anomalously high Bell violation in a suggested experiment using the OAM of light [131]. In such a case, one has to carefully examine the measurements used in order to determine what the relevant bound for a local-hidden variable theory is.

All this also implies that care has to be taken before assigning meaning to the coincidence counts as a function of the 'orientation' of an SLM in one beam, while keeping the SLM in the other beam fixed, in analogy with coincidence curves for polarisation experiments. Note that measurements on different subsystems are allowed to sample the Hilbert space unequally, as long as all measurements on the same subsystem sample the space equally. Whether the settings of an SLM lead to fair sampling or not does not depend on how the SLM in the other beam is configured.

4.4.1 S=4 using a classically correlated state

Consider a test of a CHSH-type inequality, and that the state space of each of the two subsystems is four-dimensional, spanned by the states $|1\rangle_i, |2\rangle_i, |3\rangle_i, |4\rangle_i$, where $i = 1,2$ refers to quantum subsystem 1 or 2. This could result from considering a four-dimensional subspace spanned by four orbital angular momentum states or any other four-dimensional space. Similar examples may be constructed using fewer dimensions, but this case is in-

teresting as it yields maximal Bell violation for measurements that are perfect projections within the subspaces. Also, assume that the source state is the separable mixture

$$\hat{\rho} = \frac{1}{4}\left(|1,1\rangle\langle 1,1| + |2,2\rangle\langle 2,2| + |3,3\rangle\langle 3,3| + |4,4\rangle\langle 4,4|\right), \tag{4.8}$$

where $|j,k\rangle$ denotes $|j\rangle_1 \otimes |k\rangle_2$. The same statistics can of course be achieved with an entirely classical joint probability distribution. Also, if each subsystem is measured in the basis $\{|1\rangle, |2\rangle, |3\rangle, |4\rangle\}$, this state displays the same coincidence statistics as a maximally entangled state $|\Psi\rangle = 1/2(|1,1\rangle + |2,2\rangle + |3,3\rangle + |4,4\rangle)$.

Let the two-outcome measurements A, B, C, D be chosen as follows. On system 1, A is a projective measurement in the basis $\{|1\rangle_1, |2\rangle_1\}$, and B in the basis $\{|3\rangle_1, |4\rangle_1\}$. State $|1\rangle_1$ corresponds to $a = +1$ and $|2\rangle_1$ to $a = -1$. State $|3\rangle_1$ corresponds to $b = +1$ and $|4\rangle_1$ to $b = -1$. On system 2, C is a projective measurement in the basis $\{|1\rangle_2, |4\rangle_2\}$, and D in the basis $\{|4\rangle_2, |2\rangle_2\}$. State $|1\rangle_2$ corresponds to $c = +1$ and $|4\rangle_2$ to $c = -1$, state $|4\rangle_2$ to $d = +1$, and $|2\rangle_2$ to $d = -1$. It is easy to see that the fair sampling assumption is not satisfied, since quite clearly $Q_A = |1\rangle_{11}\langle 1| + |2\rangle_{11}\langle 2| \neq Q_B = |3\rangle_{11}\langle 3| + |4\rangle_{11}\langle 4|$, and similarly $Q_C \neq Q_D$. Alternatively, consider that e.g. for the state $\hat{\rho} = |1\rangle_{11}\langle 1|$, where $i = 1$ or 2, it holds that $\mathcal{E}(B, |1\rangle_{11}\langle 1|) = 0$. If this factorises as a function of measurement setting and measured state, then either $\mathcal{E}(B) = 0$ or $\mathcal{E}(|1\rangle_{11}\langle 1|) = 0$. The former would imply that e.g. $\mathcal{E}(B, |3\rangle_{11}\langle 3|) = 0$, if this efficiency also factorises, which is not the case. The latter would imply that e.g. $\mathcal{E}(A, |1\rangle_{11}\langle 1|) = 0$, if this efficiency factorises, which again is not the case. Again, a similar argument may be made for C and D.

None of these measurements are complete on the four-dimensional Hilbert space, but only on two-dimensional subspaces. Within these subspaces, however, the efficiency is 100%, and the measurement operators are all pure-state projectors. It may also be argued that no real quantum measurement is complete, in the sense that there will always be more degrees of freedom than the ones tested. That is, there are possible quantum states that will never be detected using the particular experimental equipment at hand. Also, these two-dimensional measurements accurately model the measurements that one might aim for in an actual experiment using orbital angular momentum of light.

If A is measured on system 1, and C on system 2, then this will sample the 4-dimensional subspace spanned by $\{|1,1\rangle, |1,4\rangle, |2,1\rangle, |2,4\rangle\}$. As a result, $p(a = c = +1) = 1/4$, with the other probabilities $p(a = c = -1) = p(a = -c = 1) = p(a = -c = -1) = 0$. Without postselection, this gives $E(a,c) = 1/4$. In addition, half of the time, either the detector corresponding to A or the one corresponding to C would fire, but not the other. Also, 1/4 of the time neither detector would fire. This, however, does not affect our calculation of $E(a,c)$ if using Eq. (4.2). Similarly, $E(a,d) = E(b,c) = 1/4$ and $E(b,d) = -1/4$, giving $S = 1$, which does not violate Eq. (4.3).

An experimenter, however, would register count rates rather than probabilities, and use postselection when calculating the Bell parameter. Since the fair sampling condition is not satisfied, this may lead to incorrectly inferred violations of Bell inequalities. If postselection is done, ignoring the cases when only one or none of the detectors fire, and use Eq. (4.4), one obtains $\widetilde{E}(a,c) = 1$. Similarly, one obtains $\widetilde{E}(a,d) = \widetilde{E}(b,c) = 1$ and $\widetilde{E}(b,d) = -1$, giving $S = 4$ in Eq. (4.3). This not only "violates" the CHSH Bell inequality, but achieves the maximal "violation" of $S = 4$, whereas $S = 2\sqrt{2}$ is the highest value obtainable using a quantum-mechanical state if the fair sampling assumption holds [37, 121]. The anomalous Bell "violation" is due to the fact that the normalisation is not done using the correct total count rate corresponding to all of the four-dimensional space on each quantum system, in total a 16-dimensional Hilbert space for both quantum systems. Normalising only with part of the total count rate results in an incorrect value of S, four times its correct value. The fair sampling assumption is here violated irrespective of how efficient the final detection is, and irrespective of there being no loss within the sampled subspaces in the final projective measurement.

Taking into account also the cases when only one of the detectors fires will improve the situation. However, one would still be ignoring the cases when neither detector fires while there was a state present to be detected. It may be hard to experimentally determine the loss rate for different measurement settings and states in a reliable way without making non-trivial assumptions of what the different parts of the experimental setup are actually doing. Having to make such assumptions affects the confidence with which experimental violations of Bell inequalities can be viewed.

The example above is an extreme case where a totally separable state achieves maximal CHSH-Bell "violation" of $S = 4$, but effects in an actual experiment may be more subtle. If the measurement settings on one subsystem do not equally sample the same part of the Hilbert space, then incorrectly high Bell violations may be obtained for both separable and entangled states.

4.4.2 Anomalous violation of a Bell inequality for an entangled state

This section highlights another example where the measurements on one subsystem also do not sample exactly the same Hilbert space, resulting in anomalous Bell violations. This example is a modification of a "standard" test of the CHSH-Bell inequality. For standard tests of the CHSH-Bell inequality, the measurements A, B on subsystem 1 and C, D on subsystem 2 are projective measurements in some bases $\{|m_+(\theta)\rangle, |m_-(\theta)\rangle\}$, where

$$\begin{aligned} |m_+(\theta)\rangle &= \cos(\theta/2)|1\rangle + \sin(\theta/2)|2\rangle \\ |m_-(\theta)\rangle &= -\sin(\theta/2)|1\rangle + \cos(\theta/2)|2\rangle. \end{aligned} \tag{4.9}$$

The settings $\theta_a = \pi/2$, $\theta_b = 0$, $\theta_c = 3\pi/4$ and $\theta_d = \pi/4$ give the maximal violation of $2\sqrt{2}$ when the entangled state

$$|\psi\rangle = (|1,2\rangle + |2,1\rangle)/\sqrt{2} \tag{4.10}$$

is measured. Suppose now that an experimenter intends to measure the CHSH-Bell parameter using the subspace spanned by $\{|1\rangle, |2\rangle\}$ of each of two systems living in a four-dimensional Hilbert space spanned by $\{|1\rangle, |2\rangle, |3\rangle, |4\rangle\}$, with a state given by

$$|\psi_4\rangle = \tfrac{1}{\sqrt{4}}(|1,2\rangle + |2,1\rangle + |3,4\rangle + |4,3\rangle). \tag{4.11}$$

Also suppose that without the experimenter being aware of it, the measurement actually implemented is a projection in the basis $\{|\mu_+(\theta)\rangle, |\mu_-(\theta)\rangle\}$, where

$$\begin{aligned} |\mu_+(\theta)\rangle =& [\cos(\theta/2)|1\rangle + \sin(\theta/2)|2\rangle]r + [\cos(\theta)|3\rangle + \sin(\theta)|4\rangle](1-r^2)^{1/2}, \\ |\mu_-(\theta)\rangle =& [-\sin(\theta/2)|1\rangle + \cos(\theta/2)|2\rangle]r - [\cos(\theta)|3\rangle + \sin(\theta)|4\rangle](1-r^2)^{1/2}, \end{aligned} \tag{4.12}$$

and $0 < r < \frac{1}{\sqrt{2}}$. In other words, the detectors 'feel' also the parts of the total Hilbert space spanned by $|3\rangle$ and $|4\rangle$. The measurement settings A, B, C, and D remain as before, $\theta_a = \pi/2$, $\theta_b = 0$, $\theta_c = 3\pi/4$ and $\theta_d = \pi/4$. One obtains anomalous violation of Tsirelson's bound, that is, Bell violations larger than $2\sqrt{2}$, for a range of values of r. The highest violation is $S = 3.2645$ which occurs at $r = 0.6166$. The reason is that the measurements on one subsystem do not sample the same two-dimensional space, so that again, the fair sampling assumption is violated. Similar examples can be constructed for local Hilbert spaces of higher dimensions.

4.5 CHSH-Bell inequality in high dimensions with fair sampling

The following is now an example where the fair sampling condition is satisfied for a test of the CHSH-Bell inequality using high-dimensional quantum systems. The highest possible quantum mechanical violation is then $S = 2\sqrt{2}$, in agreement with Tsirelson's bound. Postselection will not introduce anomalously high Bell violations if all the different measurement settings on one quantum system sample the Hilbert space for that system in an equivalent way, as discussed in section 4.3.

Consider dichotomic measurements with measurement operators $|\phi\rangle_{ii}\langle\phi|, \hat{\mathbf{1}}_i - |\phi\rangle_{ii}\langle\phi|$, where $|\phi\rangle_i$ is a pure state, and $i = 1,2$ refers to quantum system 1 or 2. The total dimension of either quantum system 1 or 2 is not specified, and may be infinite. This is similar

to measurements of orbital angular momentum using SLMs, with the difference that now also the outcome corresponding to $\hat{\mathbf{1}}_i - |\phi\rangle_{ii}\langle\phi|$ is actively registered. Clearly, any two measurements of this type on the same quantum system will evenly sample all of the Hilbert space for a subsystem, and the fair sampling condition in section 4.3 is satisfied.

The maximal possible Bell violation for a quantum-mechanical state may be investigated in terms of the eigenvalues of a so-called Bell operator. Let Π_A^+ and Π_A^- denote the measurement operators corresponding to outcomes $+1$ and -1 for measurement A, and similar for measurements B, C and D. With $\hat{A} = \Pi_A^+ - \Pi_A^-$, and analogously for $\hat{B}$, $\hat{C}$ and $\hat{D}$, the Bell operator is defined as

$$\hat{S} = \hat{A}\otimes\hat{C} + \hat{A}\otimes\hat{D} + \hat{B}\otimes\hat{C} - \hat{B}\otimes\hat{D}, \tag{4.13}$$

so that $S = \mathrm{Tr}[\hat{\rho}\hat{S}]$, where $\hat{\rho}$ describes the bipartite quantum system on which the measurements A or B, and C or D, are made. Without loss of generality, one can write

$$\begin{aligned}
&\Pi_A^+ = |a\rangle_{11}\langle a|, \;\; \Pi_A^- = \hat{\mathbf{1}}_1 - |a\rangle_{11}\langle a|,\\
&\Pi_B^+ = |b\rangle_{11}\langle b|, \;\; \Pi_B^- = \hat{\mathbf{1}}_1 - |b\rangle_{11}\langle b|,\\
&\Pi_C^+ = |c\rangle_{22}\langle c|, \;\; \Pi_C^- = \hat{\mathbf{1}}_2 - |c\rangle_{22}\langle c|,\\
&\Pi_D^+ = |d\rangle_{22}\langle d|, \;\; \Pi_D^- = \hat{\mathbf{1}}_2 - |d\rangle_{22}\langle d|,
\end{aligned} \tag{4.14}$$

with the bases for quantum systems 1 and 2 chosen so that

$$|a\rangle_1 = |0\rangle_1, |b\rangle_1 = \cos\theta_1|0\rangle_1 + \sin\theta_1|1\rangle_1, \tag{4.15}$$

$$|c\rangle_2 = |0\rangle_2, |d\rangle_2 = \cos\theta_2|0\rangle_2 + \sin\theta_2|1\rangle_2. \tag{4.16}$$

It is then straightforward to show that the Bell operator in Eq. (4.13) takes the form

$$\begin{aligned}
\hat{S} = \hat{S}_{2D} &- 2\left(|0\rangle_{11}\langle 0| - |1\rangle_{11}\langle 1|\right)\otimes\hat{\mathbf{1}}_2' - 2\hat{\mathbf{1}}_1'\otimes\left(|0\rangle_{22}\langle 0|\right.\\
&\left. - |1\rangle_{22}\langle 1|\right) + 2\hat{\mathbf{1}}_1'\otimes\hat{\mathbf{1}}_2',
\end{aligned} \tag{4.17}$$

where $\hat{S}_{2D}$ is the Bell operator for the familiar CHSH inequality for two 2-dimensional quantum systems in the space spanned by $|00\rangle, |01\rangle, |10\rangle, |11\rangle$, and $\hat{\mathbf{1}}_i' = \hat{\mathbf{1}}_i - |0\rangle_{ii}\langle 0| - |1\rangle_{ii}\langle 1|$ are the identity operators in the remaining part of the Hilbert space for each subsystem. As is well known, the eigenvalues of $\hat{S}_{2D}$ are at most $\pm 2\sqrt{2}$ [37]. Since the remaining part of the total Bell operator is diagonal, one immediately sees that all eigenvalues corresponding to this part are ± 2. Thus the maximal Bell violation is $2\sqrt{2}$, just as for two 2-dimensional quantum systems. In particular, the maximal violation is independent of the total dimensionality of the two subsystems.

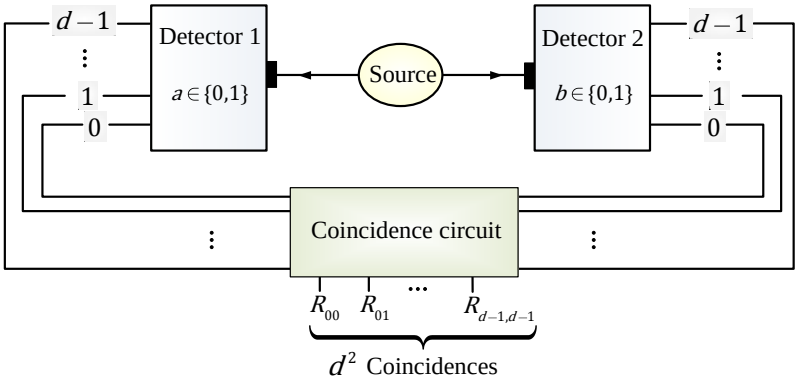

Figure 4.2: Schematic view of the Bell-type test generalised to d outcome measurements. Each of the two detectors has two possible settings. The outputs from the detectors give d^2 different pairwise coincidence rates for each combination of detector settings. The four different combinations of detector settings give in total $4d^2$ coincidence rates, which are used for calculating the generalised Bell parameter S_d.

4.6 Bell inequality violations and entanglement dimension

For high-dimensional quantum systems, one has the option to test not just CHSH-type Bell inequalities, but also Bell-type inequalities that explicitly use measurement settings with more than two outcomes [128, 135, 136]. Violation of such high-dimensional Bell-type inequalities indicate that a local hidden-variable model cannot fully describe the situation. In addition to this, a high violation of such an inequality will indicate that the state is not only entangled, but that the entanglement is of a particular kind. How high the violation should be, and exactly what is implied about the form of the entangled state, of course depends on the details of the particular Bell inequality that is tested. Such bounds are useful for experimental verification e.g. of high-dimensional entanglement. In this, one of course considers standard Bell-type experiments, with measurement settings for which the fair sampling condition (Eq. 4.7) is satisfied.

Now, how high should the violation be in order to guarantee that high-dimensional entanglement was present when the Bell-type inequalities introduced by Collins *et al.* [135] are tested experimentally? These Bell inequalities apply to two d-dimensional systems (qudits), with two observers, two detector settings for each observer, and d outcomes per detector setting (Figure 4.2). They must be satisfied for any local hidden-variable theory,

and can be written as

$$\begin{aligned} S_d &= \sum_{k=0}^{(d/2)-1} \left(1-\frac{2k}{d-1}\right) \{[P(A_0 = B_0 + k) + P(B_0 = A_1 + k + 1) \\ &+ P(A_1 = B_1 + k) + P(B_1 = A_0 + k)] - [P(A_0 = B_0 - k - 1) \\ &+ P(B_0 = A_1 - k) + P(A_1 = B_1 - k - 1) + P(B_1 = A_0 - k - 1)]\} \leq 2, \end{aligned} \tag{4.18}$$

where S_d is the Bell parameter (corresponding to I_d in Ref. [135]). The outcomes of measurements made by two local observers (Alice and Bob) are denoted by $A_a, B_b \in \{0,\ldots,d-1\}$, with the detector settings of Alice and Bob given by $a,b \in \{0,1\}$. $P(A_a = B_b + k)$ denotes the probability that the outcomes A_a and B_b of Alice's and Bob's measurements differ by k modulo d, and similarly for $P(B_b = A_a + k)$, more specifically,

$$\begin{aligned} P(A_a = B_b + k) &= \sum_{j=0}^{d-1} P\left[A_a = j, B_b = (j+k) \bmod d\right] \\ P(B_b = A_a + k) &= \sum_{j=0}^{d-1} P\left[A_a = (j+k) \bmod d, B_b = j\right]. \end{aligned} \tag{4.19}$$

The measurement bases corresponding to the detector settings of Alice and Bob are defined as

$$|v\rangle_a^A = \tfrac{1}{\sqrt{d}} \sum_{j=0}^{d-1} \exp\left[i\frac{2\pi}{d} j(v+\alpha_a)\right] |j\rangle, \;\; |w\rangle_b^B = \tfrac{1}{\sqrt{d}} \sum_{j=0}^{d-1} \exp\left[i\frac{2\pi}{d} j(-w+\beta_b)\right] |j\rangle, \tag{4.20}$$

where $v,w = 0,\ldots,d-1$ label each of the basis states and correspond to the outcomes of Alice's and Bob's measurements respectively. The parameters $\alpha_0 = 0$, $\alpha_1 = 1/2$, $\beta_0 = 1/4$, and $\beta_1 = -1/4$.

A pure state can be considered to have n-dimensional entanglement if its Schmidt number is n. A mixed state will be considered to have n-dimensional entanglement if it cannot be described by a mixture of pure states with individual Schmidt numbers all less than n (see Sec. 1.2.2). To derive a bound on how high S_d in (5.8) should be to guarantee that the state was d-dimensionally entangled, it is again useful to employ the concept of a Bell operator [137] $\hat{S}_d$, for which the Bell parameter is $S_d = Tr(\rho \hat{S}_d)$. (One could of course also derive bounds for S_d that would guarantee $(d-1)$-dimensional entanglement, $(d-2)$-dimensional entanglement, and so on.) Let $s_1, s_2, s_3, \ldots$ be the eigenvalues of $\hat{S}_d$ in descending order of magnitude, and let $|s_1\rangle, |s_2\rangle, |s_3\rangle \ldots$ be the corresponding eigenstates. Then

$$\hat{S}_d = \sum_k s_k |s_k\rangle\langle s_k|, \;\; \text{and} \;\; S_d = \mathrm{Tr}(\hat{\rho}\hat{S}_d) = \sum_k s_k \langle s_k|\hat{\rho}|s_k\rangle. \tag{4.21}$$

Therefore, in order to produce a large violation, $\langle s_k|\hat{\rho}|s_k\rangle$ would need to be large for the

eigenstates $|s_k\rangle$ corresponding to the largest eigenvalues s_k. More precisely, if $\langle s_1|\hat{\rho}|s_1\rangle \leq q$, then it will hold that $S_d \leq qs_1 + (1-q)s_2$. Equivalently,

$$S_d = \mathrm{Tr}(\hat{\rho}\hat{S}_d) > qs_1 + (1-q)s_2 \implies \langle s_1|\hat{\rho}|s_1\rangle > q. \tag{4.22}$$

The state with at most $(d-1)$-dimensional entanglement and the largest possible $\langle s_1|\hat{\rho}|s_1\rangle$ can be constructed in the following way. It is found here that all the $|s_1\rangle$ have the form $|s_1\rangle = \sum_{k=1}^{d} c_k|k,k\rangle$ with all c_k real for $d = 2,\ldots,32$ (and conjectured that this holds for all d). Here $|k,j\rangle \equiv |k\rangle \otimes |j\rangle$. The state with the greatest overlap with $|s_1\rangle$ but having only $(d-1)$-dimensional entanglement is then given by $\hat{\rho} = |\tilde{s}_1\rangle\langle\tilde{s}_1|$, with

$$|\tilde{s}_1\rangle = K \sum_{\substack{j=1 \\ j\neq j_0}}^{d} c_j|j,j\rangle; \quad |c_{j_0}| = \min_j\{|c_j|\}, \tag{4.23}$$

where $K = (\sum_{\substack{j=1 \\ j\neq j_0}}^{d} |c_j|^2)^{-1/2}$.

Therefore, if the Bell violation S_d for a tested state $\hat{\rho}$ exceeds the level S_d^{bound},

$$S_d > S_d^{\mathrm{bound}} = |\langle\tilde{s}_1|s_1\rangle|^2 s_1 + (1-|\langle\tilde{s}_1|s_1\rangle|^2)s_2, \tag{4.24}$$

then it must hold that $\langle s_1|\hat{\rho}|s_1\rangle > |\langle\tilde{s}_1|s_1\rangle|^2$. Violations above S_d^{bound} cannot be produced unless the tested state has (at least) d-dimensional entanglement. This bound is not tight, that is, the true bound for S_d above which the state must contain d-dimensional entanglement is somewhat lower. However, the calculation of the tight bound would involve much more complicated optimisation procedures. Also, given other actual experimental data, a more involved maximisation procedure can be performed to ascertain how many dimensions must have been involved in the entanglement when $S_d < S_d^{\mathrm{bound}}$ [136]. Even obtaining an explicit value for the "simple" bound in (4.24) of course involves diagonalising the Bell operators $\hat{S}_d$.

Fig. 4.3 shows four kinds of Bell violations as functions of d for up to $d = 32$. Numerical values are found in Table 4.1. The plots show the maximum possible violations of the inequalities $S_d \leq 2$, that is, s_1 as a function of d, using black dots. This is the maximum eigenvalue s_1 of the corresponding Bell operator. For comparison, the plot also shows the second largest eigenvalues, s_2, again as a function of d, using filled dark blue squares. The open green diamonds show the violations produced by maximally entangled states of the form $|\psi_{\mathrm{me}}\rangle = (1/\sqrt{d})\sum_{k=0}^{d-1}|k\rangle \otimes |k\rangle$. Finally, the red stars show the bound S_d^{bound}. Above this level, the violation could not have been produced by a state with only $(d-1)$-dimensional entanglement.

From Fig. 4.3 (and Table 4.1) one sees that below $d = 6$, the violation produced by a maximally entangled state cannot be reproduced by a $(d-1)$-dimensionally entangled

Table 4.1: Table of s_1, s_2, and numerical values of a bound on the generalised Bell parameter for states having no more than $(d-1)$-dimensional entanglement, S_d^{bound}.

No. of dimensions d	Largest eigenvalue of $\hat{S}_d$, s_1	2nd largest eigenvalue of $\hat{S}_d$, s_2	Bound S_d^{bound}
2	2.82843	0.	0.
3	2.91485	1.1547	2.36241
4	2.9727	1.59551	2.67794
5	3.01571	1.84344	2.84728
6	3.0497	2.00816	2.92993
7	3.07765	2.12826	2.99175
8	3.10128	2.22113	3.03333
9	3.12168	2.29593	3.06793
10	3.13959	2.35799	3.09462
11	3.1555	2.41067	3.11795
12	3.16979	2.45618	3.13728
13	3.18274	2.49606	3.15464
14	3.19457	2.53143	3.16967
15	3.20543	2.56311	3.1834
16	3.21546	2.59172	3.1956
17	3.22477	2.61774	3.2069
18	3.23346	2.64157	3.21714
19	3.24158	2.6635	3.2267
20	3.24921	2.68378	3.23549
21	3.2564	2.70262	3.24376
22	3.26318	2.7202	3.25144
23	3.26961	2.73664	3.2587
24	3.27571	2.75208	3.2655
25	3.28151	2.76661	3.27197
26	3.28704	2.78033	3.27806
27	3.29232	2.79331	3.28388
28	3.29737	2.80562	3.28939
29	3.3022	2.81731	3.29466
30	3.30684	2.82845	3.29968
31	3.31129	2.83907	3.3045
32	3.31558	2.84921	3.30911

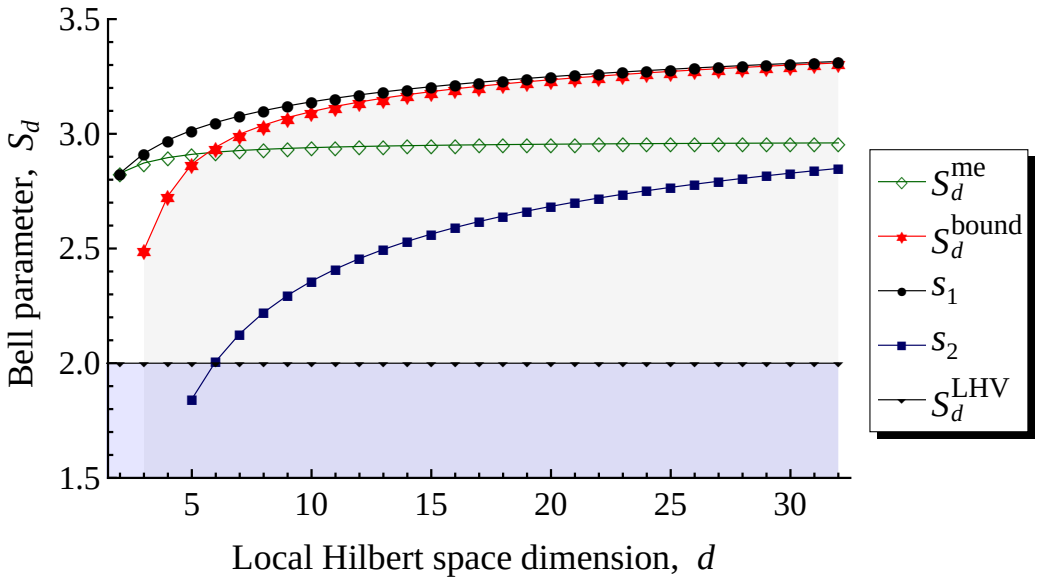

Figure 4.3: Plots of Bell parameters as a function of the number of dimensions d. The figure shows the first and second largest eigenvalues of the Bell operator $\hat{S}_d$, s_1 and s_2 respectively; Bell violation with a maximally entangled state S_d^{me}; the maximum possible violation with a state with at most $(d-1)$-dimensional entanglement, S_d^{bound}; and the local hidden-variable (LHV) limit S_d^{LHV}. The numerical values are shown in Table 4.1.

state. To witness the entanglement dimension for $d \geq 6$ using our bound, one would need to obtain violations larger than can be produced by a state maximally entangled in d dimensions, and the margin of difference increases with d. As mentioned above, it is possible, with very similar methods, to derive bounds for whether the state was entangled in at least $(d-2)$, $(d-3)$, ... dimensions. To highlight the experimental feasibility of verifying high-dimensional entanglement using this bound with current or shortly available technologies, note that a standard deviation of 0.02 is sufficient in experiments with up to $d = 16$. Also, using this bound, the single result of $S_4 = 2.87 \pm 0.04$ of the experiment reported in Chapter 5 is a demonstration of 4-dimensional entanglement.

4.7 Conclusions

In tests of Bell inequalities, the fair sampling assumption is violated if different measurements on one subsystem do not sample the state space in an equivalent way. This is relevant especially when using high-dimensional quantum systems, for which violation of fair sampling may result even if detection efficiency is perfect within the sampled subspaces. If care is not taken, then the fair sampling assumption may be violated in explicit ways for current experimental setups. This was illustrated by examples.

In experiments to test Bell inequalities, it is crucial to check whether the measurements one aims to use do satisfy the fair sampling condition, and if not, what the appropri-

ate bounds are for local hidden-variable theories, separable quantum states and entangled quantum states. Experimental violation of Tsirelson's bound is due to a violation of the fair sampling condition and does not necessarily indicate that more than 2-dimensional entanglement was present.

For d-dimensional quantum systems, one can also test Bell-type inequalities that use measurements with d outcomes per measurement setting. A high enough violation of such a generalised Bell inequality indicates that the state not only must have been entangled, but that the entanglement must have been of a particular kind. A simple bound is derived in this chapter which guarantees that the tested state must have been d-dimensionally entangled. Such bounds are useful for experimental verification of high-dimensional entanglement. Interestingly, combinations of tests using different values of d can provide more relaxed bounds on the dimensionality of entanglement as further explored in Chapter 5.

CHAPTER 5

Experimental eleven-dimensional entanglement

5.1 Introduction

Quantum entanglement [34, 138] plays a vital role in many quantum information and communication tasks [139]. Entangled states of higher dimensional systems are of great interest due to the extended possibilities they provide. For example, they allow the realisation of new types of quantum information schemes that can offer higher information-density coding and greater resilience to errors than can be achieved with entangled two-dimensional systems (see [140] and references therein). Closing the detection loophole in Bell test experiments is also more experimentally feasible when higher dimensional entangled systems are used [116]. This chapter describes experiments which measure previously untested correlations between two photons to experimentally demonstrate high-dimensional entangled states. The experimental techniques and measurement methods enable violations of Bell-type inequalities generalised to d-dimensional systems [135] with up to $d = 12$. Furthermore, the violations are strong enough to indicate genuine 11-dimensional entanglement. The experiments use photons entangled in orbital angular momentum (OAM) [134], generated through spontaneous parametric down-conversion (SPDC) [7, 141], and manipulated using computer controlled holograms. The main contributions highlighted in this chapter are the experimental methods used to detect high-dimensional entanglement through Bell inequality violation, the analysis of the experimental results, and the numerical work involved in proving high-dimensional entanglement.

Quantum information tasks requiring high dimensional bipartite entanglement include teleportation using qudits [10, 20], generalised dense coding (i.e., with pairs of entangled d-level systems) [21], and some quantum key distribution protocols [9]. More generally, schemes like quantum secret sharing [22], and measurement based quantum computation [23], apply multi-particle entanglement. These are promising applications, especially in view of recent progress in the development of quantum repeaters (see [142] and references therein). However, practical applications of such protocols are only conceivable when it is possible to experimentally prepare, and moreover, detect high-dimensional en-

tangled states. Therefore, the ability to verify high-dimensional entanglement between physical qudits is of crucial importance. Indeed, much progress has generally been made on the generation and detection of high-dimensional entangled states (please see [143] and references within).

This chapter reports the experimental investigation of high-dimensional, two-photon entangled states. It focuses on photon OAM entangled states generated by SPDC, and demonstrates genuine high-dimensional entanglement using violations of generalised Bell-type inequalities [135]. Previously, qutrit Bell-type tests have been performed using photon OAM to verify 3-dimensional entanglement (see [128] and references within). In addition to testing whether correlations in nature can be explained by local realist theories [144], the violation of Bell-type inequalities may be used to demonstrate the presence of entanglement. Bell-type experiments have been performed using two-dimensional subspaces of the OAM state space of photons [130, 145] and experiments have demonstrated 2-dimensional entanglement using up to twenty different 2-dimensional subspaces [146]. Careful studies have also been carried out to describe how specific detector characteristics bound the dimensionality of the measured OAM states in photons generated by SPDC using Shannon dimensionality [147].

This chapter explores the generation and detection of entanglement in larger subspaces. This experimental study of high-dimensional entanglement is based on the theoretical work of Collins *et al.* [135] mentioned in Chapter 4, which was applied in experiments for qutrits encoded in the OAM states of photons [128, 129]. The experimental study reported here involves encoding qudits using the OAM states of photons, with eigenstates defined by the azimuthal index ℓ. These states arise from the solution of the paraxial wave equation in its cylindrical co-ordinate representation, and are the Laguerre-Gaussian modes $LG_{p,\ell}$, so called because they are light beams having a Laguerre-Gaussian amplitude distribution.

5.2 Generalised Bell inequalities

Collins *et al.* [135] showed that, for correlations which can be described by theories based on local realism [34], a family of Bell-type parameters S_d satisfy the inequalities

$$S_d^{(\text{localrealism})} \leq 2, \text{ for all } d \geq 2. \tag{5.1}$$

Alternatively, if quantum mechanics is assumed to hold, then the violation of an inequality of type (5.1) indicates the presence of entanglement.

The parameters S_d are calculated using coincidence probabilities for measurements made locally by two observers, 'Alice' and 'Bob', on their respective subsystems, which

in this case are the signal and idler photons from an SPDC source. Alice's detector has two settings labelled by $a \in \{0,1\}$ with d outcomes for each setting, and similarly for Bob's detector with settings $b \in \{0,1\}$. The measurement bases corresponding to the detector settings of Alice and Bob are defined as

$$|v\rangle_a^A = \tfrac{1}{\sqrt{d}} \sum_{j=0}^{d-1} \exp\left[i\frac{2\pi}{d} j(v+\alpha_a)\right] |j\rangle, \tag{5.2}$$

$$|w\rangle_b^B = \tfrac{1}{\sqrt{d}} \sum_{j=0}^{d-1} \exp\left[i\frac{2\pi}{d} j(-w+\beta_b)\right] |j\rangle, \tag{5.3}$$

where v and w both run from 0 to $d-1$ and denote the outcomes of Alice's and Bob's measurements respectively, and the parameters $\alpha_0 = 0$, $\alpha_1 = 1/2$, $\beta_0 = 1/4$, and $\beta_1 = -1/4$.

The measurement bases $\{|v\rangle_a^A\}$ and $\{|w\rangle_a^A\}$ have been shown [116, 148] to maximise the violations of inequality (5.1) for the maximally entangled state of two d-dimensional systems given by $|\psi\rangle = \frac{1}{\sqrt{d}} \sum_{j=0}^{d-1} |j\rangle_A \otimes |j\rangle_B$. It turns out that we are able to parametrise these d-dimensional measurement basis states with 'mode analyser' angles θ_A and θ_B, and write them in terms of photon OAM in the form

$$|v\rangle_a^A \equiv |\theta_A^a\rangle = \frac{1}{\sqrt{d}} \sum_{\ell=-[d/2]}^{\ell=+[d/2]} \exp\left[i\theta_A^a g(\ell)\right] |\ell\rangle, \text{ and}$$

$$|w\rangle_b^B \equiv |\theta_B^b\rangle = \frac{1}{\sqrt{d}} \sum_{\ell=-[\frac{d}{2}]}^{\ell=+[\frac{d}{2}]} \exp\left[i\theta_B^b g(\ell)\right] |\ell\rangle, \tag{5.4}$$

where $\theta_A^a = (v + a/2)\, 2\pi/d$, and $\theta_B^b = \left[-w + 1/4\,(-1)^b\right] 2\pi/d$. The function $g(\ell)$ is defined as

$$g(\ell) = \ell + [\tfrac{d}{2}] + (d \bmod 2)\mathrm{u}(\ell), \tag{5.5}$$

where $[x]$ is the integer part of x, and $\mathrm{u}(\ell)$ is the discrete unit step function.

For a maximally entangled state

$$|\Phi\rangle = \tfrac{1}{\sqrt{d}} \sum_{\ell=-[d/2]}^{[d/2]} h(\ell) |\ell\rangle_A \otimes |-\ell\rangle_B, \tag{5.6}$$

where $h(\ell) = 1$ for all ℓ when d is odd, and $h(\ell \neq 0) = 1$, $h(0) = 0$ when d is even, the coincidence rate of detecting one photon in state $|\theta_A\rangle$ and the other in state $|\theta_B\rangle$ is

proportional to

$$C(\theta_A,\theta_B) = |\langle\theta_A|\langle\theta_B||\Phi\rangle|^2 \propto \frac{\cos(d(\theta_A-\theta_B))-1}{d^3[\cos(\theta_A-\theta_B)-1]}. \tag{5.7}$$

5.2.1 Bell operator

The Bell parameter S_d can be expressed as the expectation value of a quantum mechanical observable, referred to here as the *generalised Bell operator* and denoted as $\hat{S}_d$. The expressions for $\hat{S}_d$ and the operators $\hat{S}_2$, $\hat{S}_3$ are obtained below. The generalised Bell-type parameter derived in [135] can be written as

$$\begin{aligned} S_d = \sum_{k=0}^{[d/2]-1} \left(1-\tfrac{2k}{d-1}\right)\{ &+[P(A_0=B_0+k)+P(B_0=A_1+k+1)+P(A_1=B_1+k) \\ &+P(B_1=A_0+k)]-[P(A_0=B_0-k-1)+P(B_0=A_1-k) \\ &+P(A_1=B_1-k-1)+P(B_1=A_0-k-1)]\}. \end{aligned} \tag{5.8}$$

Here, d is the number of dimensions, and S_d is the Bell parameter, denoted as I_d in [135]. The measurement outcomes $A_i, B_i \in \{0,\ldots,d-1\}$. $P(A_a = B_b)$ denotes the probability that the outcome A_a of Alice's measurement is the same as the outcome B_b of Bob's measurement, for the respective detector settings $a,b \in \{0,1\}$, (denoted in [135] as $a,b \in \{1,2\}$). That is,

$$P(A_a = B_b) = \sum_{j=0}^{d-1} P(A_a = j, B_b = j). \tag{5.9}$$

In a similar way,

$$P(A_a = B_b + k) = \sum_{j=0}^{d-1} P\left[A_a = j, B_b = (j+k) \bmod d\right] \tag{5.10}$$

is the probability that the outcome B_b differs from A_a by k, modulo d. We also have

$$P(B_b = A_a + k) = \sum_{j=0}^{d-1} P\left[A_a = (j+k) \bmod d, B_b = j\right]. \tag{5.11}$$

Each joint probability is obtained from the photon coincidence count rate $C(A_a = i, B_b = j)$ divided by the sum $C_T(a,b)$ of all coincidence rates for a given combination of detector settings for Alice and Bob, $C_T(a,b) = \sum_{i',j'=0}^{d-1} C(A_a = i', B_b = j')$.

The d basis states correspond to orbital angular momentum (OAM) eigenstates, with an OAM of $\ell\hbar$ per photon. For odd d, ℓ runs from $-(d-1)/2$ to $(d-1)/2$, and for even d, ℓ runs from $-d/2$ to $+d/2$, but without the $\ell = 0$ state. These basis states are denoted as

$|j\rangle$, where $j = 0,\ldots,d-1$. For the signal photon state and odd d, we choose $j = \ell + (d-1)/2$, and for even d, similarly, $j = 0$ corresponds to $\ell = d/2$, $j = 1$ corresponds to $\ell = d/2+1$, and so on, until $j = d-1$ which corresponds to $\ell = d/2$ ($\ell = 0$ is missing for even d). For the idler photon the ordering is the opposite, with low values of j corresponding to high values of ℓ. That is, $j = -\ell + (d-1)/2$ for odd d, and for even d, $j = 0$ corresponds to $\ell = d/2$ and so on, until $j = d-1$ which corresponds to $\ell = -d/2$ (again without the $\ell = 0$ state). In short, a state $|\ell\rangle \otimes |-\ell\rangle = |j\rangle \otimes |j\rangle = |j,j\rangle$, with the connection between ℓ and j as above.

As mentioned above, the Bell-type parameter S_d can be written for a given state $\hat{\rho}$ as the expectation value of a Bell operator $\hat{S}_d$, that is,

$$S_d(\hat{\rho}) = Tr(\hat{S}_d\hat{\rho}).$$

Let us define operators $\hat{P}(A_a = B_b + k)$ as

$$\hat{P}(A_a = B_b + k) = \sum_{r=0}^{d-1} |r\rangle_a^A |(r+k) \bmod d\rangle_b^{BB}\langle(r+k) \bmod d|_a^A\langle r|, \tag{5.12}$$

and operators $\hat{P}(B_b = A_a + k)$ as

$$\hat{P}(B_b = A_a + k) = \sum_{r=0}^{d-1} |(r+k) \bmod d\rangle_a^A |r\rangle_b^{BB}\langle r|_a^A\langle(r+k) \bmod d|, \tag{5.13}$$

where the measurement basis states $|v\rangle_a^A$, $|w\rangle_b^B$ for measurement settings a and b and $v,w = 0,\ldots,d-1$ are as defined in Equations (5.2) to (5.5).

From Equation 5.8, the generalised Bell operator can then be written as

$$\begin{aligned}\hat{S}_d = \sum_{k=0}^{[d/2]-1} \left(1 - \tfrac{2k}{d-1}\right) \{ &+ [\hat{P}(A_0 = B_0 + k) + \hat{P}(B_0 = A_1 + k + 1) + \\ &\hat{P}(A_1 = B_1 + k) + \hat{P}(B_1 = A_0 + k)] - [\hat{P}(A_0 = B_0 - k - 1) + \\ &\hat{P}(B_0 = A_1 - k) + \hat{P}(A_1 = B_1 - k - 1 + \hat{P}(B_1 = A_0 - k - 1)]\}. \end{aligned} \tag{5.14}$$

For example, the Bell operators for $d = 2$ and $d = 3$ are

$$\hat{S}_2 = \begin{pmatrix} 0 & 0 & 0 & 2\sqrt{2} \\ 0 & 0 & 0 & 0 \\ 0 & 0 & 0 & 0 \\ 2\sqrt{2} & 0 & 0 & 0 \end{pmatrix}, \quad \hat{S}_3 = \begin{pmatrix} 0 & 0 & 0 & 0 & \frac{2}{\sqrt{3}} & 0 & 0 & 0 & 2 \\ 0 & 0 & 0 & 0 & 0 & \frac{2}{\sqrt{3}} & 0 & 0 & 0 \\ 0 & 0 & 0 & 0 & 0 & 0 & 0 & 0 & 0 \\ 0 & 0 & 0 & 0 & 0 & 0 & 0 & \frac{2}{\sqrt{3}} & 0 \\ \frac{2}{\sqrt{3}} & 0 & 0 & 0 & 0 & 0 & 0 & 0 & \frac{2}{\sqrt{3}} \\ 0 & \frac{2}{\sqrt{3}} & 0 & 0 & 0 & 0 & 0 & 0 & 0 \\ 0 & 0 & 0 & 0 & 0 & 0 & 0 & 0 & 0 \\ 0 & 0 & 0 & \frac{2}{\sqrt{3}} & 0 & 0 & 0 & 0 & 0 \\ 2 & 0 & 0 & 0 & \frac{2}{\sqrt{3}} & 0 & 0 & 0 & 0 \end{pmatrix}, \tag{5.15}$$

where the basis states are ordered as $|0,0\rangle$, $|0,1\rangle$, $|0,2\rangle$, …, $|0,d-1\rangle$, $|1,0\rangle$, $|1,1\rangle$, …, $|1,d-1\rangle$, $|2,0\rangle$, …, $|d-1,d-1\rangle$.

Careful inspection shows that all diagonal elements of $\hat{S}_d$ are equal to zero in the OAM basis $|j,k\rangle$, as all diagonal elements of the operators $\hat{P}(A_a = B_b + k)$ and the operators $\hat{P}(B_b = A_a + k)$ are equal to $1/d^2$. Also, we note that all elements S_{jk} of the Bell operators, written in the OAM basis, are nonnegative. This in fact holds for all Bell operators until $d = 32$, which leads one to suspect that it holds generally.

Clearly, the maximal value of the Bell parameter, that is, the maximal Bell violation, is the largest eigenvalue of the Bell operator, and this largest violation is obtained for the corresponding eigenstate. Interestingly, this eigenstate is not in general equal to a maximally entangled state. Table 5.1 lists the Bell parameter values theoretically obtained for the maximally entangled state $|\psi\rangle = (1/\sqrt{d})\sum_{j=0}^{d-1}|j,j\rangle$, together with the maximal values of the Bell parameter, which, as already stated above, are equal to the largest eigenvalue of the respective Bell operator [137]. For any $\hat{\rho}$, the corresponding Bell violation is a linear combination of the eigenvalues of $\hat{S}_d$, since

$$S_d = Tr(\hat{\rho}\hat{S}_d) = \sum_k s_k \langle s_k|\hat{\rho}|s_k\rangle, \tag{5.16}$$

where s_k and $|s_k\rangle$ are the eigenvalues and eigenvectors of $\hat{S}_d$, and therefore $\sum_k \langle s_k|\hat{\rho}|s_k\rangle = \mathrm{Tr}\hat{\rho} = 1$. The five largest eigenvalues s_k of $\hat{S}_{11}$ are shown in Table 5.2, along with the form of the corresponding eigenstates $|s_k\rangle$.

5.3 Experimental setup

In the experimental setup (see Figure 5.1), OAM entangled photons are generated through a frequency degenerate type-I SPDC process, and the OAM state is manipulated with

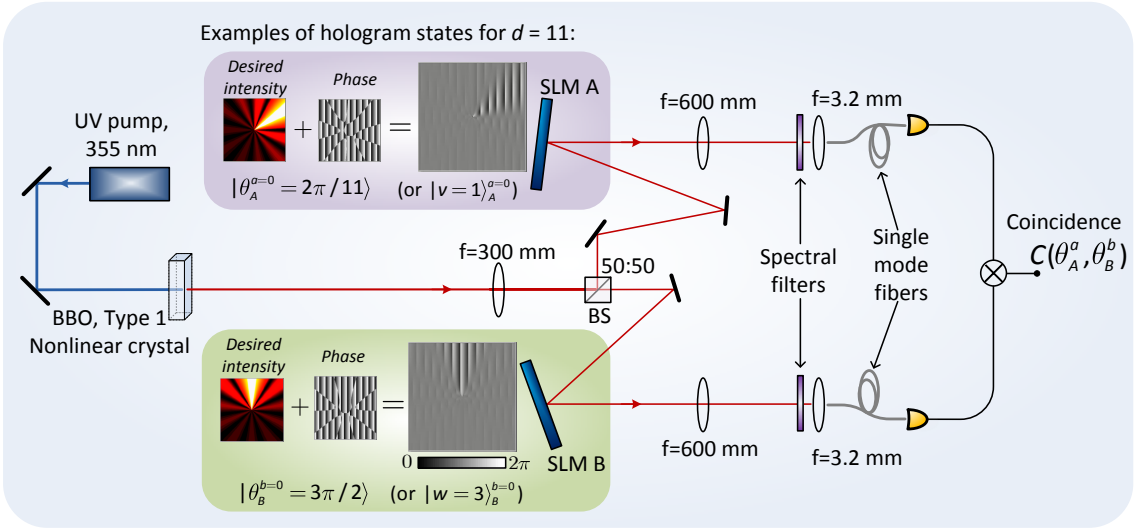

Figure 5.1: Schematic of experimental setup for violations of Bell-type inequalities. $C(A_a = v, B_b = w)$ or $C(\theta_A^a, \theta_B^b)$ is the coincidence count rate when SLM A is in state $|v\rangle_a^A$ or $|\theta_A^a\rangle$ and SLM B is in state $|w\rangle_b^B$ or $|\theta_B^b\rangle$ respectively.

computer controlled spatial light modulators (SLM) acting as reconfigurable holograms. Conservation of angular momentum ensures that if the signal photon is in the mode specified by $|\ell\rangle$, the corresponding idler photon can only be in the mode $|-\ell\rangle$. Assuming that angular momentum is conserved [141], a pure state of the two photon field produced will have the form

$$|\Psi\rangle = \sum_{\ell=-\infty}^{\ell=\infty} c_\ell \, |\ell\rangle_A \otimes |-\ell\rangle_B, \tag{5.17}$$

where subscripts A and B label the signal and idler photons respectively, $|c_\ell|^2$ is the probability to create a photon pair with OAM $\pm\ell\hbar$ and $|\ell\rangle$ is the OAM eigenmode with mode number ℓ.

5.4 Experimental methods

In the experiments, computer controlled SLMs (Hamamatsu) operating in reflection mode with a resolution of 600×600 pixels manipulate/select OAM states for detection. In the detection, the SLMs are prepared in the states defined in Equations (5.4) respectively. By the expression that the SLM is 'prepared' in a given state $|\psi\rangle$, it is meant here that, on reflection, it transforms the OAM state $|\psi\rangle$ to a Gaussian beam state $|\ell = 0\rangle$. The reflected photon is then coupled into a single-mode fibre which feeds a single photon detector. Since only the $|\ell = 0\rangle$ mode couples into the fibre, a count in the detector indicates a detection of the state in which the SLM was prepared. The hologram generation algorithm introduced in [149] is applied to configure the SLMs.

Figure 5.1 shows the schematic diagram of the experimental setup as well as examples

of SLM settings used where $d = 11$. For the SPDC, the experiment uses a pump beam, with $\ell = 0$, produced by a frequency tripled, mode-locked Nd-YAG laser with an average output power of 150 mW at 355 nm. The collimated laser beam is normally incident on a 3 mm long BBO crystal cut for type-I collinear phase matching. A 50:50 beam splitter (BS) then separates the co-propagating OAM entangled photons probabilistically into the signal and idler paths. Spectral filters with 10 nm bandwidth are used to reduce the detection of noise photons. The coincidence resolving time is 10 ns and an integration time of 20 s is used for the measurements.

For tests within a d-dimensional subspace and for odd d, we choose the modes $\ell = -(d-1)/2, \ldots, 0, \ldots, (d-1)/2$ as the computational basis states $|j\rangle$ in Equations 5.2 and 5.3, where $j = 0, \ldots d-1$. For even d, we use $\ell = -d/2, \ldots, -1, 1, \ldots, d/2$, omitting the $\ell = 0$ mode. A projection of the SPDC output state onto a d-dimensional subspace results in a non-maximally entangled state due to the limited *spiral bandwidth* [150].

The spiral bandwidth is an important factor affecting the amount of entanglement of the OAM correlated photons for a given selected subspace of the OAM Hilbert space. The square of a Lorentzian function

$$f(\ell, \gamma) = A\gamma / \left(\gamma^2 + \ell^2\right), \tag{5.18}$$

gives a good fit to the experimentally measured coincidence rates, which are proportional to $|c_\ell|^2$ and presented in Figure 5.2. The parameter γ specifies the half-width at half-maximum (HWHM) of $f(\ell, \gamma)$, and A is a normalisation constant. We identify γ with the effective quantum spiral bandwidth. For the SPDC source used here, γ is obtained to be 7.58. As mentioned before, the finiteness of the spiral bandwidth causes a projection of the SPDC output state onto a d-dimensional subspace to result in a non-maximally entangled state, which in turn might not violate the tested Bell inequality.

5.5 Procrustean entanglement concentration

To enhance the detectable entanglement, we use the so-called procrustean method of entanglement concentration [132]. This is generally done by means of a filtering technique which equalises the mode amplitudes, thereby probabilistically enhancing the entanglement of the two-photon state [151]. This can be achieved by applying local operations to one or both of the signal and idler photons. We choose local operations matched to the spiral bandwidth measurement for the SPDC source (please see below), so as to obtain a close approximation to a maximally entangled state. The method applied in [133] uses lenses for equalising amplitudes in a superposition of three OAM modes. We however use alterations of the diffraction efficiencies of blazed phase gratings in the SLMs to achieve

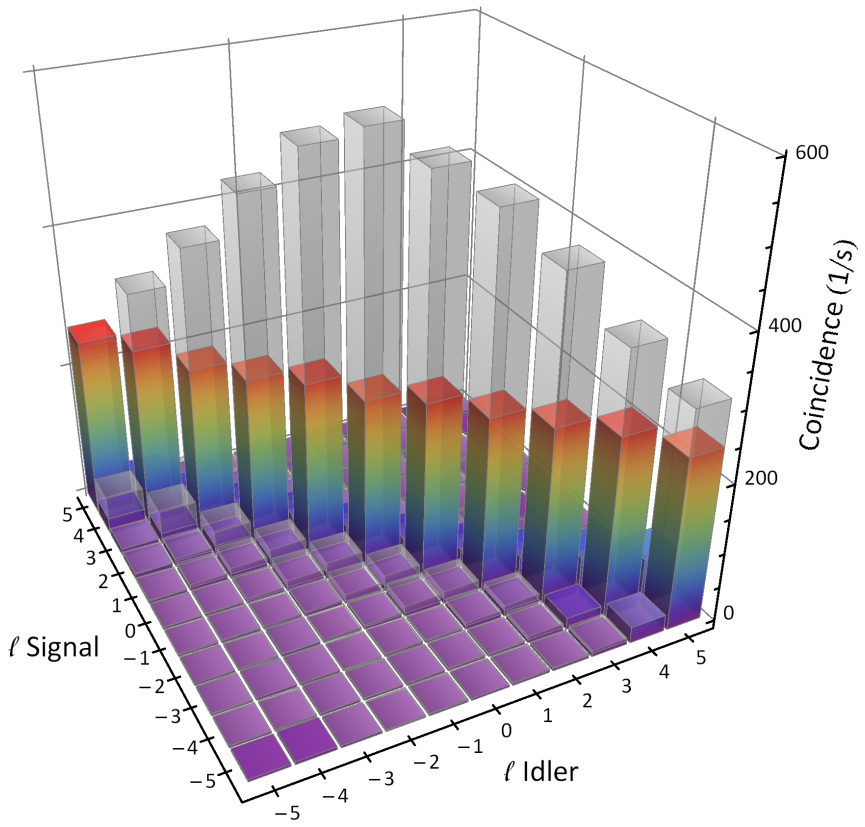

Figure 5.2: Experimental coincidence rates proportional to the probability of measuring the state $|\ell_s\rangle \otimes |\ell_i\rangle$ with $\ell_s, \ell_i = -5, \ldots, +5$. The coloured and greyed-out bars depict the measurement results with and without the application of procrustean filtering respectively (see Section 5.5). The measurement time was 20 s for each combination of ℓ_s and ℓ_i.

this goal for up to fourteen modes. Figure 5.2 contrasts the results of coincidence measurements with and without procrustean filtering, with the SLMs in the state $\{|\ell_A\rangle \otimes |\ell_B\rangle\}$ where $\ell_A, \ell_B \in \{-5, \ldots, +5\}$.

The effect of procrustean filtering is described below in terms of measurement operators. Let us denote the unfiltered state from the SPDC source as $\hat{\rho}_i$. The procrustean entanglement concentration we perform can be considered to be a two-outcome generalised measurement (POM or probability operator measure) with measurement operators $\hat{O}_1^\dagger \hat{O}_1$ and $\hat{O}_2^\dagger \hat{O}_2$. The Hermitian operators $\hat{O}_1$ and $\hat{O}_2$ satisfy $\hat{O}_1^\dagger \hat{O}_1 + \hat{O}_2^\dagger \hat{O}_2 = \mathbf{1}$ in the relevant Hilbert space. Furthermore, the procedure can be performed using only local operations on the signal and idler beams. The filtered state is obtained conditioned on outcome 1, and is given by

$$\hat{\rho}_f = \frac{\hat{O}_1^\dagger \hat{\rho}_i \hat{O}_1}{\mathrm{Tr}(\hat{O}_1^\dagger \hat{\rho}_i \hat{O}_1)}. \tag{5.19}$$

If outcome 2 is obtained, then the filtering has failed, and in the experiment, one can think

of the photon as having been absorbed, leaving the vacuum state,

$$\hat{O}_2^\dagger \hat{\rho}_i \hat{O}_2 / \mathrm{Tr}[\hat{O}_2^\dagger \hat{\rho}_i \hat{O}_2)] = |\mathrm{vac}\rangle\langle\mathrm{vac}|. \tag{5.20}$$

Using the filtered state $\hat{\rho}_f$, the parameter S_d is

$$S_d = Tr(\hat{\rho}_f \hat{S}_d) = \mathrm{Tr}\left[\frac{\hat{O}^\dagger \hat{\rho}_i \hat{O}}{\mathrm{Tr}(\hat{O}^\dagger \hat{\rho}_i \hat{O})} \hat{S}_d\right]. \tag{5.21}$$

Since the purpose of the experiment is to demonstrate entanglement, within the framework of quantum mechanics (i.e., assuming that we are testing some quantum mechanical state for entanglement), it is important to note that the local filtering can produce neither the appearance of entanglement nor the violation of a Bell inequality from a separable state. Any separable state can be written as $\hat{\rho} = \sum_m p_m \hat{\rho}_{m,A} \otimes \hat{\rho}_{m,B}$. After filtering, we have $\hat{\rho}_f \propto \hat{O_1}^\dagger \hat{\rho} \hat{O_1} = \sum_m p_m (\hat{o}\hat{\rho}_{m,A}\hat{o}) \otimes (\hat{o}\hat{\rho}_{m,B}\hat{o})$, which is just another separable state. No separable state can produce a violation of any of the inequalities $S_d \leq 2$.

5.6 Experimental results

The key result of this chapter is displayed in Figure 5.3, which shows a plot of experimental values of parameter S_d as a function of the number of dimensions d, using $LG_{p,\ell}$ with all radial modes (all p), i.e., the ℓ states of the photons are used irrespective of their radial state (denoted by p). The plot compares theoretically predicted violations for a maximally entangled state, the experimental readings and the local hidden variable (LHV) limit. The maximum possible violations (shown in Table 5.1) are slightly larger than the corresponding violations produced by a maximally entangled state. Violations persist up to as much as $d = 12$ when entanglement concentration [132] is applied. We find $S_{11} = 2.39 \pm 0.07$ and $S_{12} = 2.24 \pm 0.08$, which clearly violate $S_d \leq 2$ (see also Table 5.3). In the corresponding experiment using $LG_{p,\ell}$ modes with only $p = 0$, violations are obtained up to $d = 11$. Without procrustean entanglement concentration, violations persist for only up to $d = 9$ (please see Figure 5.4). Above $d \sim 11$, and the strength of the filtered signal becomes so low that noise begins to overshadow the quantum correlations.

The procrustean filter applied for all the experiments was by means of local operations of the form $\hat{O}_1 = \hat{O}_A \otimes \hat{O}_B$, where $\hat{O}_A = \hat{O}_B \equiv \hat{o}$ is approximately a diagonal matrix. For d=11, $\hat{o}$ has diagonal elements (1.00, 0.97, 0.94, 0.92, 0.91, 0.90, 0.91, 0.92, 0.93, 0.95, 0.97). Figure 5.2 compares the results of coincidence measurements with and without the use of procrustean entanglement concentration.

The disadvantage of the procrustean method is the associated reduction in the number of detected photons and larger experimental error bars on the Bell parameters. The plot

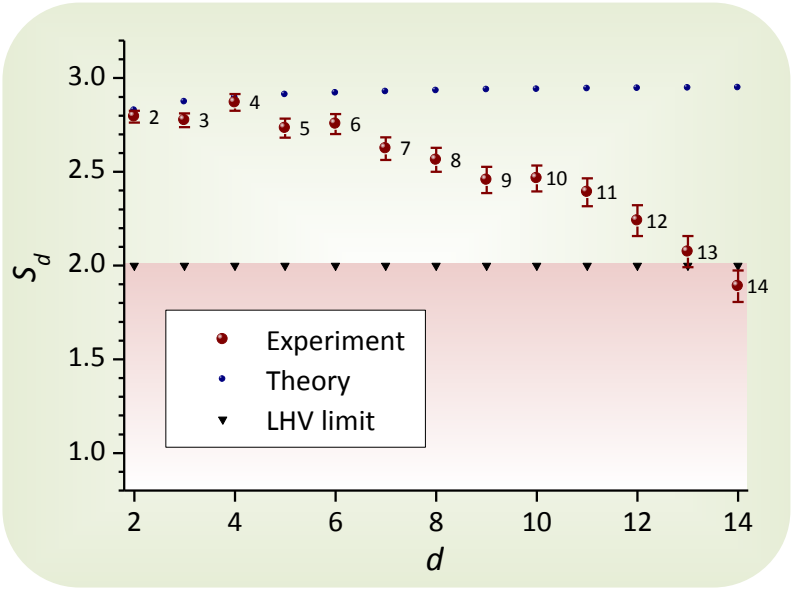

Figure 5.3: Experimental Bell-type parameter S_d versus number of dimensions d. $S_d > 2$ violates local realism for any $d \geq 2$. The plot compares the theoretically predicted violations by a maximally entangled state and the local hidden variable (LHV) limit with the experiments. Violations are observed for up to $d = 12$. The experimental error bars account only for uncertainty due to measurement shot noise (Poisson statistics).

of S_d versus d using $LG_{p,\ell}$ (all p) modes with no procrustean filtering is shown in Figure 5.4 (a). The plotted numerical values are displayed in Table 5.4. The results obtained with procrustean filtering applied (Figure 5.3) show larger error bars than the those without procrustean filtering (Figure 5.4 (a)). Even larger errors bars were obtained when the experiment was performed with radial index p of the detected beams restricted to only $p = 0$, i.e., using $LG_{p=0,\ell}$ modes. In this case, the state $|\ell\rangle$ means $|p = 0, \ell\rangle$. The data (Table 5.5) is plotted in Figure 5.4 (b). This figure compares theoretically predicted violations for a maximally entangled state, the experimental results and the local hidden variable (LHV) limit. Again, the corresponding theoretical maximal violations are shown in Table 5.1. Using only modes with radial index p=0, one observes increased error bars and violations only up to $d = 11$. This is due to the reduced count rates resulting from the detection of only $p = 0$ states.

Figure 5.5 shows an example of the experimental data points for the self normalised coincidence rates as function of the relative angle $(\theta_A - \theta_B)$ using $d = 11$. There, the theoretical prediction for the coincidence function in Equation 5.7 for a state with maximal 11-dimensional entanglement is fitted to the experimental coincidence data obtained using the mode analyser settings defined in Equation 5.4 for $d = 11$, with only the vertical offset and amplitude left as free parameters. The observed fringes are seen to closely match those theoretically obtained for a state with maximal 11-dimensional entanglement. Coincidence curves are also obtained using $LG_{p=0,\ell}$ modes, i.e. with the radial index p

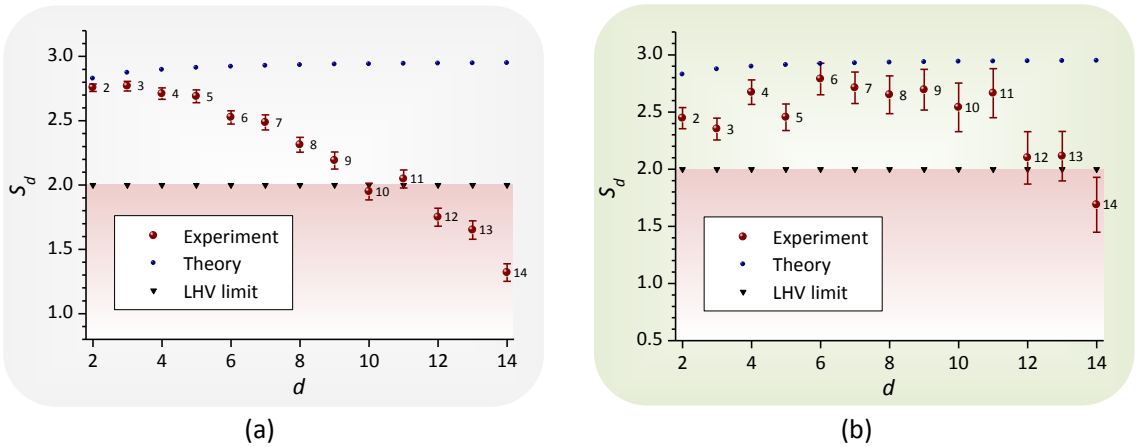

Figure 5.4: Experimental results for S_d versus number of dimensions d using (a) all p modes and no procrustean filtering and (b) only $p = 0$ modes with procrustean filtering. $S_d > 2$ violates local realism for any $d \geq 2$. The plots compares the theoretically predicted violations by a maximally entangled state and the local hidden variable (LHV) limit with the experiments. Violations are observed using up to $d = 11$ dimensions for each qudit. Errors were calculated assuming Poisson statistics for the photon counting processes. The measurement time was 20 s per point.

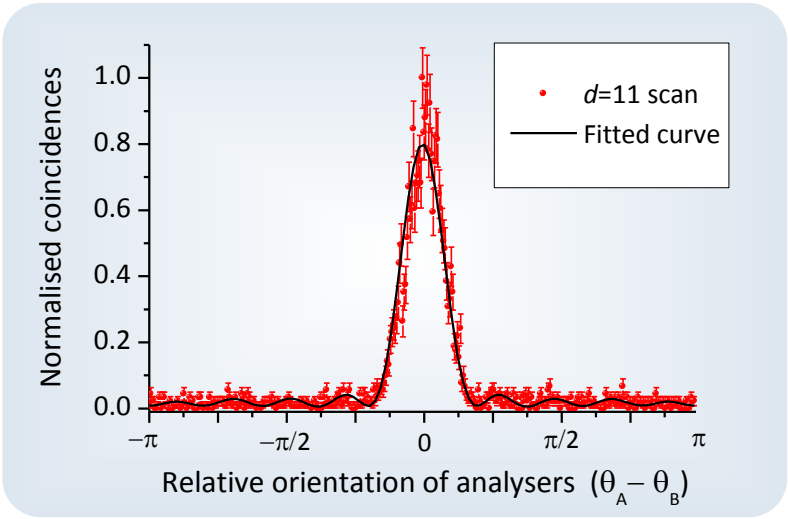

Figure 5.5: Coincidence count rates (self normalised) as a functions of relative orientation angles between state analysers $(\theta_A - \theta_B)$. Equation 5.7 for a state with maximal 11-dimensional entanglement is fitted to the experimental data with the vertical offset and amplitude left as free parameters. The experimental error bars account only for uncertainty due to measurement shot noise (Poisson statistics).

restricted to $p = 0$. The results in this case, shown in Figure 5.6(a) and Figure 5.6(b) also indicate reasonable agreement between the experimental coincidence measurements and the theoretical predictions for maximally entangled states (Equation 5.7).

The violation of a Bell inequality in $d \times d$ dimensions directly indicates that the measured state was entangled. It remains to determine how many dimensions were involved in the entanglement. Measuring the coincidence probabilities, i.e., of having the joint

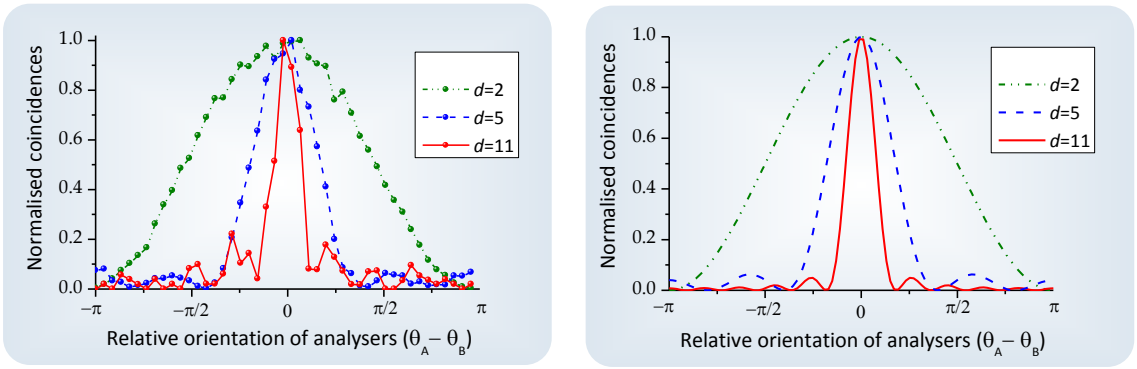

(a) Experiment (b) Theory

Figure 5.6: Coincidence count rates (self normalised) as a functions of relative orientation angles between state analysers $(\theta_A - \theta_B)$. The figures depict (a) experimental coincidence curves and (b) theoretical prediction for maximally entangled states of two d-dimensional systems with mode analyser settings defined in Equations 5.4 using $d = 2, 5$, and 11, as examples. Only modes with $p = 0$ are used here. The observed fringes are typical of genuine 2-, 5-, and 11-dimensional entanglement, respectively.

state $|\ell_s\rangle \otimes |\ell_i\rangle$ (Figure 5.2), together with the parameters S_d for different d, can be seen as a partial tomography of the SPDC source state. Numerical investigations indicate that a state having the experimentally observed coincidence probabilities and parameters $S_2, S_3, \ldots, S_{11}$ must contain genuine 11-dimensional entanglement. In other words, it is not possible to obtain the observed levels of violation with a state that contains entanglement involving only 10 dimensions or less. The analysis carried out here assumes a special form of the states, based on the coincidence measurement results shown in Figure 5.2. Further details are given below.

5.7 Evidence for high-dimensional entanglement

Violation of a Bell inequality indicates that the measured state was entangled, but does not directly give information of how many dimensions were involved in the entanglement. The following analysis of coincidence measurements results of the SPDC output, shown in Figure 5.2, together with the obtained Bell violations for different d, shows that the high levels of violations of the tested Bell inequalities indicate that the SPDC state is indeed a high-dimensional entangled state. The problem of finding a lower bound on the dimensionality required to produce certain quantum correlations has been studied by Acin *et al.* in [152], where they present examples of correlations that require measurements on quantum systems of dimension greater than two for their generation. Although, the depth

of analysis presented there would require immense computational efforts for 11 dimensions, additional experimental results and considerations below allow a simplification of the analysis carried out here. A more specific problem of finding a lower bound on the dimensionality required to produce certain Bell inequality violations is studied in Chapter 4. Although the bound derived shows that the single result of $S_4 = 2.87 \pm 0.04$ is a direct demonstration of 4-dimensional entanglement, the single values of S_d experimentally obtained here for $d > 4$ do not satisfy the derived bounds. However, combinations of Bell test results for different values of d provide more relaxed bounds on the dimensionality of entanglement as demonstrated below.

Assuming conservation of OAM, meaning that j is always the same for signal and idler photons, both the filtered and unfiltered SPDC source states can be written in the form

$$\hat{\rho} = \sum_{j,k=0}^{d-1} c_{jk} |j,j\rangle\langle k,k|. \tag{5.22}$$

As seen from Figure 5.2, for high $|\ell|$, there are nonzero coincidence counts even when j for the signal and idler photons differ by ± 1. This occurs for approximately 8% of the total count rate. Conservation of angular momentum in parametric down-conversion is, however, a theoretically and experimentally well-documented phenomenon (please see [141]). One is therefore justified in assuming a state of the form in Equation (5.22), and that any coincidence counts indicating unequal j for signal and idler photons are due to measurement errors, i.e. imperfect selection of OAM modes by the SLMs, which gets worse with increasing $|\ell|$.

A state of the form in Equation (5.22), which in addition has only at most $(d-1)$-dimensional entanglement, can be written as a mixture of pure states $|\psi_m\rangle = \sum_{j=0}^{d-1} a_{mj} |j,j\rangle$, where for each $|\psi_m\rangle$, it holds that $a_{mj} = 0$ for at least one j. By grouping terms with different $|\psi_m\rangle$ together, one can further write a state with at most $(d-1)$-dimensional entanglement as a mixture of no more than d mixed states, $\hat{\rho} = \sum_{n=0}^{d-1} r_n \hat{\rho}_n$, where each $\hat{\rho}_n$ is a mixture of states $|\psi_m\rangle$ for which $a_{mn} = 0$. That is, if $\hat{\rho}_n = \sum_{j,k=0}^{d-1} c_{n,jk} |j,j\rangle\langle k,k|$, then $c_{n,jk} = 0$ whenever one or both of j,k are equal to n.

By varying the r_n and the $c_{n,jk}$ in

$$\hat{\rho} = \sum_{n=0}^{d-1} r_n \hat{\rho}_n = \sum_{n=0}^{d-1} r_n \sum_{j,k=0}^{d-1} c_{n,jk} |j,j\rangle\langle k,k|, \tag{5.23}$$

one may now investigate what level of Bell violations may be obtained for a state with at most $(d-1)$-dimensional entanglement.

Clearly, if there are no constraints in the maximisation, then the maximum violation for such a state is attained when it is pure. When constraints are included, it is possible in general that there is no pure state which satisfies all of them, so that the maximum

is obtained with a mixed state. For example, three constraints on the Bloch vector of a 2-dimensional state may force it to be mixed. For $d \geq 4$ it is in fact enough to consider pure states $\hat{\rho}_n = |\psi_n\rangle\langle\psi_n|$. This follows since, for any mixed $\hat{\rho}_n$, there is a corresponding pure state with the same diagonal components $c_{n,jj}$, and the same Bell violations for $S_2, S_3, \ldots, S_d$. To see this, note that in addition to the $d-1$ diagonal components of $\hat{\rho}_n$, constraining the values of $d-1$ Bell parameters as done here constitutes in total $2d-2$ constraints on $\hat{\rho}_n$, which has $(d-1)^2-1$ free parameters. These parameters can be thought of as the diagonal components of $\hat{\rho}_n$, plus the real and imaginary parts of its off-diagonal elements. We can also think of them as the components of the generalised Bloch vector for $\hat{\rho}_n$. If the constraints leave at least one component of the generalised Bloch vector free, then this last component can be chosen large enough for $\hat{\rho}_n$ to be a pure state. We thus require that $(d-1)^2-1 > 2d-2$, which is satisfied for $d \geq 4$. For $d \geq 5$, the $\hat{\rho}_n$ can in fact be chosen, not only to be pure, but also to have only real matrix elements, since then the number of independent off-diagonal matrix elements in $\hat{\rho}_n$ is strictly greater than the number of Bell inequalities, that is, $(d-1)(d-2)/2 > d-1$ if $d \geq 5$. This considerably simplifies the numerical maximisation, which otherwise would be relatively demanding.

For $d = 11$, the corresponding state space is thus spanned by the OAM basis states $|j\rangle \otimes |k\rangle = |j,k\rangle$, with $j,k \in \{0,\ldots,10\}$. For $d = 11$, the experimentally obtained diagonal coincidence probabilities P_{jj}, with $j = 0,\ldots,10$, and the experimental values of $S_2, S_3, \ldots, S_{10}$ serve as constraints. All these quantities are allowed to vary within the experimental error bars which are estimated assuming Poisson statistics for the photon counting processes. Numerical maximisation using *Mathematica*® shows that the largest value of S_{11} that can be obtained with a state of the form in Equation (5.23) is $S_{11} = 2.14$. As mentioned above we measure S_{11} to be 2.39 ± 0.07 using all p modes. Using only $p = 0$, we find 2.67 ± 0.22. These and the other experimentally obtained Bell parameters are listed in Tables 5.3 and 5.4. In other words, the largest violation S_{11} that can be obtained with a state that has at most 10-dimensional entanglement is smaller than the experimentally measured violation, with more than three standard deviations for all p modes, and with more than two standard deviations for $p = 0$. One may therefore conclude, with high confidence, that the SPDC output state measured here does contain 11-dimensional entanglement.[1]

[1] The level of violation for $d = 12$ is too low to permit a similar argument.

No. of Dimensions d	Violation for $\|\psi\rangle$	Maximum possible violation
2	2.8284	2.8284
3	2.8729	2.9149
4	2.8962	2.9727
5	2.9105	3.0157
6	2.9202	3.0497
7	2.9272	3.0776
8	2.9324	3.1013
9	2.9365	3.1217
10	2.9398	3.1396
11	2.9425	3.1555
12	2.9448	3.1698
13	2.9467	3.1827
14	2.9483	3.1946

Table 5.1: Violation of the inequality $S_d \leq 2$ for two d-dimensional qudits, up to $d = 14$. This table shows theoretically predicted values obtained for the maximally entangled state $|\psi\rangle$ (depicted in Figure 5.3) and the maximum possible violation corresponding to the largest eigenvalue of the Bell operator $\hat{S}_d$.

Eigenvalue of $\hat{S}_{11}$	Eigenstate	...-dimensional entanglement
3.1555	$\|s_1\rangle \equiv \sum_{n=0}^{10} C_{1,n}\|n,n\rangle$	11
2.4107	$\|s_2\rangle \equiv \sum_{n=0}^{9} C_{2,n}\|n,n+1\rangle$	10
2.4107	$\|s_3\rangle \equiv \sum_{n=0}^{9} C_{3,n}\|n+1,n\rangle$	10
1.9709	$\|s_4\rangle \equiv \sum_{n=0}^{8} C_{4,n}\|n,n+2\rangle$	9
1.9709	$\|s_5\rangle \equiv \sum_{n=0}^{8} C_{5,n}\|n+2,n\rangle$	9

Table 5.2: Five largest eigenvalues of $\hat{S}_{11}$ and the form of the corresponding eigenstate.

5.8 Conclusion

These results hold much promise for applications requiring entangled qudits in general. As mentioned earlier, progress in the development of quantum repeaters (see [142] and references therein) would make quantum key distribution using high-dimensional entangled states [9] a possible application. Conventional quantum communication will fail for sufficiently large transmission distances because of loss, and quantum repeaters are one possible solution to this problem. Although experimental quantum key distribution has been demonstrated with OAM qutrits [129], the findings reported here provide experimental evidence that such protocols could be implemented using photons entangled in OAM in up to 11 dimensions, resulting in a considerable increase in information coding density.

A possible extension to the work reported in this chapter could be to investigate the generation of multi-photon, high-dimensional OAM entanglement. One can conceive of

No. of Dimensions d	2	3	4	5	6	7	8	9
Parameter S_d	2.79	2.78	2.87	2.73	2.76	2.62	2.56	2.46
Standard deviation σ	0.03	0.04	0.04	0.05	0.06	0.07	0.07	0.07

No. of Dimensions d	10	11	12	13	14
Parameter S_d	2.47	2.39	2.24	2.07	1.89
Standard deviation σ	0.07	0.07	0.08	0.08	0.08

Table 5.3: Experimental Bell-type parameter S_d as a function of the number of dimensions d. All radial modes (all p) are used here, and violations of $S_d \leq 2$ are observed for up to $d = 12$.

No. of Dimensions d	2	3	4	5	6	7	8	9
Parameter S_d	2.76	2.77	2.71	2.69	2.53	2.49	2.31	2.19
Standard deviation σ	0.03	0.04	0.04	0.05	0.05	0.06	0.06	0.07

No. of Dimensions d	10	11	12	13	14
Parameter S_d	1.95	2.05	1.75	1.65	1.32
Standard deviation σ	0.07	0.07	0.07	0.07	0.07

Table 5.4: Experimental Bell-type parameter S_d as a function of the number of dimensions d without procrustean filtering/entanglement concentration. Violations of $S_d \leq 2$ are observed for up to $d = 9$. All p modes are used here.

No. of Dimensions d	2	3	4	5	6	7	8	9
Parameter S_d	2.45	2.4	2.67	2.46	2.79	2.71	2.65	2.7
Standard deviation σ	0.09	0.1	0.11	0.12	0.14	0.14	0.16	0.2

No. of Dimensions d	10	11	12	13	14
Parameter S_d	2.54	2.67	2.1	2.11	1.69
Standard deviation σ	0.21	0.22	0.2	0.22	0.24

Table 5.5: Experimental Bell-type parameter S_d as a function of the number of dimensions d. Only OAM modes with $p = 0$ are used here, and violations of $S_d \leq 2$ are observed for up to $d = 11$.

achieving this using a cascade of down-conversion crystals for generating multipartite entangled photons, which has been done for polarisation entangled photons [143]. It also appears to be within reach to combine the high-dimensional photon OAM entanglement with entanglement in the polarisation and path degrees of freedom, creating even larger hyper-entangled states (please see [143] and Refs. within).

On a more fundamental note, Bell test experiments performed to date have one or both of two main loopholes, namely the locality and detection loopholes. However, a recent theoretical work reveals that even low dimensional qudits can provide a significant advantage over qubits for closing the detection loophole [116]. In fact, it was found that as much as 38.2% loss can be tolerated using 4-dimensional entanglement. The results of this chapter raise interesting possibilities regarding the role higher-dimensional entangled qudits could play in closing this loophole. It should be emphasised that neither the detection nor the locality loophole has been closed in the experiments reported here, because the overall efficiency of the experimental setup is $1-2\%$, and the switching time for the measurement devices (SLMs) is of the order of tens of ms. However, closing these loopholes was not the immediate goal of the experiments. Instead, they provide a verification of high-dimensional entanglement using the violation of Bell inequalities, up to fair sampling assumptions, and within the framework of quantum mechanics.

In summary, this chapter has reported the experimental violations of Bell-type inequalities generalised to d-dimensional systems [135] with up to $d = 12$, enough to indicate genuine 11-dimensional entanglement in the orbital angular momentum of signal and idler photons in parametric down-conversion. It appears that this could be extended to even higher dimensions by using a brighter source of entangled photons.

CHAPTER 6

Conclusions and future outlook

6.1 Conclusions

This thesis has explored aspects of implementing optimal quantum measurements. The unavailability of deterministic photon-photon interactions motivates the exploitation of non-photonic platforms for quantum information processing, of which the implementation of optimal quantum measurements is an important and integral part. This was addressed in the second and third chapters of this thesis. Also, tests of Bell inequalities are a useful way of demonstrating genuine entanglement since they relate directly to certain applications. To violate Bell inequalities, however, the measurements performed need to be optimised based on the form of the entangled state and the particular Bell inequality. This will not only give the largest possible violation, but also enable the detection of information about the nature of the entangled state that might otherwise be undetectable from the Bell test. This was the focus of the fourth and fifth chapters of this thesis. Experiments performed using such methods provided evidence for genuine eleven-dimensional entanglement.

This thesis has proposed and explained explicit schemes for implementing two generalised quantum measurement strategies using atoms in cavity QED, since atoms can interact strongly with each other via cavity fields. The measurements considered were unambiguous discrimination of two non-orthogonal quantum states, the so-called IDP measurement, and the measurement to demonstrate superadditive quantum coding using a ternary quantum alphabet. It was also shown that the proposed realisations are feasible using current or shortly available cavity QED technologies. This was by means of a simple proof confirming the optimality of the realisation of the measurement that demonstrates quantum superadditivity in terms of cavity usage. The effect of imperfect detection of the basis states on superadditive quantum coding gain was investigated. The results showed that even with rather high levels of such experimental imperfections, a reasonable amount of superadditivity can be seen. Similar methods can be applied to implement *any* generalised quantum measurement using cavity QED-type systems.

The thesis also presents a discussion of an experimental realisation and comparison of three different measurement schemes to distinguish between non-orthogonal quantum states using nitrogen nuclear spins associated NV^- centres. The measurements were opti-

mal unambiguous state discrimination and the minimum-error or Helstrom measurement. Previously, optimal unambiguous state discrimination had only been realised using photons [50, 93]. The ability to perform generalised measurements on NV^- centres is of great interest for implementations of solid-state quantum computing. The realised IDP measurement for NV^- centres outperforms standard projective measurements, and gives further evidence that NV^- centres in diamond are a favourable candidate for solid state quantum information processing at room temperature.

This thesis considered some questions relevant to tests of Bell inequalities when the local Hilbert space dimension is greater two. Subtle ways in which fair sampling can be violated were explained. In particular, this can happen easily when the different measurements on one subsystem do not sample the state space in an equivalent way, i.e. if the resulting efficiency of detection is not factorable into a function of the state and another of the measurement choice. This is relevant especially when using high-dimensional quantum systems such as photon orbital angular momentum, for which violation of fair sampling may result even if detection efficiency is perfect within the sampled subspaces. A simple bound on the violation of generalised bell inequalities was presented with which it can be guaranteed that a tested state must have been entangled in a given number of dimensions. Such bounds are useful for experimental verification of high-dimensional entanglement. Through an experiment demonstrating genuine eleven-dimensional entanglement, it was further shown how combinations experimental results of tests using different values of d can provide more accessible bounds on the dimensionality of entanglement.

6.2 Outlook

The realisation of quantum measurements using atoms is clearly advantageous as a result of a better potential for scalability. For example, as earlier mentioned, the fact that atoms can interact strongly via cavity fields makes it possible to experimentally investigate the implementation of superadditive coding with longer code words (and increased quantum coding gain) using cavity QED-type systems. The methods described in this thesis can also be applied using circuit QED [153] based technologies. It is also interesting to further study realisations of other optimal quantum measurements that are difficult to realise using linear optics, such as other schemes involving measurements using entangled measurement basis states.

A clear and direct application of the demonstration of high-dimensional two-photon entanglement is using it in a generalised protocol for entanglement based quantum key distribution [9, 154] in such a way as to take advantage of the high-information capacity provided by high-dimensional entanglement [27, 28]. This would however require full projective measurements in the OAM basis. Another possible extension would be to

investigate the generation of multi-photon, high-dimensional OAM entanglement. This might be achieved using a cascade of down-conversion crystals for generating multipartite entangled photons, which has been done for polarisation entangled photons [143]. Larger hyper-entangled states (please see [143] and references within) might be generated by combining the high-dimensional photon OAM entanglement with entanglement in the polarisation and path degrees of freedom using current or shortly available technologies.

Of fundamental interest is the fact that Bell test experiments performed to date have one or both of two main loopholes, namely the locality and detection loopholes. However, a recent theoretical work reveals that even multilevel entanglement allows for less stringent detection efficiency requirements and can provide a significant advantage over two-qubit entanglement for closing the detection loophole [116]. The results of this thesis then raise interesting possibilities regarding the role higher-dimensional entangled qudits could play in closing this loophole.

References

[1] Nielsen, M. A. and Chuang, I. L. *Quantum Computation and Quantum Information*, pp. 1–4. Number ISBN 0-521-63503-9 in Cambridge Series on Information and the Natural Sciences. Cambridge University Press, New York, (2000). 1

[2] Pusey, M. F., Barrett, J., and Rudolph, T. **On the reality of the quantum state**. *Nat Phys*, **8**, 475–478, (2012). 1

[3] Peres, A. *Quantum Theory: Concepts and Methods*. Kluwer Academic Publishers, Dordrecht, (1993). 1, 13

[4] Paraoanu, G. S. **Extraction of information from a single quantum**. *Phys. Rev. A*, **83**, 044101, (2011). 1

[5] von Neumann, J. *Mathematical Foundations of Quantum Mechanics*. Princeton University Press, (1996). 1

[6] Ghosh, R. and Mandel, L. **Observation of nonclassical effects in the interference of two photons**. *Phys. Rev. Lett.*, **59**, 1903–1905, (1987). 1

[7] Kwiat, P. G., Mattle, K., Weinfurter, H., Zeilinger, A., Sergienko, A. V., and Shih, Y. **New High-Intensity Source of Polarization-Entangled Photon Pairs**. *Phys. Rev. Lett.*, **75**, 4337–4341, (1995). 1, 67

[8] Burnham, D. C. and Weinberg, D. L. **Observation of Simultaneity in Parametric Production of Optical Photon Pairs**. *Phys. Rev. Lett.*, **25**, 84–87, (1970). 1

[9] Ekert, A. K. **Quantum cryptography based on Bell's theorem**. *Phys. Rev. Lett.*, **67**, 661–663, (1991). 1, 2, 67, 82, 86

[10] Bennett, C. H., Brassard, G., Crépeau, C., Jozsa, R., Peres, A., and Wootters, W. K. **Teleporting an unknown quantum state via dual classical and Einstein-Podolsky-Rosen channels**. *Phys. Rev. Lett.*, **70**, 1895–1899, (1993). 1, 2, 67

[11] Nobelprize.org. **The Nobel Prize in Physics 2012**. (2012). 1

[12] Walther, H., Varcoe, B. T. H., Englert, B.-G., and Becker, T. **Cavity quantum electrodynamics**. *Reports on Progress in Physics*, **69**, 1325, (2006). 1

[13] Neumann, P., Mizuochi, N., Rempp, F., Hemmer, P., Watanabe, H., Yamasaki, S., Jacques, V., Gaebel, T., Jelezko, F., and Wrachtrup, J. **Multipartite Entanglement Among Single Spins in Diamond**. *Science*, **320**, 1326–1329, (2008). 1, 37

[14] Balasubramanian, G., *et al.* **Ultralong spin coherence time in isotopically engineered diamond**. *Nature Materials*, **8**, 383–387, (2009). 1, 37, 39

[15] Batalov, A., Zierl, C., Gaebel, T., Neumann, P., Chan, I.-Y., Balasubramanian, G., Hemmer, P. R., Jelezko, F., and Wrachtrup, J. **Temporal Coherence of Photons Emitted by Single Nitrogen-Vacancy Defect Centers in Diamond Using Optical Rabi-Oscillations**. *Phys. Rev. Lett.*, **100**, 077401, (2008). 1

[16] Knill, E., Laflamme, R., and Milburn, G. J. **A scheme for efficient quantum computation with linear optics**. *Nature*, **409**, 46–52, (2001). 2, 17

[17] Kok, P., Munro, W. J., Nemoto, K., Ralph, T. C., Dowling, J. P., and Milburn, G. J. **Linear optical quantum computing with photonic qubits**. *Rev. Mod. Phys.*, **79**, 135–174, (2007). 2, 17

[18] Chefles, A. **Quantum States: Discrimination and Classical Information Transmission. A Review of Experimental Progress**. In *Quantum State Estimation,* Paris, M. and Řeháček, J., editors, volume 649 of *Lecture Notes in Physics*, 467–511. Springer Berlin Heidelberg, (2004). 2

[19] Barnett, S. M. and Croke, S. **Quantum state discrimination**. *Adv. Opt. Photon.*, **1**, 238–278, (2009). 2

[20] You-Bang, Z., Qun-Yong, Z., Yu-Wu, W., and Peng-Cheng, M. **Schemes for Teleportation of an Unknown Single-Qubit Quantum State by Using an Arbitrary High-Dimensional Entangled State**. *Chinese Physics Letters*, **27**, 10307–10310, (2010). 2, 67

[21] Bennett, C. H. and Wiesner, S. J. **Communication via one- and two-particle operators on Einstein-Podolsky-Rosen states**. *Phys. Rev. Lett.*, **69**, 2881–2884, (1992). 2, 67

[22] Hillery, M., Bužek, V., and Berthiaume, A. **Quantum secret sharing**. *Phys. Rev. A*, **59**, 1829–1834, (1999). 2, 67

[23] Raussendorf, R., Browne, D. E., and Briegel, H. J. **Measurement-based quantum computation on cluster states**. *Phys. Rev. A*, **68**, 022312, (2003). 2, 67

[24] Li, C.-M., Chen, K., Reingruber, A., Chen, Y.-N., and Pan, J.-W. **Verifying Genuine High-Order Entanglement**. *Phys. Rev. Lett.*, **105**, 210504, (2010). 2

[25] Stucki, D., Zbinden, H., and Gisin, N. **A Fabry–Perot-like two-photon interferometer for high-dimensional time-bin entanglement**. *Journal of Modern Optics*, **52**, 2637–2648, (2005). 2

[26] Ali-Khan, I. and Howell, J. C. **Experimental demonstration of high two-photon time-energy entanglement**. *Phys. Rev. A*, **73**, 031801, (2006). 2

[27] Dixon, P. B., Howland, G. A., Schneeloch, J., and Howell, J. C. **Quantum Mutual Information Capacity for High-Dimensional Entangled States**. *Phys. Rev. Lett.*, **108**, 143603, (2012). 2, 86

[28] Brougham, T. and Barnett, S. M. **Information communicated by entangled photon pairs**. *Phys. Rev. A*, **85**, 032322, (2012). 2, 86

[29] Sheridan, L. and Scarani, V. **Security proof for quantum key distribution using qudit systems**. *Phys. Rev. A*, **82**, 030301, (2010). 2

[30] Nielsen, M. A. and Chuang, I. L. *Quantum Computation and Quantum Information*, Chap. 2. Number ISBN 0-521-63503-9 in Cambridge Series on Information and the Natural Sciences. Cambridge University Press, New York, (2000). 4

[31] Barnett, S. *Quantum Information (Oxford Master Series in Physics: Atomic, Optical, and Laser Physics)*. Oxford University Press, USA, (2009). 4

[32] Barenco, A., Bennett, C. H., Cleve, R., DiVincenzo, D. P., Margolus, N., Shor, P., Sleator, T., Smolin, J. A., and Weinfurter, H. **Elementary gates for quantum computation**. *Phys. Rev. A*, **52**, 3457–3467, (1995). 6

[33] Werner, R. F. **Quantum states with Einstein-Podolsky-Rosen correlations admitting a hidden-variable model**. *Phys. Rev. A*, **40**, 4277–4281, (1989). 10

[34] Einstein, A., Podolsky, B., and Rosen, N. **Can Quantum-Mechanical Description of Physical Reality Be Considered Complete?** *Phys. Rev.*, **47**, 777–780, (1935). 10, 67, 68

[35] Bell, J. S. **On the Einstein Podolsky Rosen Paradox**. *Physics*, **1**, 195–200, (1964). 10, 49, 51

[36] Clauser, J. F., Horne, M. A., Shimony, A., and Holt, R. A. **Proposed Experiment to Test Local Hidden-Variable Theories**. *Phys. Rev. Lett.*, **23**, 880–884, (1969). 11, 49, 50, 51

[37] Cirel'son, B. S. **Quantum generalizations of Bell's inequality**. *Letters in Mathematical Physics*, **4**, 93–100, (1980). 10.1007/BF00417500. 12, 50, 52, 58, 60

[38] Pérez-García, D., Wolf, M., Palazuelos, C., Villanueva, I., and Junge, M. **Unbounded Violation of Tripartite Bell Inequalities**. *Communications in Mathematical Physics*, **279**, 455–486, (2008). 10.1007/s00220-008-0418-4. 12

[39] Fujiwara, M., Takeoka, M., Mizuno, J., and Sasaki, M. **Exceeding the Classical Capacity Limit in a Quantum Optical Channel**. *Phys. Rev. Lett.*, **90**, 167906, (2003). 13, 16, 17, 24, 25

[40] Sasaki, M., Kato, K., Izutsu, M., and Hirota, O. **Quantum channels showing superadditivity in classical capacity**. *Phys. Rev. A*, **58**, 146–158, (1998). 13, 15, 17, 23, 25

[41] Helstrom, C. W. *Quantum detection and estimation theory*. Academic Press: New York, (1976). 16, 19, 35, 37, 45

[42] Chefles, A. **Quantum State Discrimination**. *Contemporary Physics*, **41**, 401–424, (2000). 16, 17

[43] Ivanovic, I. D. **How to differentiate between non-orthogonal states**. *Phys. Lett. A*, **123**, 257 – 259, (1987). 16, 18, 37, 38, 43

[44] Dieks, D. **Overlap and distinguishability of quantum states**. *Phys. Lett. A*, **126**, 303 – 306, (1988). 16, 18, 37, 38, 43

[45] Peres, A. **How to differentiate between non-orthogonal states**. *Phys. Lett. A*, **128**, 19 – 19, (1988). 16, 18, 37, 38, 43

[46] Brougham, T., Andersson, E., and Barnett, S. M. **Cloning and joint measurements of incompatible components of spin**. *Phys. Rev. A*, **73**, 062319, (2006). 17

[47] Gisin, N., Ribordy, G., Tittel, W., and Zbinden, H. **Quantum cryptography**. *Rev. Mod. Phys.*, **74**, 145–195, (2002). 17

[48] Bennett, C. H. **Quantum cryptography using any two nonorthogonal states**. *Phys. Rev. Lett.*, **68**, 3121–3124, (1992). 17, 38

[49] Huttner, B., Muller, A., Gautier, J. D., Zbinden, H., and Gisin, N. **Unambiguous quantum measurement of nonorthogonal states**. *Phys. Rev. A*, **54**, 3783–3789, (1996). 17

[50] Clarke, R. B. M., Chefles, A., Barnett, S. M., and Riis, E. **Experimental demonstration of optimal unambiguous state discrimination**. *Phys. Rev. A*, **63**, 040305, (2001). 17, 38, 42, 48, 86

[51] Mohseni, M., Steinberg, A. M., and Bergou, J. A. **Optical Realization of Optimal Unambiguous Discrimination for Pure and Mixed Quantum States**. *Phys. Rev. Lett.*, **93**, 200403, (2004). 17

[52] Franke-Arnold, S., Andersson, E., Barnett, S. M., and Stenholm, S. **Generalized measurements of atomic qubits**. *Phys. Rev. A*, **63**, 052301, (2001). 17, 42, 43

[53] Andersson, E. **Generalized measurements on atoms in microtraps**. *Phys. Rev. A*, **64**, 032303, (2001). 17

[54] Roa, L., Retamal, J. C., and Saavedra, C. **Quantum-state discrimination**. *Phys. Rev. A*, **66**, 012103, (2002). 17

[55] Gopinath, T., Das, R., and Kumar, A. **Programmable quantum-state discriminator by nuclear magnetic resonance**. *Phys. Rev. A*, **71**, 042307, (2005). 17

[56] Takeoka, M., Fujiwara, M., Mizuno, J., and Sasaki, M. **Implementation of generalized quantum measurements: Superadditive quantum coding, accessible information extraction, and classical capacity limit**. *Phys. Rev. A*, **69**, 052329, (2004). 17, 24, 32

[57] Mitsumori, Y., Vaccaro, J. A., Barnett, S. M., Andersson, E., Hasegawa, A., Takeoka, M., and Sasaki, M. **Experimental Demonstration of Quantum Source Coding**. *Phys. Rev. Lett.*, **91**, 217902, (2003). 17

[58] Hagley, E., Maître, X., Nogues, G., Wunder lich, C., Brune, M., Raimond, J. M., and Haroche, S. **Generation of Einstein-Podolsky-Rosen Pairs of Atoms**. *Phys. Rev. Lett.*, **79**, 1–5, (1997). 17, 31

[59] Rauschenbeutel, A., Nogues, G., Osnaghi, S., Bertet, P., Brune, M., Raimond, J. M., and Haroche, S. **Coherent Operation of a Tunable Quantum Phase Gate in Cavity QED**. *Phys. Rev. Lett.*, **83**, 5166–5169, (1999). 17

[60] Guerlin, C., Bernu, J., Deleglise, S., Sayrin, C., Gleyzes, S., Kuhr, S., Brune, M., Raimond, J.-M., and Haroche, S. **Progressive field-state collapse and quantum non-demolition photon counting**. *Nature*, **448**, 889–893, (2007). 18

[61] Brune, M., Hagley, E., Dreyer, J., Maître, X., Maali, A., Wunderlich, C., Raimond, J. M., and Haroche, S. **Observing the Progressive Decoherence of the "Meter" in a Quantum Measurement**. *Phys. Rev. Lett.*, **77**, 4887–4890, (1996). 18, 23, 34

[62] Lindström, T., Webster, C. H., Healey, J. E., Colclough, M. S., Muirhead, C. M., and Tzalenchuk, A. Y. **Circuit QED with a flux qubit strongly coupled to a coplanar transmission line resonator**. *Superconductor Science and Technology*, **20**, 814, (2007). 18

[63] Vuckovic, J. and Yamamoto, Y. **Photonic crystal microcavities for cavity quantum electrodynamics with a single quantum dot**. *Applied Physics Letters*, **82**, 2374 –2376, (2003). 18

[64] Reck, M., Zeilinger, A., Bernstein, H. J., and Bertani, P. **Experimental realization of any discrete unitary operator**. *Phys. Rev. Lett.*, **73**, 58–61, (1994). 20, 28, 43

[65] Andersson, E. and Oi, D. K. L. **Binary search trees for generalized measurements**. *Phys. Rev. A*, **77**, 052104, (2008). 20

[66] Haroche, S. and Raimond, J.-M. *Exploring the Quantum: Atoms, Cavities, and Photons (Oxford Graduate Texts)*. Oxford University Press, USA, 1st ed edition, (2006). 22, 27

[67] Filipovicz, P., Meystre, P., Rempe, G., and Walther, H. **Rydberg Atoms: A Testing Ground for Quantum Electrodynamics**. *Journal of Modern Optics*, **32**, 1105–1123, (1985). 22

[68] Walther, H., Varcoe, B. T. H., Englert, B.-G., and Becker, T. **Cavity quantum electrodynamics**. *Reports on Progress in Physics*, **69**, 1325–1382, (2006). 23

[69] Jones, M., Sanguinetti, B., Majeed, H., and Varcoe, B. **Evolutionary optimization of state selective field ionization for quantum computing**. *Applied Soft Computing*, **11**, 2079 – 2082, (2011). The Impact of Soft Computing for the Progress of Artificial Intelligence. 23

[70] Tada, M., Kishimoto, Y., Shibata, M., Kominato, K., Yamada, S., Haseyama, T., Ogawa, I., Funahashi, H., Yamamoto, K., and Matsuki, S. **Manipulating ionization path in a Stark map: Stringent schemes for the selective field ionization in highly excited Rb Rydberg**. *Physics Letters A*, **303**, 285–291, (2002). 23

[71] Gürtler, A. and van der Zande, W. J. **l-state selective field ionization of rubidium Rydberg states**. *Physics Letters A*, **324**, 315–320, (2004). 23

[72] Peres, A. and Wootters, W. K. **Optimal detection of quantum information**. *Phys. Rev. Lett.*, **66**, 1119–1122, (1991). 23, 24

[73] Buck, J. R., van Enk, S. J., and Fuchs, C. A. **Experimental proposal for achieving superadditive communication capacities with a binary quantum alphabet**. *Phys. Rev. A*, **61**, 032309, (2000). 23

[74] Shor, P. W. **The adaptive classical capacity of a quantum channel, or Information capacities of three symmetric pure states in three dimensions**. *IBM Journal of Research and Development*, **48**, 115 –137, (2004). 24

[75] Zheng, S.-B. and Guo, G.-C. **Efficient Scheme for Two-Atom Entanglement and Quantum Information Processing in Cavity QED**. *Phys. Rev. Lett.*, **85**, 2392–2395, (2000). 26, 27, 31, 32

[76] Everitt, M. S., Jones, M. L., Varcoe, B. T. H., and Dunningham, J. A. **Creating and observing N -partite entanglement with atoms**. *Journal of Physics B: Atomic, Molecular and Optical Physics*, **44**, 035504, (2011). 26

[77] Lazarou, C. and Garraway, B. M. **Adiabatic entanglement in two-atom cavity QED**. *Phys. Rev. A*, **77**, 023818, (2008). 27, 31

[78] Andersson, E. and Barnett, S. M. **Bell-state analyzer with channeled atomic particles**. *Phys. Rev. A*, **62**, 052311, (2000). 28

[79] Vliegen, E. and Merkt, F. **Normal-Incidence Electrostatic Rydberg Atom Mirror**. *Phys. Rev. Lett.*, **97**, 033002, (2006). 30

[80] Merimeche, H. **Atomic beam focusing with a curved magnetic mirror**. *Journal of Physics B: Atomic, Molecular and Optical Physics*, **39**, 3723, (2006). 30

[81] Zhang, J., Vala, J., Sastry, S., and Whaley, K. B. **Geometric theory of nonlocal two-qubit operations**. *Phys. Rev. A*, **67**, 042313, (2003). 31

[82] Croke, S., Andersson, E., Barnett, S. M., Gilson, C. R., and Jeffers, J. **Maximum Confidence Quantum Measurements**. *Phys. Rev. Lett.*, **96**, 070401, (2006). 31

[83] Croke, S., Andersson, E., and Barnett, S. M. **No-signaling bound on quantum state discrimination**. *Phys. Rev. A*, **77**, 012113, (2008). 31

[84] Mosley, P. J., Croke, S., Walmsley, I. A., and Barnett, S. M. **Experimental Realization of Maximum Confidence Quantum State Discrimination for the Extraction of Quantum Information**. *Phys. Rev. Lett.*, **97**, 193601, (2006). 31

[85] Osnaghi, S., Bertet, P., Auffeves, A., Maioli, P., Brune, M., Raimond, J. M., and Haroche, S. **Coherent Control of an Atomic Collision in a Cavity**. *Phys. Rev. Lett.*, **87**, 037902, (2001). 34

[86] Purcell, E. M. **Spontaneous emission probabilities at radio frequencies**. *Physical Review*, **69**, 681+, (1946). 34

[87] Deleglise, S., Dotsenko, I., Sayrin, C., Bernu, J., Brune, M., Raimond, J.-M., and Haroche, S. **Reconstruction of non-classical cavity field states with snapshots of their decoherence**. *Nature*, **455**, 510–514, (2008). 34

[88] Andersson, E., Barnett, S. M., Gilson, C. R., and Hunter, K. **Minimum-error discrimination between three mirror-symmetric states**. *Phys. Rev. A*, **65**, 052308, (2002). 35

[89] Hamilton, C. S., Lavička, H., Andersson, E., Jeffers, J., and Jex, I. **Quantum public key distribution with imperfect device components**. *Phys. Rev. A*, **79**, 023808, (2009). 36

[90] Bergou, J. A., Herzog, U., and Hillery, M. *Quantum state estimation*. Springer, Berlin, (2004). 37

[91] van Enk, S. J. **Unambiguous state discrimination of coherent states with linear optics: Application to quantum cryptography**. *Phys. Rev. A*, **66**, 042313, (2002). 38

[92] Delgado, A., Roa, L., Retamal, J. C., and Saavedra, C. **Entanglement swapping via quantum state discrimination**. *Phys. Rev. A*, **71**, 012303, (2005). 38

[93] Dada, A. C., Andersson, E., Jones, M. L., Kendon, V. M., and Everitt, M. S. **Quantum measurements of atoms using cavity QED**. *Phys. Rev. A*, **83**, 042339, (2011). 38, 44, 48, 86

[94] Neumann, P., Beck, J., Steiner, M., Rempp, F., Fedder, H., Hemmer, P. R., Wrachtrup, J., and Jelezko, F. **Single-Shot Readout of a Single Nuclear Spin**. *Science*, **329**, 542–544, (2010). 38, 39, 40

[95] Gruber, A., Draebenstedt, A., Tietz, C., Fleury, L., Wrachtrup, J., and Borczyskowski, C. v. **Scanning Confocal Optical Microscopy and Magnetic Resonance on Single Defect Centers**. *Science*, **276**, 2012–2014, (1997). 39

[96] Jelezko, F., Gaebel, T., Popa, I., Domhan, M., Gruber, A., and Wrachtrup, J. **Observation of Coherent Oscillation of a Single Nuclear Spin and Realization of a Two-Qubit Conditional Quantum Gate**. *Phys. Rev. Lett.*, **93**, 130501, (2004). 39

[97] Childress, L., Gurudev Dutt, M. V., Taylor, J. M., Zibrov, A. S., Jelezko, F., Wrachtrup, J., Hemmer, P. R., and Lukin, M. D. **Coherent Dynamics of Coupled Electron and Nuclear Spin Qubits in Diamond**. *Science*, **314**, 281–285, (2006). 39

[98] Robledo, L., Childress, L., Bernien, H., Hensen, B., Alkemade, P. F. A., and Hanson, R. **High-fidelity projective read-out of a solid-state spin quantum register**. *Nature*, **477**, 574–578, (2011). 39

[99] Waldherr, G., Neumann, P., Huelga, S. F., Jelezko, F., and Wrachtrup, J. **Violation of a Temporal Bell Inequality for Single Spins in a Diamond Defect Center**. *Phys. Rev. Lett.*, **107**, 090401, (2011). 40, 48

[100] Freedman, S. J. and Clauser, J. F. **Experimental Test of Local Hidden-Variable Theories**. *Phys. Rev. Lett.*, **28**, 938–941, (1972). 49, 50

[101] Aspect, A., Dalibard, J., and Roger, G. **Experimental Test of Bell's Inequalities Using Time- Varying Analyzers**. *Phys. Rev. Lett.*, **49**, 1804–1807, (1982). 49

[102] Weihs, G., Jennewein, T., Simon, C., Weinfurter, H., and Zeilinger, A. **Violation of Bell's Inequality under Strict Einstein Locality Conditions**. *Phys. Rev. Lett.*, **81**, 5039–5043, (1998). 49

[103] Rowe, M. A., Kielpinski, D., Meyer, V., Sackett, C. A., Itano, W. M., Monroe, C., and Wineland, D. J. **Experimental violation of a Bell's inequality with efficient detection**. *Nature*, **409**, 791–794, (2001). 49

[104] Pearle, P. M. **Hidden-Variable Example Based upon Data Rejection**. *Phys. Rev. D*, **2**, 1418–1425, (1970). 49

[105] Fine, A. **Hidden Variables, Joint Probability, and the Bell Inequalities**. *Phys. Rev. Lett.*, **48**, 291–295, (1982). 49

[106] Larsson, J.-Å. **Modeling the singlet state with local variables**. *Physics Letters A*, **256**, 245 – 252, (1999). 49

[107] Branciard, C. **Detection loophole in Bell experiments: How postselection modifies the requirements to observe nonlocality**. *Phys. Rev. A*, **83**, 032123, (2011). 49

[108] Lo, T. K. and Shimony, A. **Proposed molecular test of local hidden-variables theories**. *Phys. Rev. A*, **23**, 3003–3012, (1981). 49

[109] Garg, A. and Mermin, N. D. **Detector inefficiencies in the Einstein-Podolsky-Rosen experiment**. *Phys. Rev. D*, **35**, 3831–3835, (1987). 49

[110] Santos, E. **Critical analysis of the empirical tests of local hidden-variable theories**. *Phys. Rev. A*, **46**, 3646–3656, (1992). 49

[111] Eberhard, P. H. **Background level and counter efficiencies required for a loophole-free Einstein-Podolsky-Rosen experiment**. *Phys. Rev. A*, **47**, R747–R750, (1993). 49

[112] Gisin, N. and Gisin, B. **A local hidden variable model of quantum correlation exploiting the detection loophole**. *Physics Letters A*, **260**, 323 – 327, (1999). 49

[113] Massar, S. **Nonlocality, closing the detection loophole, and communication complexity**. *Phys. Rev. A*, **65**, 032121, (2002). 49

[114] Cabello, A. and Larsson, J.-A. **Minimum Detection Efficiency for a Loophole-Free Atom-Photon Bell Experiment**. *Phys. Rev. Lett.*, **98**, 220402, (2007). 49

[115] Brunner, N., Gisin, N., Scarani, V., and Simon, C. **Detection Loophole in Asymmetric Bell Experiments**. *Phys. Rev. Lett.*, **98**, 220403, (2007). 49

[116] Vértesi, T., Pironio, S., and Brunner, N. **Closing the Detection Loophole in Bell Experiments Using Qudits**. *Phys. Rev. Lett.*, **104**, 060401, (2010). 49, 67, 69, 84, 87

[117] Larsson, J. A. and Gill, R. D. **Bell's inequality and the coincidence-time loophole**. *EPL (Europhysics Letters)*, **67**, 707–713, (2004). 50

[118] Semenov, A. A. and Vogel, W. **Fake violations of the quantum Bell-parameter bound**. *Phys. Rev. A*, **83**, 032119, (2011). 50

[119] Clauser, J. F. and Shimony, A. **Bell's theorem. Experimental tests and implications**. *Reports on Progress in Physics*, **41**, 1881, (1978). 50

[120] Aspect, A., Grangier, P., and Roger, G. **Experimental Tests of Realistic Local Theories via Bell's Theorem**. *Phys. Rev. Lett.*, **47**, 460–463, (1981). 50

[121] Berry, D. W., Jeong, H., Stobińska, M., and Ralph, T. C. **Fair-sampling assumption is not necessary for testing local realism**. *Phys. Rev. A*, **81**, 012109, (2010). 50, 53, 58

[122] Gisin, N. **Hidden quantum nonlocality revealed by local filters**. *Physics Letters A*, **210**, 151 – 156, (1996). 50

[123] Berndl, K. and Teufel, S. **Comment on "Hidden quantum nonlocality revealed by local filters"**. *Phys. Lett. A*, **224**, 314, (1997). 50

[124] Cabello, A. **Violating Bell's Inequality Beyond Cirel'son's Bound**. *Phys. Rev. Lett.*, **88**, 060403, (2002). 50

[125] Chen, Y.-A., Yang, T., Zhang, A.-N., Zhao, Z., Cabello, A., and Pan, J.-W. **Experimental Violation of Bell's Inequality beyond Tsirelson's Bound**. *Phys. Rev. Lett.*, **97**, 170408, (2006). 50

[126] Marcovitch, S., Reznik, B., and Vaidman, L. **Quantum-mechanical realization of a Popescu-Rohrlich box**. *Phys. Rev. A*, **75**, 022102, (2007). 50

[127] Tasca, D. S., Walborn, S. P., Toscano, F., and Souto Ribeiro, P. H. **Observation of tunable Popescu-Rohrlich correlations through postselection of a Gaussian state**. *Phys. Rev. A*, **80**, 030101, (2009). 50

[128] Vaziri, A., Weihs, G., and Zeilinger, A. **Experimental Two-Photon, Three-Dimensional Entanglement for Quantum Communication**. *Phys. Rev. Lett.*, **89**, 240401, (2002). 50, 55, 61, 68

[129] Gröblacher, S., Jennewein, T., Vaziri, A., Weihs, G., and Zeilinger, A. **Experimental quantum cryptography with qutrits**. *New Journal of Physics*, **8**, 75, (2006). 50, 55, 68, 82

[130] Leach, J., Jack, B., RitschMarte, M., Boyd, R. W., K.Jha, A., Barnett, S. M., Franke-Arnold, S., and Padgett, M. J. **Violation of a Bell inequality in two-dimensional orbital angular momentum state-spaces**. *Optics Express*, **17**, 8287–8293, (2009). 50, 55, 68

[131] Oemrawsingh, S. S. R., Aiello, A., Eliel, E. R., Nienhuis, G., and Woerdman, J. P. **How to Observe High-Dimensional Two-Photon Entanglement with Only Two Detectors**. *Phys. Rev. Lett.*, **92**, 217901, (2004). 50, 56

[132] Bennett, C. H., Bernstein, H. J., Popescu, S., and Schumacher, B. **Concentrating partial entanglement by local operations**. *Phys. Rev. A*, **53**, 2046–2052, (1996). 54, 74, 76

[133] Vaziri, A., Pan, J.-W., Jennewein, T., Weihs, G., and Zeilinger, A. **Concentration of Higher Dimensional Entanglement: Qutrits of Photon Orbital Angular Momentum**. *Phys. Rev. Lett.*, **91**, 227902, (2003). 54, 74

[134] Allen, L., Beijersbergen, M. W., Spreeuw, R. J. C., and Woerdman, J. P. **Orbital angular momentum of light and the transformation of Laguerre-Gaussian laser modes**. *Phys. Rev. A*, **45**, 8185–8189, (1992). 55, 67

[135] Collins, D., Gisin, N.-l., Linden, N., Massar, S., and Popescu, S. **Bell Inequalities for Arbitrarily HighDimensional Systems**. *Phys. Rev. Lett.*, **88**, 040404, (2002). 61, 62, 67, 68, 70, 84

[136] Dada, A. C., Leach, J., Buller, G. S., Padgett, M. J., and Andersson, E. **Experimental high-dimensional two-photon entanglement and violations of generalized Bell inequalities**. *Nature Physics*, **7**, 677–680, (2011). 61, 63

[137] Acín, A., Durt, T., Gisin, N., and Latorre, J. I. **Quantum nonlocality in two three-level systems**. *Phys. Rev. A*, **65**, 052325, (2002). 62, 72

[138] Schrödinger, E. **Die gegenwärtige Situation in der Quantenmechanik**. *Naturwissenschaften*, **23**, 807–812; 823–828; 844–849, (1935). 67

[139] Nielsen, M. A. and Chuang, I. L. *Quantum Computation and Quantum Information*, p. 11. Number ISBN 0-521-63503-9 in Cambridge Series on Information and the Natural Sciences. Cambridge University Press, New York, (2000). 67

[140] Durt, T., Kaszlikowski, D., Chen, J.-L., and Kwek, L. C. **Security of quantum key distributions with entangled qudits**. *Phys. Rev. A*, **69**, 032313, (2004). 67

[141] Walborn, S. P., de Oliveira, A. N., Thebaldi, R. S., and Monken, C. H. **Entanglement and conservation of orbital angular momentum in spontaneous parametric down-conversion**. *Phys. Rev. A*, **69**, 023811, (2004). 67, 73, 80

[142] Yuan, Z.-S., Chen, Y.-A., Zhao, B., Chen, S., Schmiedmayer, J., and Pan, J.-W. **Experimental demonstration of a BDCZ quantum repeater node**. *Nature*, **454**, 1098–1101, (2008). 67, 82

[143] Gao, W.-B., Lu, C.-Y., Yao, X.-C., Xu, P., Guhne, O., Goebel, A., Chen, Y.-A., Peng, C.-Z., Chen, Z.-B., and Pan, J.-W. **Experimental demonstration of a hyper-entangled ten-qubit Schrödinger cat state**. *Nature Physics*, **6**, 331–335, (2010). 68, 84, 87

[144] Aspect, A., Grangier, P., and Roger, G. **Experimental Realization of Einstein-Podolsky-Rosen-Bohm Gedankenexperiment: A New Violation of Bell's Inequalities**. *Phys. Rev. Lett.*, **49**, 91–94, (1982). 68

[145] Jack, B., Yao, A. M., Leach, J., Romero, J., Franke-Arnold, S., Ireland, D. G., Barnett, S. M., and Padgett, M. J. **Entanglement of arbitrary superpositions of modes within two-dimensional orbital angular momentum state spaces**. *Phys. Rev. A*, **81**, 043844, (2010). 68

[146] Jack, B., Leach, J., Ritsch, H., Barnett, S. M., Padgett, M. J., and Franke-Arnold, S. **Precise quantum tomography of photon pairs with entangled orbital angular momentum**. *New Journal of Physics*, **11**, 103024, (2009). 68

[147] Pors, J. B., Oemrawsingh, S. S. R., Aiello, A., van Exter, M. P., Eliel, E. R., 't Hooft, G. W., and Woerdman, J. P. **Shannon Dimensionality of Quantum Channels and Its Application to Photon Entanglement**. *Phys. Rev. Lett.*, **101**, 120502, (2008). 68

[148] Durt, T., Kaszlikowski, D., and Żukowski, M. **Violations of local realism with quantum systems described by N-dimensional Hilbert spaces up to** $N = 16$. *Phys. Rev. A*, **64**, 024101, (2001). 69

[149] Leach, J., Dennis, M. R., Courtial, J., and Padgett, M. J. **Vortex knots in light**. *New Journal of Physics*, **7**, 55, (2005). 73

[150] Torres, J. P., Alexandrescu, A., and Torner, L. **Quantum spiral bandwidth of entangled two-photon states**. *Phys. Rev. A*, **68**, 050301, (2003). 74

[151] Law, C. K. and Eberly, J. H. **Analysis and Interpretation of High Transverse Entanglement in Optical Parametric Down Conversion**. *Phys. Rev. Lett.*, **92**, 127903, (2004). 74

[152] Brunner, N., Pironio, S., Acin, A., Gisin, N., Méthot, A. A., and Scarani, V. **Testing the Dimension of Hilbert Spaces**. *Phys. Rev. Lett.*, **100**, 210503, (2008). 79

[153] Blais, A., Huang, R.-S., Wallraff, A., Girvin, S. M., and Schoelkopf, R. J. **Cavity quantum electrodynamics for superconducting electrical circuits: An architecture for quantum computation**. *Phys. Rev. A*, **69**, 062320, (2004). 86

[154] Kaszlikowski, D., Oi, D. K. L., Christandl, M., Chang, K., Ekert, A., Kwek, L. C., and Oh, C. H. **Quantum cryptography based on qutrit Bell inequalities**. *Phys. Rev. A*, **67**, 012310, (2003). 86